



UNIVERSIDADE FEDERAL DE MINAS GERAIS
ESCOLA DE ENGENHARIA
DEPARTAMENTO DE ENGENHARIA NUCLEAR
PÓS-GRADUAÇÃO EM CIÊNCIAS E TÉCNICAS NUCLEARES

CARLOS JULIO MONTAÑO VALENCIA

Investigação de cimentos radioativos de Y-90 e Ho-166 para
tratamentos de metástases ósseas por carcinomas de mama

Belo Horizonte
2019

CARLOS JULIO MONTAÑO VALENCIA

INVESTIGAÇÃO DE CIMENTOS RADIOATIVOS DE Y-90
E Ho-166 PARA TRATAMENTOS DE METÁSTASES
ÓSSEAS POR CARCINOMAS DE MAMA.

Tese apresentada ao Programa de Pós-graduação em Ciências e Técnicas Nucleares como requisito parcial à obtenção do título de Doutor em Ciências e Técnicas Nucleares.

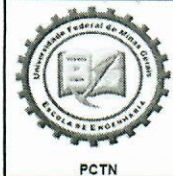
Área de concentração: Ciências das Radiações

Orientador: Dr. Tarcísio Passos Ribeiro de Campos

BELO HORIZONTE
2019

Ficha Catalográfica

M765i	<p>Montaño Valencia, Carlos Julio. Investigação de cimentos radioativos de Y-90 e Ho-166 para tratamentos de metástases ósseas por carcinomas de mama [recurso eletrônico] / Carlos Julio Montaño Valencia. - 2019. 1 recurso online (168 f. : il., color.) : pdf. Orientador: Tarcísio P. Ribeiro de Campos.</p> <p>Tese (doutorado) - Universidade Federal de Minas Gerais, Escola de Engenharia.</p> <p>Apêndices e anexos: f. 138-167.</p> <p>Inclui bibliografias. Exigências do sistema: Adobe Acrobat Reader.</p> <p>1. Engenharia nuclear - Teses. 2. Braquiterapia - Teses. 3. Radiação - Dosimetria - Teses. 4. Análise térmica - Teses. 5. Análise elástica - (Engenharia) - Teses. 6. Análise plástica (Teoria das estruturas) - Teses. 7. Metástase - Teses. I. Campos, Tarcísio Passos Ribeiro de. II. Universidade Federal de Minas Gerais. Escola de Engenharia. III. Título.</p> <p style="text-align: right;">CDU: 621.039(043)</p>
-------	---



FOLHA DE APROVAÇÃO

Investigação de cimentos radioativos de Y-90, Ho-166 e Sm-153 para tratamentos de metástases ósseas por carcinomas de mama.

CARLOS JULIO MONTAÑO VALENCIA

Tese submetida à Banca Examinadora designada pelo Colegiado do Programa de Pós-Graduação em CIÊNCIAS E TÉCNICAS NUCLEARES, como requisito parcial para obtenção do grau de Doutor em CIÊNCIAS E TÉCNICAS NUCLEARES, área de concentração CIÊNCIAS DAS RADIAÇÕES.

Aprovada em 27 de junho de 2019, pela banca constituída pelos membros:

Prof. Tarcísio Passos Ribeiro de Campos - Orientador
Departamento de Engenharia Nuclear - UFMG

Profa. Maria Irene Yoshida
Departamento de Química - ICEx/UFMG

Dr. Bruno Melo Mendes
CDTN/CNEN

Profa. Luciana Batista Nogueira
Departamento de Anatomia e Imagem - UFMG

Dr. Celso Vieira Lima
Departamento de Engenharia Nuclear - UFMG

Dr. André Lima de Souza Castro
Hospital Felício Rocho

Belo Horizonte, 27 de junho de 2019.

AGRADECIMENTOS

Meus sinceros agradecimentos ao professor Tarcísio Passos Ribeiro de Campos pelo acolhimento, convívio, ensinamentos e por contribuir e tornar possível meu desenvolvimento acadêmico e profissional.

Aos amigos do Núcleo de Radiação Ionizante pela amizade, companheirismo e ajuda.

*Agradeço também a minha esposa Olga Lucía Maquilon Moreno por estar ao meu lado durante esses anos, e em especial a minha mãe **María Leonisa Valencia de Montaña**. A meus irmãos Oscar de Jesús Montaña e Gonzalo Montaña por todo seu apoio desde minha criação até agora, no qual está próximo para finalizar minha formação. Também aproveito para deixar na memória de meu pai José Antonio Montaña Triana e meus irmãos Pablo e Jorge este importante logro.*

Agradeço à agência de financiamento para a manutenção com bolsa para o doutorado CAPES – Coordenação de Aperfeiçoamento de Pessoal de Nível Superior. Finalmente, agradeço a oportunidade brindada pelo Grupo Coimbra de Universidades Brasileiras - GCUB e ao Departamento de Talento Humano da Organização dos Estados Americanos - OEA por ter me oferecido essa oportunidade de experimentar deste intercâmbio educativo para minha formação profissional e pessoal aqui no Brasil, além da confiança depositada na minha escolha por meio do processo seletivo de méritos PAEC OEA-GCUB 2014.

RESUMO

A presente tese abordou a Radiovertebroplastia. O objetivo do trabalho foi ampliar os estudos dos materiais envolvidos na técnica, e a resposta dosimétrica em condições simuladas. Foi também avaliada a resposta radiológica do compósito *in situ*, e feita a análise de toxicidade.

O biomaterial, dito cimento ósseo radioativo, foi preparado com PMMA (Polimetilmetacrilato) e Hidroxiapatita (HAp). As concentrações e proporção dos compostos possuem propriedades físico-químicas importantes para otimizar o tratamento. O PMMA é um polímero de natureza hidrofóbica com baixa porosidade em comparação aos tecidos ósseos trabeculares. O perfil térmico estudado apresentou uma fase exotérmica de mais de 60 °C o que poderia produzir necrose celular. Foi observado também que se o PMMA aplicado em implante trabecular, devido a sua pobre porosidade, poderá impedir a difusão de células da medula óssea reduzindo os processos da dinâmica celular e adesão frequente pelas células osteoblásticas e osteoclásticas no microambiente. Tais condições levaram à análise de materiais com concentrações diferenciadas em HAp, incorporadas ao cimento ósseo.

O biomaterial foi sintetizado por cinco distintas razões de concentração do sistema HAp+PMMA. No caso o HAp foi adicionado ao PMMA como uma função estequiométrica $(1-x)\text{PMMA}-x\text{HAp}$ de tal forma que em uma proporção 1:1 a fase exotérmica do material cimentício foi reduzida à temperatura ambiente. Estudos de análise térmica (DSC e TGA), confirmaram a existência de uma transição vítrea reversível ao redor de 103 °C. Por outro lado, posterior a essa transição acontecem fenômenos de degradação liberando CO_2 e H_2O nos segmentos poliméricos. Essa degradação contribui macroscopicamente ao aumento da porosidade no material. Os resultados do estudo mecânico mostrou uma relação inversamente proporcional entre o aumento da concentração do HAp e a diminuição do módulo da resistência à compressão. Outro achado foi a proximidade da resistência à compressão do material cimentício polimerizado em bloco com os valores de resistência à compressão do osso trabecular altamente poroso. Além disso, foi possível concluir que esse aumento de HAp acrescentou a porosidade do implante ósseo, teoricamente devido às reações de segregação sobre as moléculas da água

presas no HAp e expostas ao PMMA na hora da mistura dos componentes.

Os radionuclídeos estudados para compor o cimento foram o Ho-166, Y-90 e Sm-153 por serem emissores de partículas beta energéticas, com meia vida reduzida, e abundância natural do isótopo, a relação custo-benefício de sua produção. Simulações computacionais feitas em modelos vertebrais com metástases ósseas mostraram uma melhor distribuição espacial da dose absorvida do Y-90 em comparação com os outros radionuclídeos alcançando mais do 90% do volume da metástase com uma dose depositada de 65 Gy. Entretanto, Ho-166 também atendeu a proposta terapêutica da Radiovertebroplastia.

Estudos quantitativos de contraste radiológico mostraram resposta radiológica diferenciada do compósito em implantes em vértebras, indicando a possível redução ou eliminação do uso de meios de contraste como o sulfato de bário (BaSO_4) em uma mescla de proporção 1:1 do material cimentício. Testes de citotoxicidade feitos a frio do cimento ósseo radioativo mostraram adesão dos monócitos em meio de cultura e biocompatibilidade do material conferindo outros estudos que apresentam relação entre a ativação dos monócitos em macrófagos e sua função fagocítica para partículas de PMMA menores a 10 μm , indicando uma possível sinalização dos biocerâmicos para reabsorção por osteoclastos.

Palavras chave: Radiovertebroplastia; PMMA; HAp; Cimento Ósseo Radioativo; Y-90; Ho- 166; Análise Térmica; Resistência à Compressão; Dosimetria Computacional; Citotoxicidade.

ABSTRACT

The present thesis has aboard Radiovertebroplasty. The work's objective was to broaden the studies of the materials involved in the technique, and the dosimetric response under simulated conditions. The *in situ* composite radiological response and toxicity analysis were also evaluated.

The biomaterial, said radioactive bone cement, was prepared by PMMA (Polymethylmethacrylate) and Hydroxyapatite (HAp). The concentrations and proportion of the compounds have important physicochemical properties to optimize the treatment. The PMMA is a hydrophobic polymer with low porosity compared to trabecular bone tissue. The thermal profile studied showed an exothermic phase of more than 60 °C which could produce cellular necrosis. It was also observed that if the PMMA applied in a trabecular implant, due to its poor porosity, could prevent the diffusion of cells of the bone marrow reducing the processes of the cellular dynamics and frequent adhesion by the osteoblastic and osteoclastic cells in the microenvironment. Such conditions led to the analysis of materials with different concentrations in HAp, incorporated into the bone cement.

The biomaterial was composed from five different concentration ratios of the HAp+PMMA system. In the case the HAp was added to PMMA as a $(1-x)\text{PMMA}-x\text{HAp}$ stoichiometric function in such a way that in a 1:1 ratio the exothermic phase of the cementitious material was reduced to room temperature. Thermal analysis studies (DSC and TGA) confirmed the existence of a reversible glass transition around 103 °C. On the other hand, subsequent to this transition occur degradation phenomena releasing CO_2 and H_2O in the polymer segments. This degradation contributes macroscopically to the increased porosity on material. The mechanical study results showed an inversely proportional relationship between the increase of the HAp concentration and the decrease of the compressive strength modulus. Another finding was the proximity in the compressive strength of the block polymerized cementitious material to the compressive strength values of the highly porous trabecular bone. In addition, it was possible to conclude that this increase of HAp added the porosity of the bone implant, theoretically due to the segregation reactions on water molecules trapped in the HAp and exposed to PMMA at the mixing time to all components.

The radionuclides studied to compose the cement were Ho-166, Y-90 and Sm-153 due to the emission of energetic beta particles, with reduced half-life, and natural abundance of the isotope, the cost-benefit ratio of their production. Computational simulations on vertebral models with bone metastases showed a better spatial distribution of the absorbed dose of Y-90 compared to the other radionuclides reaching more than 90% of the volume of metastasis with a deposited dose of 65 Gy. However, Ho-166 also met the therapeutic proposal of Radiovertebroplasty.

Quantitative radiological contrast studies showed a differentiated radiological response of the composite in implants in vertebrae, indicating the possible reduction or elimination in the use for contrast agents such as barium sulphate (BaSO_4) in a 1:1 blend of cementitious material. Cold cytotoxicity tests with radioactive bone cement showed monocyte adhesion in culture medium and biocompatibility for material conferring other studies that show a relationship between the activation of monocytes in macrophages and their phagocytic function for PMMA particles smaller until 10 μm , indicating a possible bioceramic signaling for osteoclast reabsorption.

Keywords: Vertebroplasty; PMMA; HAp; Bone Radioactive Cement; Y-90; Ho-166; Thermal Analysis; Compressive Strength; Dosimetry; Cytotoxicity.

Lista de ilustrações

Figura 1.1 Imagens radiográficas de corpo de vértebra com indicativo para Vertebroplastia, com metástases interna. (A) no diagnóstico – complementado com RMN e Cintilografia; (B) Vertebroplastia aplicada e teleterapia externa; (C) falha com colapsamento da vertebra. Fonte: (MACEDO, 2005)	32
Figura 1.2 Distribuição de isodoses produzidas por três campos de irradiação, proposto no planejamento radioterápico, e dimensões do campo externo centrado na vertebra alvo FONTE: (CASTRO, et al. 2002) http://dx.doi.org/10.1590/S0100-39842002000300010 .	34
Figura 1.3 Imagem do planejamento de radioterapia de corpo vertebral, como modelo padrão ouro em radioterapia.	35
Figura 1.4 Imagens estereoscópicas (x80) do cimento radioativo ósseo, frio, após preparo e pega, com razão de concentração entre Polimetilmetacrilato e Hidroxiapatita, incorporando Ho-165 em sua matriz de Ca e P, de 1:0,01 e 0.1:1, isto é, de 100x para 0,1x. Fonte: acervo do autor.	37
Figura 1.5 Distribuição de dose produzida pelo cimento ósseo radioativo posicionado ao lado da coluna vertebral(DONANZAM B. A., 2012).	40
Figure 2.1 Minimal invasive procedures: anatomical position of vertebrae. (A) Vertebroplasty; (B) anatomical regions of the vertebrae according to Harrington; (C) Kit and Vertebroplasty simulation (GEORGY, 2008).	52
Figure 2.2 Computational model with MCNP5/Siscodes - BED. (A) vertebral model of the spine and isodose distribution. (B) accumulated dose curve for cement bound with Ho-166 (DONANZAM B. A., 2012).....	55
Figure 3.1 X-ray and ultrasound images in vitro from vertebrae model is presented. In (a) antero-posterior-AP incidence plane (b) lateral incidence plane (c) and (d), there are ultrasound images; and, (d), a dynamic anomaly shows the insertion of the needle.....	64
Figure 3.2 Radiological images of four vertebral models. In (a) the vertebrae have molten lead (b) PMMA injected. (c) PMMA + 10% BaSO ₄ were injected. (d) x = 0.5 of the bone cement.....	66
Figure 3.3 Contrast Analysis with ImageJ free software. In (a) and (c) implant's surface plot and the vertebra image has molten lead, respectively. In (b) and (d) hole's surface plot and the vertebra image has a hole, respectively	67

Figure 3.4 Plot profile of a vertebra in the implant region. (a) Vertebra with lead molten.	
(b) Vertebra's image with hole.....	68
Figure 3.5 (a) Analysis of profiles plots for different implants to a length equivalent. (b)	
Attenuation factor for all implants download from NIST, online free XCOM	
(https://physics.nist.gov/PhysRefData/Xcom/html/xcom1.html).....	69
Figure 4.1 TGA heating profiles for x_i ($i=1-6$) concentrations of the $(1-x)$ PMMA- x HAp	
binary system in the interest temperature range between 45 – 180 °C approximately to	
determine system's mass loss, where (a) to PMMA(Copolymer)-HAp polymerized system,	
and (b) to PMMA-HAp system in powder.	78
Figure 4.2 DSC heating curves for the six $[x]$ concentrations of the $(1-x)$ PMMA- x HAp	
binary system in the interest temperature range between 60 – 180 °C. The Heat Flux is	
presented in [mJ/s]. All curves were normalized with the maximum heat flux.	79
Figure 4.3 Compression profiles for the mechanical assay on the blocks with x_i ($i=1-5$)	
concentrations of the $(1-x)$ PMMA- x HAp binary system, where (a) PMMA-HAp	
polymerized system without thermal treatment with a fracture domain at 0.30 – 0,42 %	
compression strain; and (b) PMMA-HAp polymerized system with thermal treatment of 30	
min at T_g glass transition temperature.	81
Figure 4.4 Stereoscopic images of the block surfaces, where (a) to PMMA only or x_1	
concentration without thermal treatment; (b) to x_5 concentration parameter with thermal	
treatment for 30 min at the T_g glass transition temperature.	82
Figure 5.1 Shows the change in temperature as a function of time for each of the samples.	
Macroaggregate thermology in the bone cement. (a) Thermal profiles varying x_n in the $(1-$	
$x)$ PMMA- x HAp system. (b) Fit exponential curve for the x_1 concentration.	93
Figure 5.2 ^1H MAS NMR spectra of ACP-CaHA (red) and nanostructured CaHA (blue).	
Taken from the reference (KLIMAVICIUS et al. 2014).	94
Figure 6.1 XY-planes characteristics of the vertebral models with mammary metastasis. (a)	
Bone Implant XY-planes for Vert. A between $z = -7$ and $z = 7$. (b) Bone Metastasis XY-	
planes only for Vert. A for $(-43 < z < -8)$ and $(8 < z < 43)$. (c) Bone tissue only for Vert. A	
$(-47 < z < -44)$ and $(44 < z < 47)$. (d) Bone Implant XY-planes for Vert. B between $z = -7$	
and $z = 7$. (e) Bone Implant XY-planes for Vert. B $(-31 < z < -8)$ and $(8 < z < 31)$. (f) Bone	
Metastasis XY-planes only for Vert. B for $(-39 < z < -32)$ and $(32 < z < 39)$. (g) Bone	
tissue only for Vert. A $(-47 < z < -40)$ and $(40 < z < 47)$	104
Figure 6.2 Radiological images of four vertebral models. In (a) the vertebrae have molten	
lead with ROI defined as 84 pxls x 80 pxls on vertebral body. (b) PMMA injected. (c)	

0.9PMMA + 0.1BaSO ₄ were injected. (d) x = 0.5 concentration of the HAp for the bone cement.....	106
Figure 6.3 The gray-profiles in the spatial domain of the I(x,y) and FFT 2D images of their respective ROIs. Example for a gray profile in (a) straight lines parallel to x = 0 and y = 0; (b) FFT 2D for ROI with the lead implant; (c) FFT 2D for ROI with PMMA implant; (d) FFT 2D for ROI with the 0.9PMMA + 0.1BaSO ₄ implant; and, (e) FFT 2D for ROI with PMMA+HAp implant and 1:1 ratio.	108
Figure 6.4 FFT 2D curves from ROIs and Gauss surface fit. (a) Plotting Surface of the FFT 2D corresponds to ROI with lead implant. (b) Plotting Surface of the FFT 2D corresponds to ROI with PMMA implant. (c) Plotting Surface of the FFT 2D corresponds to ROI with the 0.9PMMA + 0.1BaSO ₄ implant. (d) Plotting Surface of the FFT 2D corresponds to ROI with PMMA+HAp implant, and 1:1 ratio. (e) Gauss surface fit for the lead implant (f) Gauss surface for case (e).....	109
Figure 6.5 Computational dosimetric evaluating in the vertebrae models. Dose spatial distribution for Vert A model: (a) Ho-166 coupled source (b) Sm-153 coupled source (c) Y-90 coupled source. Dose spatial distribution for VertB model: (d) Ho-166 coupled source (e) Sm-153 coupled source (f) Y-90 coupled source. The dose for the b-emission for all models was limited to 72 Gy.	111
Figure 6.6 Dose spatial distribution for lumbar vertebral model. Ho-166 coupled source: (a) Transverse XY-plane (b) Coronal XZ-plane (d) Sagittal YZ-plane. Sm-153 coupled source: (a) Transverse XY-plane (b) Coronal XZ-plane (d) Sagittal YZ-plane. Y-90 coupled source: (a) Transverse XY-plane (b) Coronal XZ-plane (d) Sagittal YZ-plane. .	113
Figure 6.7 Dose-Volume Histograms for PTV and OAR in vertebral models with 90% Dref=72 Gy. (a) OAR 1 for spinal cord at z = 0 in Vert. A and Vert. B (b) OAR 2 for bone tissue at z = 0 in Vert. A and Vert. B (c) PTV for metastasis at z = 0 in Vert. A and Vert. B (d) PTV for bone cement in model without metastasis (e) OAR 1 for spinal cord in model without metastasis (f) OAR 2 for bone tissue in model without metastasis.....	114
Figure 6.8 Volume Percentage with 90% of the Reference Dose as a time decay function for Ho-166 and Y-90 with a bone cement 6,77 g simulated in the Vert. B model.....	116
Figure 7.1 Chip-shaped samples of PMMA+HAp bone cement (1:1 ratio) and PMMA..	125
Figure 7.2 ANOVA results for the time kinetic of the diverse studied groups at (a) 24 h (b) 48 h (c) 72 h and (d) all times inter-groups.	127
Figure 7.3 ANOVA Cell count for analysis of cellular field microphotography in kinetic time function (500 x 500 μm ² cellular field) at (a) 0 h (b) 24 h (c) 48 h and (d) 72 h.	128

Figure 7.4 Microphotographs on cell proliferation and aggregation to bone cement samples. (a) Initial cell density at $t = 24$ hours distant from the bone implant sample. (b) Increase in cell density at $t = 24$ hours close to the chip. (c) Increase in cell density at $t = 24$ hours below of the chip. (d) Aggregation and cell adhesion detected at the chip edge at $t = 72$ hours 130

Lista de tabelas

Tabela 1.1 Doses e BED para diferentes técnicas de radioterapia e ^{166}Ho Radiovertebroplastia.....	41
Table 3.1 Concentrations [x] bone cement to produce 1 g of the binary system (1-x)PMMA-xHAp	63
Table 4.1 Thermomechanical properties of (1-x)PMMA-xHAp System.....	82
Table 5.1 Viscous phase polymerization time of the cement based in the (1-x)PMMA-xHAp system are numbered with Roman numerals.	94
Table 6.1 Evaluation of the Radiological Contrast by means of the FWHM due to the implants.	110
Table 6.2 Therapeutic Dose Deposited and Radiotoxicity for PTV and OAR – Volume percentage estimated for 90% of the Reference Dose (72 Gy) concerning to TD 50/5 for each organ.....	116

Lista de abreviaturas e siglas

^1H NMR	Espectro de Ressonância Magnética Nuclear para Hidrogênio
2D	Bidimensional
3D	Tridimensional
^{166}Ho	Hólmio-166
^{153}Sm	Samário-153
^{90}Y	Ítrio-90
μ	Coefficiente de atenuação
CTV	Volume alvo clínico
CS	Compressive Strength
DNA	Ácido Desoxirribonucleico
DO	Densidade óptica
DSC	Differential Scanning Calorimetry
GTV	Volume tumoral bruto
H	Hidrogênio
HAp	Hidroxiapatita
ICRP	<i>International Commission on Radiological Protection</i>
ICRU	<i>International Commission on Radiations Units and Measurements</i>
IMRT	Radioterapia por intensidade modulada
LET	Transferência linear de energia
MCNP	<i>Monte Carlo N-particle</i>
MCNPx	<i>Monte Carlo N-particle x</i>
O	Oxigênio
OAR	Órgãos de risco
PET	Tomografia por emissão de pósitron
PMMA	Polimetilmetacrilato
PTV	Volume alvo planejado
PRV	Volume de órgãos de risco planejados
RGB	Vermelho, verde, azul
RMN	Ressonância Magnética Nuclear
RT	Radioterapia
TGA	Thermogravimetric Analysis
T _g	Temperatura de Transição vítrea
TC	Tomografia Computadorizada
TLD	Dosímetro termoluminescente
TPS	Treatment Planning System
TPS 3D	Sistemas de planejamento de tratamento tridimensionais
Z	Número atômico
Z _{eff}	Número atômico efetiva

SUMÁRIO

AGRADECIMENTOS	V
RESUMO	VI
ABSTRACT	VIII
LISTA DE ILUSTRAÇÕES	X
LISTA DE TABELAS	XIV
LISTA DE ABREVIATURAS E SIGLAS	XV
SUMÁRIO	XVI
I. INTRODUÇÃO	19
II. OBJETIVOS	21
A. OBJETIVOS GERAIS	21
B. OBJETIVOS ESPECÍFICOS	21
C. METAS.....	21
III. CONSIDERAÇÕES METODOLÓGICAS	22
A. MATERIAIS	22
B. IMPLANTES E RESPOSTA RADIOLÓGICA	22
C. ESTUDOS EM DOSIMETRIA.....	22
D. ANÁLISE DE RESPOSTA BIOLÓGICA DEVIDO À EXPOSIÇÃO AO CIMENTO	23
IV. ORGANIZAÇÃO DA TESE	24
CAPITULO 1	27
1. POSSIBILIDADES DE UM CIMENTO ÓSSEO RADIOATIVO EM METÁSTASES ÓSSEAS – UMA REVISÃO	27
1.1. APRESENTAÇÃO DO TEMA	27
1.2. JUSTIFICATIVA	29
1.3. SOBRE A VERTEBROPLASTIA	30
1.4. VERTEBROPLASTIA E ONCOLOGIA	31
1.5. A VERTEBROPLASTIA E A RADIOTERAPIA.....	33
1.6. NOVO MATERIAL E SUAS PERSPECTIVAS	35
1.7. CONSTITUIÇÃO DO CIMENTO ÓSSEO RADIOATIVO	37
1.8. ATIVAÇÃO DO CIMENTO ÓSSEO.....	38
1.9. DOSIMETRIA NO CIMENTO ÓSSEO RADIOATIVO	39
1.10. CONSIDERAÇÕES	41
1.11. REFERÊNCIAS	42
CAPÍTULO 2	46
2. RADIOACTIVE CEMENT OF PMMA AND HAP-¹⁵³SM, ¹⁶⁶HO, OR ¹⁸⁸RE FOR BONE METASTASIS TREATMENT	46
ABSTRACT	46

2.1.	INTRODUCTION	47
2.2.	SOME CANCER EPIDEMIOLOGICAL DATA IN BRAZIL	49
2.3.	ANATOMIC CLASSIFICATION AND STRUCTURAL MECHANICAL FUNCTIONS OF THE BONE TISSUE	50
2.4.	BONE DISEASES, TYPES OF METASTASIS	51
2.5.	BONE CEMENT, STRUCTURE AND COMPOSITION	51
2.6.	THERAPEUTIC TREATMENT AND PERCUTANEOUS PROCEDURES	51
2.7.	RADIOACTIVE MATERIAL PRODUCTION, VERTEBRAL MODEL AND COMPUTATIONAL DOSIMETRY.....	54
2.8.	FINAL REMARKS	56
2.9.	REFERENCES.....	56
CAPITULO 3.....		60
3. PHYSICAL DISTRIBUTION AND RADIOLOGICAL CONTRAST OF CEMENTS IMPLANTED IN VITRO VERTEBRAE		60
	ABSTRACT	60
3.1.	INTRODUCTION	61
3.2.	METHODS	62
3.2.1.	<i>In vitro anatomical sample preparation.</i>	62
3.2.2.	<i>Synthesis of the composite.</i>	62
3.2.3.	<i>Cement injection.</i>	63
3.2.4.	<i>Radiological contrast.</i>	63
3.2.5.	<i>Ultrasonography images.</i>	64
3.3.	RESULTS.....	64
3.4.	CONCLUSIONS	70
3.5.	REFERENCES.....	71
CAPITULO 4.....		73
4. HYDROXYAPATITE INFLUENCE ON THE THERMAL AND MECHANICAL PROPERTIES OF A POSSIBLE RADIOACTIVE BONE CEMENT.....		73
	ABSTRACT	73
4.1.	INTRODUCTION	74
4.2.	MATERIALS AND METHODS.....	76
4.2.1.	<i>HAp Synthesis.</i>	76
4.2.2.	<i>PMMA-HAp composite preparation.</i>	77
4.2.3.	<i>Calorimetry DSC and Thermogravimetric TGA assays.</i>	77
4.3.	RESULTS.....	78
4.4.	DISCUSSION	82
4.5.	CONCLUSION	84
4.6.	REFERENCES.....	85
CAPITULO 5.....		87
5. INFLUENCE OF HAP ON THE POLYMERIZATION PROCESSES OF A POSSIBLE RADIOACTIVE BONE CEMENT.....		87
	ABSTRACT	87
5.1.	INTRODUCTION	88
5.2.	MATERIALS AND METHODS.....	91
5.2.1.	<i>Bone cement synthesis.</i>	91

5.2.2. <i>Macroaggregate thermology</i>	92
5.3. RESULTS AND DISCUSSION	92
5.4. CONCLUSION	95
5.5. REFERENCES.....	95
CAPITULO 6.....	98
6. COMPUTATIONAL DOSIMETRIC EVALUATION USING A RADIOACTIVE BONE CEMENT BASED ON PMMA+HAP WITH OPTIMAL RADIOLOGICAL CONTRAST.....	98
ABSTRACT	98
6.1. INTRODUCTION	99
6.2. MATERIALS AND METHODS.....	102
6.2.1. <i>The RB cement synthesis</i>	102
6.2.2. <i>Radiological Analysis</i>	102
6.2.3. <i>Computational vertebrae models</i>	103
6.3. RESULTS.....	105
6.3.1. <i>Radiological contrast</i>	105
6.3.2. <i>Computational dosimetric evaluation of the vertebrae models</i>	110
6.4. DISCUSSION	116
6.5. CONCLUSION	118
6.6. REFERENCES.....	118
CAPITULO 7	121
7. CYTOTOXICITY STUDY IN PBMC CULTURES DUE TO EXPOSITION OF A POSSIBLE RADIOACTIVE-BONE CEMENT BASED IN PMMA-HAP.	121
ABSTRACT	121
7.1. INTRODUCTION	122
7.2. MATERIALS AND METHODS.....	124
7.2.1. <i>The RB cement synthesis</i>	124
7.2.2. <i>Toxicity experiments</i>	125
7.3. RESULTS.....	126
7.3.1. <i>ANOVA Cell viability</i>	126
7.4. DISCUSSION	129
7.5. CONCLUSION	132
7.6. REFERENCES.....	133
8. CONSIDERAÇÕES FINAIS.....	136
A. APÊNDICE - FUNDAMENTOS DA TERMODINÂMICA	138
A TRANSIÇÕES DE FASE.....	138
B. ANÁLISE TÈRMICA	143
B. APÊNDICE – ALGUNS FUNDAMENTOS DE DOSIMETRIA.....	148
A. GERALIDADES DA DOSIMETRIA	148
B. MODELO FÍSICO DA TERMOLUMINISCÊNCIA.....	150
C. DOSIMETRIA COM FILME RADIOCRÔMICO.....	155
C. APÊNDICE – ANÁLISE MECÂNICA	159
D. REFERÊNCIAS DOS APÊNDICES	162
E. ANEXOS	163

A.	IMAGEM MÉDICA.....	163
B.	ANALISE TÉRMICA	164
C.	ANÁLISE MECÂNICA.....	164
D.	CITOTOXICIDADE.....	165
E.	TRABALHOS PUBLICADOS EM REVISTAS, CONGRESSOS E EM PROCESSO DE SUBMISSÃO	
	166	

I. INTRODUÇÃO

Desde 1981 quando foi proposto o uso do Metilmetacrilato polimerizado para estabilização de corpos vertebrais causado por fraturas e luxações induzidas pelas metástases devido a um aumento da pressão interna do corpo vertebral e como consequência disso o compromisso neurológico para o paciente apresentou-se uma solução para a redução da dor. Alguns efeitos térmicos indesejados de tipo exotérmico foram encontrados pelo processo de polimerização do Metilmetacrilato. Pesquisas feitas em procedimentos pós-cirúrgicos mostraram uma excelente melhora na dor com a estabilização da coluna vertebral graças ao uso do cimento polimérico. Entretanto, manteve-se em adição às terapias de radiação já protocolizadas nos serviços oncológicos. Naquela época, a fonte de radiação ainda não havia se inserido ao cimento restaurador e só se pretendia no momento melhorar a estabilidade do corpo vertebral.

Durante os anos 90, os cimentos ósseos foram utilizados em fraturas como mecanismo para a estabilização de corpos vertebrais e como parte do tratamento na Radioterapia das metástases ósseas com aceleradores lineares utilizando o método do IMRT (*Intensity Modulation Radiotherapy*), o qual apresenta um bom desempenho em comparação com outras técnicas radioterápicas de megavoltagem, reduzindo a dose nos tecidos sadios. Mas envolve um maior custo de operação devido à complexidade dos algoritmos para definir o volume alvo e a dose. Além disso, comparado com uma técnica braquiterápica intersticial de uso *in situ* da fonte radioativa, o IMRT apresenta menor desempenho clínico. Em outros procedimentos se considerou o uso de radioisótopos como o Renio-186 e Estroncio-89 que inseridos por via intravenosa depositam uma dose de radiação abrangendo uma distribuição espacial mais ampla, obtendo um efeito clínico favorável com relação à sintomatologia referente aos problemas associados com a dor.

Em 1987 foi introduzida a técnica da Vertebroplastia e a Cifoplastia que considerou o uso do cimento de restauração óssea principalmente para os pacientes com osteoporose. Da mesma maneira como nos tratamentos paliativos de IMRT misturados com os procedimentos de Vertebroplastia e Cifoplastia o objetivo era reduzir os sintomas das

como consequência das metástases. No início dos anos 90 já existiam pesquisas com proposta para o uso de $^{153}\text{Sm-EDTMP}$ através de um procedimento percutâneo e assim melhorar a distribuição espacial de dose. O uso de Sr-186 e Re-89 fornecidos por via intravenosa sistemicamente produziam um efeito tóxico com um alto compromisso neurológico na medula devido à desmielinização. Apesar de toda a pesquisa e investimento clínico, continua-se como um desafio a necessidade da melhora na qualidade de vida dos pacientes com metástases ósseas e, portanto, o uso dos cimentos ósseos representa uma boa alternativa clínica.

Em termos gerais, a presente tese aborda um tratamento que permite inserção *in situ* no corpo da Vértebra, da região torácica ou das extremidades, um compósito biocerâmico constituído por um radioisótopo de emissão beta como: ^{90}Y ou ^{166}Ho , incorporado a um cimento ósseo acrílico, de forma a depositar uma dose de radiação em condições suficientes e desejadas nas lesões metastáticas reproduzindo uma situação clínica de menor exposição aos tecidos sadios adjacentes, evitando assim possíveis procedimentos cirúrgicos altamente invasivos para o paciente ou doses radiotóxicas acima dos níveis de tolerância, melhorando significativamente a janela terapêutica para os protocolos radioterápicos em pacientes oncológicos com metástases ósseas. Outras características radiológicas, de resposta citotóxica e propriedades físicas do cimento são apresentadas nas discussões dos capítulos.

II. OBJETIVOS

a. Objetivos Gerais

Ampliar os conhecimentos do PMMA-HAp para uso terapêutico em tratamentos de metástases por carcinomas de mama. Investigar a dosimetria do Y-90 e Ho-166 incorporado no cimento ósseo e suas distribuições espaciais de dose. Investigar as propriedades mecânicas do cimento ósseo. Apresentar um protocolo de sínteses do PMMA-biocerâmicas que amplie o tempo clínico para procedimentos percutâneos minimamente invasivos.

b. Objetivos Específicos

- Revisar diferentes procedimentos de restauração de tecidos ósseos que sejam minimamente invasivos.
- Revisar os diferentes estudos apresentados sobre cimentos ósseos para uso terapêutico.
- Preparar a síntese do PMMA-HAp a frio e estudar suas propriedades mecânicas, compara-lo com tecido ósseo e PMMA.
- Estudar as propriedades termodinâmicas do PMMA-Biocerâmicas.
- Elaborar um estudo dosimétrico computacional do cimento nos diferentes fantomas onde é provável a metástases.
- Fazer um estudo radiobiológico in vitro dos carcinomas e dos tecidos saudáveis mediante controle de padrões físico-químicos.

c. Metas

- Aumentar o tempo clínico do PMMA para uso terapêutico em procedimentos percutâneos.
- Investigar um protocolo paliativo de menor impacto nos tecidos saídos com o uso do Y-90 e Ho-166 incorporado ao cimento ósseo.
- Fazer a respectiva divulgação científica do trabalho conforme com os requerimentos do programa e CAPES.

III. CONSIDERAÇÕES METODOLÓGICAS

a. Materiais

Investigar a natureza dos materiais que compõem o cimento ósseo na perspectiva físico-química com base na ciência dos materiais:

- i. Síntese dos materiais. Sínteses e caracterização dos materiais que compõem o cimento como: PMMA e biofosfatos.
- ii. Caracterização dos materiais. A caracterização termodinâmica, ótica e de propriedades elétricas magnéticas, podem ser desenvolvidas mediante técnicas calorimétricas (DSC, TG e outras). A caracterização das propriedades mecânicas do material em bloco é outra necessidade essencial para alcançar a respectiva comparação com o tecido ósseo natural e outros sintéticos que sejam utilizados frequentemente em procedimentos ortopédicos.

b. Implantes e resposta radiológica

- i. P&D em instrumentação médica em protocolos de implante. Investigar procedimentos percutâneos e o uso de cimentos ósseos para a restauração e recomposição anatômica, complementado com o tratamento terapêutico que envolve fatores dosimétricos, com a elaboração e adequação de instrumentação médica para tal fim.
- ii. Reprodução por imagens radiológicas. Estudos de imagem dos fantasmas mediante radiografias ou tomografias computadorizadas para que sejam outros elementos importantes de muito impacto anatômico.

c. Estudos em dosimetria

Estudos dosimétricos computacionais com geração de distribuições de doses absorvidas e biologicamente equivalentes em situações clínicas e em fantasmas *in vitro*. Do mesmo

modo, com recursos computacionais, elaborar simulações de distribuições de dose absorvidas e biologicamente equivalentes (BED), em fantasmas computacionais reprodutivos de situações clínicas humanas ou situações *in vitro*, que precisam elementos básicos da dosimetria clínica.

d. Análise de resposta biológica devido à exposição ao cimento

- i. P&D em instrumentação para investigação físico-químico em estudos radiobiológico. Investigar e elaborar programas computacionais de controle em LabView e Arduino, reproduzindo fundamentos teóricos de automatização e o controle, para ser aplicados no estudo biológico, com mensuração e monitorização de pH, temperatura.
- ii. Testes biológicos em instrumentação desenvolvida. A montagem e a monitorização do modelo biológico *in vitro* para avaliar o comportamento à exposição de culturas celulares PBMC ao implante é outro aspecto fundamental neste trabalho.
- iii. Range e percurso de radiações em tecidos ósseos. Investigar e ampliar a compreensão precisa da aplicação de núclídeos radioativos, de seus decaimentos radioativos, seus ranges de percurso em diversos tecidos, que no campo clínico fazem parte da medicina nuclear, referente a exploração de seu uso em procedimentos percutâneos e em cimentos ósseos.

IV. ORGANIZAÇÃO DA TESE

Este trabalho é apresentado segundo os requerimentos de formatação do Colegiado do programa de Pós-graduação em Ciências e Técnicas Nucleares do Departamento de Engenharia Nuclear da UFMG. Os primeiros cinco capítulos a seguir foram publicados ou apresentados em revistas especializadas ou congressos da área nuclear. O presente documento é do domínio total com fins acadêmicos da Universidade Federal de Minas Gerais e para evitar conflito de interesse com as revistas foram mantidas a linguagem do texto original dos capítulos que foram publicados. Os últimos dois capítulos encontram-se em processo de ajuste para submissão às revistas. A tese está organizada como segue:

Capítulo 1. Neste capítulo está apresentada uma revisão geral de conceitos e desenvolvimentos no âmbito do estado da arte em tratamentos de pacientes oncológicos com metástases ósseas. Foram abordados tanto questões atuais em sistemas de planejamentos de radioterapia - TPS (*Treatment Planning Systems*) em condições paliativas, como os avanços e as propostas desenvolvidas em nosso grupo de pesquisa em matéria dos cimentos ósseos para tratamentos *in situ*. São abordados os procedimentos ortopédicos de uso de técnicas minimamente invasivas; as vantagens terapêuticas de nossa proposta, em função da dosimetria comparativa com outras técnicas radioterapêuticas convencionais; e, a redução da dose e BED (*Biologically Effective Dose*) na medula espinhal para metástases na coluna vertebral. Baseado nessa revisão, foi elaborada a proposta de pesquisa identificando os objetivos e as metas para este trabalho.

Capítulo 2. Nesse capítulo foi feita uma abordagem dos fundamentos teóricos em relação ao cimento radioativo com o acoplamento do Sm-153 ou Ho-166 ou Re-188. Nesta revisão apresenta-se desde a origem dos cimentos ósseos para a Vertebroplastia até nossa proposta radioterápica com ajuda do material cimentício radioativo. São abordados também os benefícios para os pacientes na redução da dor e diminuição da dose nos tecidos sadios.

Capítulo 3. Neste capítulo foi desenvolvido um fantoma de coluna *in vitro* com

características ecográficas e foi estudado o seu contraste radiológico em função da aplicação do material cimentício para concentrações altas de Hidroxiapatita (HAp) em comparação com o uso do polímero PMMA (Polimetilmetacrilato) misturado com meios de contraste radiológico como o sulfato de bário BaSO_4 . O trabalho do contraste é referenciado com o controle positivo com uma aplicação de chumbo em uma vértebra de referência. Este fantoma é base de futuros implantes do cimento ósseo radioativo à quente para avaliação empírica da dose e a BED.

Capítulo 4. Neste capítulo fêz-se um estudo térmico e mecânico assim como a síntese da Hidroxiapatita e o planejamento estequiométrico das distintas concentrações em um sistema binário $(1-x)\text{PMMA}-x\text{HAp}$ para desenvolver os experimentos para a análise térmica e mecânica. A análise térmica foi feita basicamente por duas técnicas: a calorimetria de exploratória diferencial (DSC) e a termogravimetria (TG). A análise mecânica foi feita para estudar o comportamento mecânico do material à resistência à compressão. Neste trabalho pretende-se caracterizar o material em função do incremento da matriz de cálcio ou HAp e a proximidade dele com o comportamento mecânico dos tecidos porosos. Outro aspecto importante é a vantagem que pode ter a degradação do polímero depois da transição vítrea aos $103\text{ }^\circ\text{C}$ em relação com a formação de macroporos.

Capítulo 5. Neste capítulo foi apresentada um estudo dos perfis térmicos do cimento em função do incremento do HAp no sistema e a redução da fase exotérmica no material. Também foi feita uma revisão de estudos de espectros de ressonância magnética no HAp que mostram a formação de dipolos eléctricos por acoplamento de ^{31}P (Fósforo-31) com grupos hidroxilas o que teoricamente favorece a captação da água na rede da Hidroxiapatita pela interação dipolo-dipolo. O aumento do HAp no sistema binário $(1-x)\text{PMMA}-x\text{HAp}$ aumenta o potencial para gerar reações de segregação devido à natureza hidrofóbica do polímero.

Capítulo 6. Neste trabalho avalia-se computacionalmente a dose depositada em um modelo vertebral animal com uma metástase no corpo da vértebra na situação potencialmente mais complexa para tratar. A dose depositada máxima possível é definida baseado no máximo de dose radiotóxica que podem receber alguns tecidos sadios

próximos à metástase. Nesse caso, o máximo possível de dose de tolerância para os tecidos ósseos é 65 Gy e a mesma faixa a medula espinhal. O modelo computacional foi construído das imagens radiológicas de testes de implantes feitos no capítulo 3. O modelo computacional desenvolvido foi desenhado para o programa MCNPx o qual permite simular a dose por meio de métodos estocásticos.

Capítulo 7. Neste último capítulo foram apresentadas as perspectivas finais da pesquisa. Aqui mostrou-se um possível trabalho de citotoxicidade, no qual, desejou-se avaliar a adesão celular como uma possível resposta inflamatória das células PBMC (*Peripheral Blood Mononuclear*) expostas ao cimento em condições de culturas in vitro. Além da sinalização que os monócitos podem desenvolver e a ativação a macrófagos para fagocitose parcial dos componentes do material de implante. A viabilidade celular fornece informação importante sobre a citotoxicidade do material em cultivo.

CAPITULO 1

1. Possibilidades de um cimento ósseo radioativo em metástases ósseas – Uma revisão

1.1. Apresentação do tema

Na atualidade existem poucos procedimentos para atender os inumeráveis casos relacionados com câncer em estádios avançados com metástases confirmadas. Estes são os casos mais críticos, isto é, quando a doença se espalha saindo de in situ para loco-regional direcionada a todo o corpo e se convertendo em sistêmica, conseqüentemente afetando outros órgãos e provavelmente o sistema esquelético. Nesse estágio, a medicina não traz esperança para os pacientes, sendo que a morte pode acontecer semanas ou meses depois de confirmado diagnóstico, com conseqüente deterioramento da qualidade de vida do paciente. Muitos dos pacientes sofrem de traumas que geram diferentes intensidades de dor. Na maioria dos casos a dor é muito intensa como conseqüência de diversas microfraturas secundárias produzidas pelo processo metastático na estrutura óssea, sendo recomendado pelo corpo clínico a introdução de medidas que na maioria dos casos são consideradas paliativas para atingir redução da dor crônica. É compreensível visto que a doença já tenha evoluído para um estado de irreversibilidade e não é provável uma recuperação plena do paciente. Um dos possíveis tratamentos para redução de dor é o uso da morfina, entre outros medicamentos; mesmo que não atue na recuperação de fraturas e na descompressão produzida pelos tecidos cancerosos (HORN, HENN e LEMOLE, 2004).

Existem intervenções mediante a *Teleterapia*, que são menos invasiva que os procedimentos cirúrgicos; entretanto, essa técnica também pode trazer efeitos deletérios, pois mesmo com uma ótima definição dos campos e do volume alvo é inevitável expor outros órgãos ou regiões vitais do corpo à radiação ionizante; em uma condição clínica já debilitada. Quando o alvo é a estrutura óssea, é possível um procedimento cirúrgico ortopédico complexo. Entretanto, tais procedimentos em essência devem ser evitados pelos riscos que isso traz e em especial em idosos.

Desde 1981, quando Harrington K.D. propôs o uso do metil metacrilato polimerizado

para estabilização de corpos vertebrais causadas por fraturas e luxações induzidas pelas metástases, observou-se um aumento da pressão interna do corpo vertebral que compromete neurologicamente o paciente. A solução apresentada para a redução da dor envolvia o aproveitamento dos efeitos exotérmicos da polimerização do *Metilmetacrilato* (HARRINGTON, 1981; GEORGY, 2008). Em procedimentos pós-cirúrgicos entre 13 e 14 pacientes, HARRINGTON demonstrou com o uso do cimento uma excelente melhora de dor nestes pacientes incluindo a estabilização da coluna vertebral. Entretanto, manteve-se em adição a terapia de irradiação. Assim, nesse protocolo, não existia a proposta de inserção da fonte de radiação no sitio vertebral, em conjunto com o cimento restaurador. Só se pretendia no momento melhorar a estabilidade do corpo vertebral. Os benefícios clínicos com o uso do PMMA eram atingidos em uma escala temporal de 13 a 45 meses após o procedimento.

Durante os anos 90, esse cimento continuou sendo utilizado como mecanismo para a estabilização de corpos vertebrais e como etapa preliminar antes da irradiação das metástases ósseas por meio de aceleradores lineares. O protocolo preferido de irradiação consistia do IMRT (*Intensity Modulation Radiotherapy*), o qual possibilita redução de doses nos tecidos sadios (RYU, *et al.*, 2003); entretanto, envolvia maior custo de operação e maior complexidade de planejamento.

Em outros procedimentos, foi considerado o uso de radioisótopos como o Renio-186 e Estroncio-89 que inseridos por via intravenosa proporcionava uma deposição de dose absorvida abrangendo a estrutura óssea como um todo de forma ampla, porém alcançando um efeito clínico favorável à sintomatologia referente a redução de dor. Da mesma forma, o uso do cimento restaurador dos corpos vertebrais continua sendo utilizado para restauração da estrutura óssea (HIRSCH, MEDICH, ROSENSTEIN, MARTEL e HIRSCH, 2008). Em 1987, as técnicas *Vertebroplastia* e *Cifoplastia* foram introduzidas. Ambas fazem uso do cimento de restauração óssea avaliado clinicamente para regiões afetadas dos corpos vertebrais. É importante salientar que a possibilidade do uso do cimento ósseo foi introduzida por Harrington K.D. no início dos anos 80 (GALIBERT e DERAMOND, 1987) e (CARDOSO, *et al.*, 2009).

Os procedimentos de *Vertebroplastia* e *Cifoplastia* eram complementados à técnica de radioterapia IMRT para tratamento paliativo. Para reduzir os sintomas das metástases ósseas, no início dos anos 90 se propôs o uso de $^{153}\text{Sm-EDTMP}$ a nível sistêmico. Por sua vez, o uso de Sr-186 e Re-89 fornecidos por via intravenosa sistemicamente produziam um efeito tóxico com um alto comprometimento neurológico da medula por meio do efeito de desmielinização (HIRSCH, MEDICH, ROSENSTEIN, MARTEL e HIRSCH, 2008). Apesar de toda a pesquisa e investimento clínico, segue-se sendo um desafio a redução da dor óssea em situações clínicas de metástases na coluna vertebral (GERZTEN, 2007).

Em termos gerais, a presente tese aborda um tratamento que permite inserção no interior de um corpo ósseo, em especial do corpo da vertebra, da região torácica ou das extremidades, de um compósito cerâmico constituído de um radioisótopo emissor beta. Este incorpora-se a um cimento ósseo, de forma a depositar uma dose absorvida de radiação em condições suficientes e desejadas nas lesões metastáticas reproduzindo uma menor exposição dos tecidos sadios adjacentes, evitando assim possíveis procedimentos cirúrgicos altamente invasivos para o paciente (CAMPOS e MACEDO, 2010).

1.2. Justificativa

De acordo com dados estatísticos de câncer em escala global, providos pela *Globocan* 2012, no mundo adoecem cerca de 14 milhões de pessoas por câncer, sendo o câncer de mama, próstata e pulmão o responsável de cerca de 20% dos casos. Nosso país não é estranho a essa problemática e estima-se que cerca de 13 mil mulheres morreram de câncer de mama em 2010. Em décadas passadas o câncer de mama era a maior causa de mortalidade; e ainda hoje continua sendo o tipo de câncer que mais afeta à população feminina. As estatísticas mostraram que em 1986 quando se se constituiu o *Sistema Único de Saúde - SUS* no país, 12,8% das mulheres naquele ano morreram devido ao câncer, sendo que o câncer de mama foi a maior causa dessas mortes. Em 1998 o número total de casos de câncer de mama estava em 32 mil dos quais 6,6% de mulheres morreram no ano. Para o ano 2014, a região sudeste do país apresentou maior número de casos registrados por câncer seguido pela região Nordeste e Sul dos quais 60% das mortes aconteceram devido ao câncer de mama. Outros estudos mostram que os padrões mais comuns de

condições clínicas metastáticas são os viscerais (fígado, pulmão ou pleura e mama) (CECILIO, *et al.*, 2015).

Tendo em conta as considerações acima expostas, é importante o desenvolvimento de novos protocolos para equacionar a problemática que afeta à população de forma a expandir a ação do SUS nas diferentes regiões do país. Se o câncer de mama é um dos tipos de câncer que tem maior probabilidade de manifestar metástases tanto na região torácica como em outras regiões do corpo é preciso ampliar, melhorar e difundir novos métodos, técnicas e tratamentos que melhorem a qualidade de vida das pacientes e atinjam uma desejável remissão completa. Ainda nas regiões com menor concentração demográfica, os números de casos estão em menor proporção, mas seguem tendo um impacto elevado (CECILIO, *et al.*, 2015). Além disso, é indispensável o desenvolvimento e aplicação de

terapias que produzem um menor custo operacional, sejam minimamente invasivas de forma a reduzir o risco de infecções.

1.3. Sobre a Vertebroplastia

Deramond H. fez a descrição da técnica cirúrgica conhecida atualmente como *Vertebroplastia* (DERAMOND, DEPRIESTER, GALIBERT e LE GARS, 1998). Como o nome define, *Vertebroplastia* significa formato, modelagem (plastia) do corpo vertebral da coluna lombar. Esta técnica consiste em injetar o produto *Polimetilmetacrilato* (PMMA) no corpo da vertebra para recuperar a estrutura e a solidez do osso. Sua aplicação é indicada para osteoporose e em fraturas severas do corpo da vertebra, especificamente para um conjunto específico de vértebras da coluna vertebral (AMAR, *et al.*, 2001). O produto empregado na *Vertebroplastia* é o cimento acrílico PMMA, com adição de contraste radiológico. O produto usado para osteoporoses, sugerido por DERAMOND *et al.*, 1998, não é aplicado em ossos acometidos por metástases porque não atua na erradicação de células cancerosas (DERAMOND, DEPRIESTER, GALIBERT e LE GARS, 1998).

A *Vertebroplastia* é um procedimento minimamente invasivo usado para tratamentos de

patologias ósseas na ortopedia. O uso dos cimentos ósseos auxilia na cola de peças e estabilização da coluna vertebral. A *Cifoplastia* melhorou o procedimento da *Vertebroplastia* porque também restaura anatomicamente a peça óssea e sua funcionalidade, quando já colapsada, sendo que neste caso um balão infla internamente a estrutura colapsada antes da inserção do cimento. Assim, a *Vertebroplastia* se estabeleceu como uma técnica para atender pacientes com compromisso neurológico produzida pela compressão da medula espinhal.

1.4. Vertebroplastia e Oncologia

Não há indicação de aplicação da *Vertebroplastia* em corpos de vértebras com metástases que mantêm intacta sua estrutura óssea. Entretanto, é possível o uso de *Vertebroplastia* quando há fraturas severas induzidas pelo câncer. Quando estas ocorrem, podem levar ao aprofundamento do corpo da vértebra produzida pela invasão de células cancerosas. Neste caso, a *Vertebroplastia* é aplicada em vértebras que podem ou sofreram colapso com o comprometimento estrutural do corpo vertebral. Assim, a *Vertebroplastia*, ou a *Cifoplastia*, produz o restauro da estrutura vertebral colapsada, descomprimindo a medula (FOURNEY, *et al.*, 2003). Entretanto, de forma alguma tal técnica atua da erradicação das células cancerosas que agem no sítio vertebral. O calor gerado pela reação exotérmica do PMMA pode ser benéfico em esterilizar as ramificações nervosas internas, e conseqüentemente reduzir a dor, mas não é suficiente e demonstrável que possa erradicar células cancerosas.

Em verdade, a falha na *Vertebroplastia* aplicada em tumor da coluna vertebral colapsada tem sido um problema encontrado na clínica médica, por exemplo. A *Vertebroplastia* pode produzir resultados favoráveis nas primeiras semanas, entretanto com o tempo a condição clínica é deteriorada pela expansão das metástases. (VIRTO *et al.*, 2003; GUERRA, HERNÁNDEZ e SANTOS, 2010; PEÑA e VALLET-REGÍ, 2003)

Radiografias da coluna de um paciente, submetido a *Vertebroplastia* em condição de metástases e fratura severa, mostraram que a estrutura residual óssea após-*Vertebroplastia* apresenta inexistente e que o corpo da vértebra ficou resumido ao cimento acrílico

injetado. Na Figura 1.1(A) pode-se observar fratura na vértebra, induzida por metástases certificada por outras técnicas de diagnóstico. A Figura 1.1(B), mostra o status do corpo da vértebra após *Vertebroplastia*, com aumento da densidade radiográfica na periferia do corpo cimentício acrílico (PMMA) mostrando deslocamento de conteúdo interno para periferia entre o osso cortical e a superfície do bloco de cimento acrílico. Após 6 meses, Figura 1.1(C), pode-se identificar colapso da vértebra, e perda de estrutura óssea no entorno do cimento acrílico e regiões totalmente ausentes de osso estrutural (MACEDO, 2005).



(A)

(B)

(C)

Figura 1.1 Imagens radiográficas de corpo de vértebra com indicativo para *Vertebroplastia*, com metástases interna. (A) no diagnóstico – complementado com RMN e Cintilografia; (B) *Vertebroplastia* aplicada e teleterapia externa; (C) falha com colapsamento da vértebra. Fonte: (MACEDO, 2005)

Pode-se observar na Figura 1.1(B) que ao aplicar a *Vertebroplastia*, o conteúdo interno hidrofílico foi deslocado pelo cimento hidrofóbico para a periferia, que acelerou o processo de expansão tumoral e deterioração da estrutura óssea restante (MACEDO, 2005; WEILL, *et al.* 1996).

Ao injetar o PMMA, hidrofóbico, no interior da vértebra, este difunde pela estrutura fraturada ocupando o espaço que foi gerado pela expansão das células cancerosas no corpo da vértebra. Por ser hidrofóbico e aplicado em um tempo curto, não há a possibilidade do composto hidrofóbico se misturar à solução aquosa e celular presente no corpo vertebral. O conteúdo canceroso então é deslocado com a infusão do composto hidrofóbico para sua periferia. Parte pode ser removida com uma segunda cânula de descompressão (técnica

empregada atualmente), mas grande quantidade de células é deslocada para a periferia do corpo restante da vértebra e permanece *in situ*. Durante a pega (endurecimento), reações exotérmicas não controláveis podem ajudar em atenuar as células, mas não eliminam as invasões cancerosas. As temperaturas de pico, da reação exotérmica, dependem da quantidade de massa injetada, do tempo de pega do acrílico, e se reduz com a distância do centro da fonte, não sendo constante e suficientemente superior a 45 °C na periferia por tempo longo o suficiente para esterilização. (HOSONO *et al.*, 1995) Desta forma, após algum tempo, as células em seu novo ambiente, através de seu processo mitótico expansionista, desenvolvem angiogênese e continuam a evoluir microfraturando a estrutura óssea restante da periferia. Células *osteoclásticas* e *osteoblásticas* misturadas perderam a homeostase quando o osso foi comprimido e fraturado, e o balanço pode favorecer a absorção óssea pelas células *osteoclásticas*. Então, a compressão faz com que os *osteoclastos* consumam o osso. As próprias células cancerosas podem também encontrar em tais resíduos o nutriente favorável a sua evolução (DALBY, *et al.* 2002).

1.5. A Vertebroplastia e a Radioterapia

A *Vertebroplastia* é aplicada em fraturas extensas para dar sustentação mecânica e reduzir a dor induzida pela fratura. Por sua vez, as vértebras acometidas de metástases podem colapsar e produzir fraturas severas. A *Vertebroplastia* pode ser empregada para recuperar a estrutura da vertebra, ou através do PMMA acrílico direto ou em um balão expander definido pela *Cifoplastia* (KLIMO e SCHMIDT, 2004). Neste caso específico, o dano estrutural da vertebra ocorreu devido ao câncer, e a *Vertebroplastia* deve ser seguida pela radioterapia para casos específicos.

A *Vertebroplastia* e a radioterapia são conceitos e técnicas distintas. Na Figura 1.2 pode-se observar o protocolo clínico da teleterapia de megavoltagem na irradiação do corpo da vértebra (CASTRO *et al.*, 2002). No caso, não se irradia uma única vértebra, mas um campo que incorpora uma porção da coluna vertebral com o envolvimento do corpo da vértebra e da medula espinhal, bem como as grandes artérias que cruzam a região (KLIMO e SCHMIDT, 2004). Há sequelas graves agudas e tardias associadas a irradiação de parcela da coluna vertebral. As tardias podem levar o paciente a paralisia dos membros. Entretanto, possivelmente aceitável pela curta expectativa de vida do paciente oncológico. No caso,

utiliza-se duas ou três janelas transversais que são combinadas para expor a vértebra às doses clínicas, em regime fracionado. O PMMA com bário, injetado na *Vertebroplastia*, é um forte atenuador de raios X, e conseqüentemente altera a distribuição das doses absorvidas no campo de irradiação devido à forte heterogeneidade presente (no range da imagem). O cimento contrastado absorve e faz sombreamento da dose faceando a superfície do bloco cimentício e a interface com sítio metastático. Efeitos de heterogeneidade, produzida pela composição do cimento no corpo da vértebra, muitas vezes não são levados em consideração na dosimetria (TURNER, *et al.* 2008).

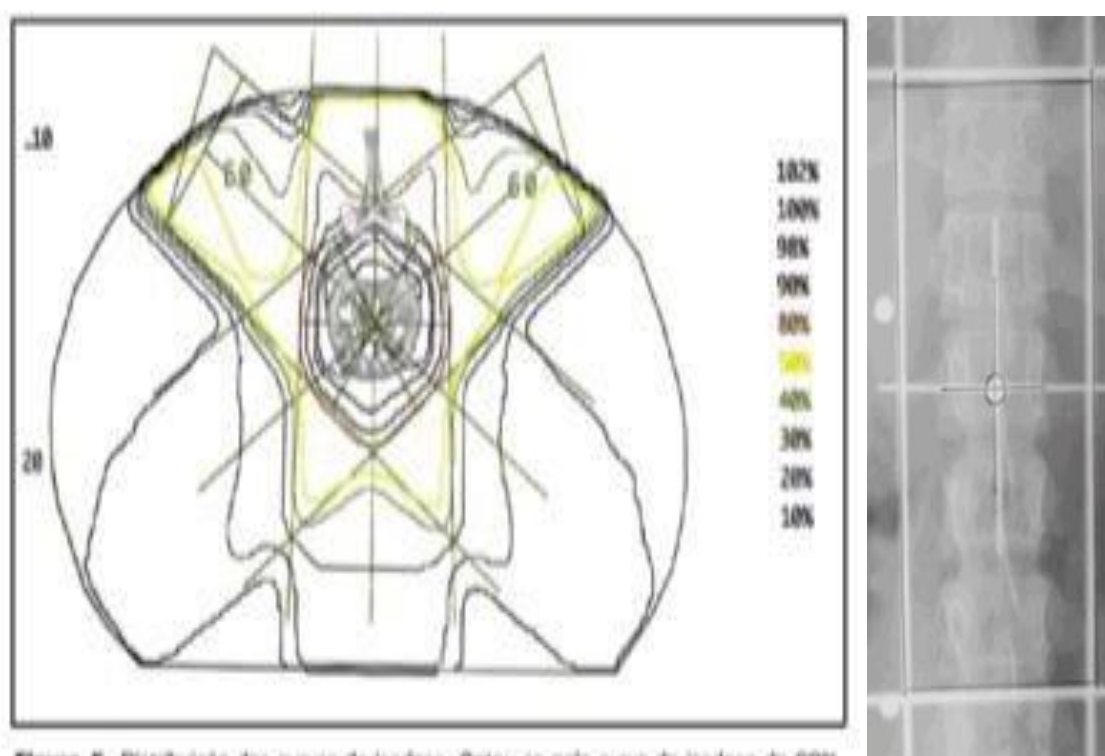


Figura 1.2 Distribuição de isodoses produzidas por três campos de irradiação, proposto no planejamento radioterápico, e dimensões do campo externo centrado na vértebra alvo FONTE: (CASTRO, *et al.* 2002) <http://dx.doi.org/10.1590/S0100-39842002000300010>

A Figura 1.2 e Figura 1.3 ilustram padrões de irradiação do corpo da vértebra com metástases, em situação clínica específica. Em radioterapia de corpo da vértebra, a radiação expõe a coluna vertebral a altas doses absorvidas (KLIMO e SCHMIDT, 2004). O efeito tardio da radioterapia de coluna é a *Mielopatia* que pode se desenvolver após radioterapia para tumores perto ou na coluna vertebral. Essa doença provoca fraqueza,

perda de sensibilidade e leva a síndrome de Brown-Séquard. Nessa síndrome, um lado da medula espinhal fica lesionada, originando fraqueza no corpo e perda da sensibilidade à dor e à temperatura. O paciente pode perder a habilidade de saber a posição das mãos e dos pés, perdendo a capacidade de se mover com coordenação (KLIMO e SCHMIDT, 2004). A *Mielopatia* por radiação do tipo tardio não se pode ser recuperada, e usualmente leva a uma paralisia (RYU *et al.*, 2007). A possibilidade de uso de irradiação da coluna vertebral, com possibilidade de efeitos tardios, está na maior probabilidade de óbito antes do aparecimento de efeitos tardios associados a medula.

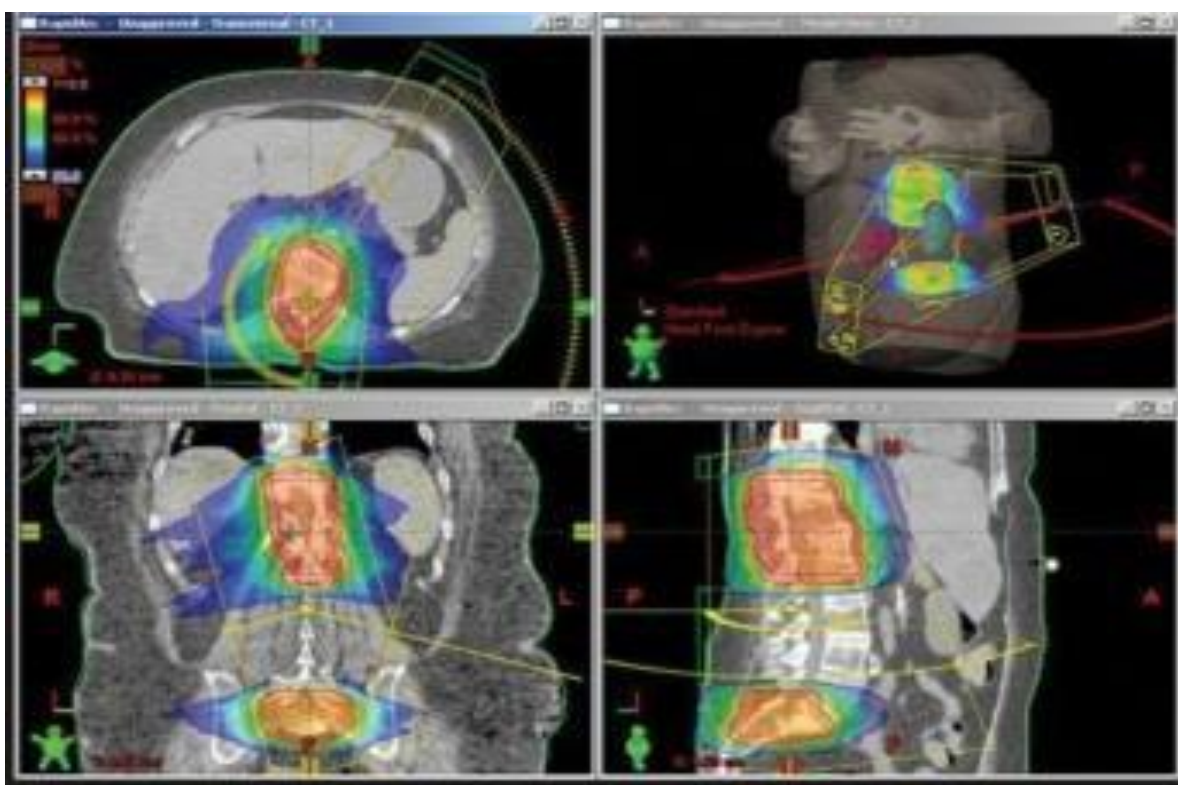


Figura 1.3 Imagem do planejamento de radioterapia de corpo vertebral, como modelo padrão ouro em radioterapia.

1.6. Novo material e suas perspectivas

Questiona-se o que pode ser empregado para combater células metastáticas deslocadas para a periferia do cimento acrílico, na interface osso residual - superfície aleatória difusa do PMMA. A solução pode estar em um cimento completo, com diversos agregados, como Hidroxiapatita, onde um constituinte radioativo deve ser incorporado à estrutura cristalina da Hidroxiapatita (CAMPOS e MACEDO, 2006; KANCKO, *et al.*, 2010). Assim,

independente da forma difusa que o cimento assume ao ser injetado e difundido na estrutura fraturada, sua superfície aleatória tomada será radioativa emissora de partículas betas de curto alcance. Neste caso, exatamente na superfície onde células cancerosas foram deslocadas e promovem angiogênese, há uma alta exposição à radiação, confinada pelo curto alcance das partículas nucleares na estrutura. Esta foi a proposta apresentada pelo grupo de pesquisa *NRI-Núcleo de Radiações Ionizantes da UFMG* (MACEDO, 2005; CAMPOS e MACEDO, 2006).

Um cimento radioativo ósseo tem condição de resolver a eliminação das células residuais cancerosas, deslocadas pelo cimento PMMA empregado pela *Vertebroplastia*, cuja técnica provocou o acúmulo destes depósitos residuais cancerosos na periferia da interface cimento acrílico – corpo cortical (MACEDO, 2005; DONANZAM *et al*, 2013). Além disso, o cimento ósseo radioativo não induz heterogeneidade da dose e expõe o entorno de sua borda com dose homogênea. A teleterapia de megavoltagem passa a ser coadjuvante após a aplicação do cimento radioativo ósseo com reduzida dose na medula; e, as doses no corpo da vértebra passam a ser elevadas e curativas.

O cimento radioativo pode ser aplicado em uma única seção. O decaimento do radioisótopo é de meia vida curta como Sm-153 (46h), Ho-166 (27h) ou Y-90(64h), e deposita toda a dose em um período de seis meias vidas. É de se esperar diferenças significativas das consequências clínicas da aplicação da técnica de teleterapia megavoltagem em relação aplicação do produto definido pelo NRI.

O cimento ósseo radioativo poderá ser aplicado em situações clínicas de metástases, exclusivamente, sendo totalmente inapropriado para a osteoporose onde a *Vertebroplastia* com cimento acrílico tem indicação. O produto pode ser aplicado mesmo onde a estrutura óssea não tenha grandes fraturas, ou que a coluna não esteja comprimida, ou que o corpo da vertebra não esteja colapsado, ou que a função não seja a recuperação da estrutura óssea. Fora das indicações da *Vertebroplastia*, o cimento radioativo pode ser aplicado em toda a estrutura óssea, independente das dimensões das trabéculas ósseas (CARDOSO *et al*, 2009; DOROZHKIN, 2009).

O procedimento favorável produzido pelo cimento ósseo radioativo proposto, agora não mais ficou restrito à vértebra, e não exatamente a *Vertebroplastia*, e pode ser aplicado aos diversos corpos ósseos, incluindo áreas muito sensíveis como as costelas, quando há metástases e infiltrações de câncer de mama, mesmo na periferia do pulmão. Por exemplo, pode ser aplicado em metástases na calota craniana, mesmo a alguns milímetros do córtex cerebral do paciente, sem perspectiva de dano algum neurológico.

1.7. Constituição do cimento ósseo radioativo

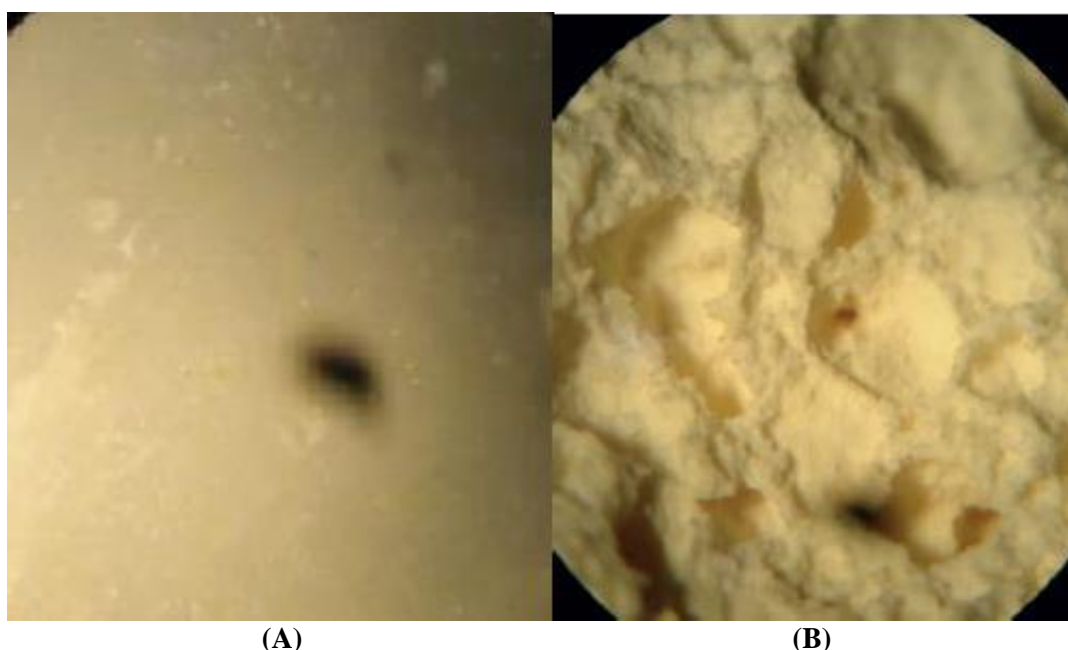


Figura 1.4 Imagens estereoscópicas (x80) do cimento radioativo ósseo, frio, após preparo e pega, com razão de concentração entre Polimetilmetacrilato e Hidroxiapatita, incorporando Ho-165 em sua matriz de Ca e P, de 1:0,01 e 0.1:1, isto é, de 100x para 0,1x. Fonte: acervo do autor.

A Figura 1.4 apresenta imagens estereoscópicas do cimento radioativo ósseo preparado com razões de proporcionalidades em peso extremas, isto é, com mínima quantidade de HAp (máximo PMMA) para a Figura 1.4(A), e de máxima quantidade de HAp (mínimo PMMA) para a Figura 1.4(B) (PEÑA e VALLET- REGÍ, 2003). Foi observado que em ambas as situações, que os compostos puderam ser misturados e ocorreu pega. A fluidez do composto é maior se PMMA é maior, e menor se a concentração de HAp é maior. Entretanto ambos são de interesse e tem praticidade e aplicabilidade. Em volumes grandes, ou em cavidades ósseas, como nasofaringe, fêmur, ou em cirurgias ortopédicas abertas é

possível aplicar ou depositar cimento ósseo radioativo com máxima proporção de HAp; enquanto, para ossos muito finos, como costelas, ossos da mão e pé, é necessária uma concentração de HAp muito baixa (DOROZHKIN, 2009).

Assim a razão de proporcionalidade entre o ligante e o agregado é assintoticamente representada por 1:0, e 0:1. Obviamente 0 (nulo) não é assumido porque foge ao escopo de um cimento por não haver HAp incorporando radioisótopo; ou apenas HAp sem ligante.

1.8. Ativação do cimento ósseo

A quantidade de atividade preconizada no agregado também depende da ativação neutrônica em reatores. O compósito cimento ósseo radioativo pode ser aplicado em diversas cavidades, estruturas trabeculares, em condição de metástases ou em infiltrações tumores que evoluem para as cavidades ósseas. Os volumes são amplos, e a expectativa de aplicação do cimento radioativo é da ordem de 10^{-6} g a 300 gramas, ou mais, dependendo da anatomia desenvolvida pela presença do tumor ou metástases.

Em relação a atividade, a ativação neutrônica depende das seções de choque de nêutrons da material base, constituído de C, H, Ca, P e do metal M, por exemplo samário. O Sm tem seção de choque de absorção de nêutrons de 40.000 b ($b=10^{-24}$ cm²), enquanto o fósforo (P) tem seção de choque de 10^{-3} b, e Ca variando conforme o isótopo chega a 0,1b, baixo o suficiente tal que qualquer contaminação radioisotópica seja aceitável (HIRSCH, MEDICH, ROSENSTEIN, MARTEL e HIRSCH, 2008). Com seções de choque tão altas do radionuclídeo, atividades de Bq a dezenas de MBq podem ser produzidas. A ativação dependerá do fluxo de nêutrons do reator, da massa do composto, do volume, das seções de choque e do tempo de irradiação. A formação matemática para equacionar a atividade pode ser obtida na literatura (DONANZAM, CAMPOS, DALMÁZIO e VALENTE, 2013). Mesmo em massas de agregados (HAp) muito menores na ordem de microgramas, ou na ordem de dezenas de gramas, é possível ativar o composto o suficiente para produzir uma eliminação das células cancerosas a 1-2 mm da superfície do bloco do cimento ósseo radioativo, após pega *in-situ*.

Observe que a deposição de energia é inversamente proporcional à distância ao

quadrado da fonte radioativa ($1/r^2$). As múltiplas emissões de raios betas dos radionuclídeos inseridos na HAp produzem para cada decaimento energia na ordem 1 a 1.8 MeV (dependendo do radionuclídeo escolhido), que são depositadas em uma massa reduzida, equivalente ao volume de 1-3 mm no entorno do cimento radioativo. A razão entre energia depositada e massa fornece o conceito de dose absorvida ($Gy = J/kg$). Conseqüentemente há a expectativa de que a dose absorvida no entorno do cimento ósseo seja muito elevada, porque a energia (J) é alta e a massa (kg) é muito pequena. A massa é limitada devido ao percurso reduzido das betas emitidas pelo radionuclídeos no cimento. Assim, doses clínicas de 20 a 140 Gy são facilmente obtidos com baixas atividades do cimento radioativo. (SILVEIRA, 2007; DONANZAM, CAMPOS, DALMÁZIO, *et al.*, 2013). Haverá sempre uma proporção de agregado e ligante, uma atividade e uma massa que atente a uma dose absorvida que possa eliminar as células cancerosas na periferia do bloco solidificado do cimento ósseo radioativo.

1.9. Dosimetria no cimento ósseo radioativo

A prescrição de uma dose clínica no corpo da vértebra, em fração única ou fracionada, para eliminar células metastáticas depende da dose de tolerância dos tecidos sadios adjacentes. Estes valores são definidos para que em cada caso clínico, as doses versus volume ($D \times V$) no tecido normal adjacente não atinja limites críticos, na qual os efeitos agudos e tardios sejam incontroláveis. O limite da dose no tumor depende então não exatamente da dose no volume tumoral, mas a dose no tecido adjacente. Para cada situação clínica há limites de dose e volumes aplicados nos tecidos adjacentes dependendo da posição da fonte, do espectro energético, dos tipos de tecidos, da Radiobiologia destes e da organização das células presentes (VAN DER LINDEN *et al.*, 2005).

A distribuição da irradiação produzida pelo cimento ósseo radioativo pode ser vista em imagem apresentada na Figura 1.5. Observe que a mesma continua no corpo da vértebra, e então não produz efeitos tardios e não leva o paciente a paralisia (DONANZAM, CAMPOS, DALMÁZIO *et al.*, 2013). Assim, há marcante diferença entre a aplicação da *Vertebroplastia* com cimento acrílico, seguindo da teleterapia que na aplicação do produto proposto: cimento ósseo radioativo.

No caso clínico do cimento ósseo radioativo, a possibilidade de anular a dose a alguns milímetros da fonte, evitando a irradiação dos órgãos vitais adjacentes, ultrapassa as expectativas da teleterapia de megavoltagem. Assim, ainda não há estudos de limites de atividade para que produzam uma dose preconizada no emprego do cimento ósseo radioativo.

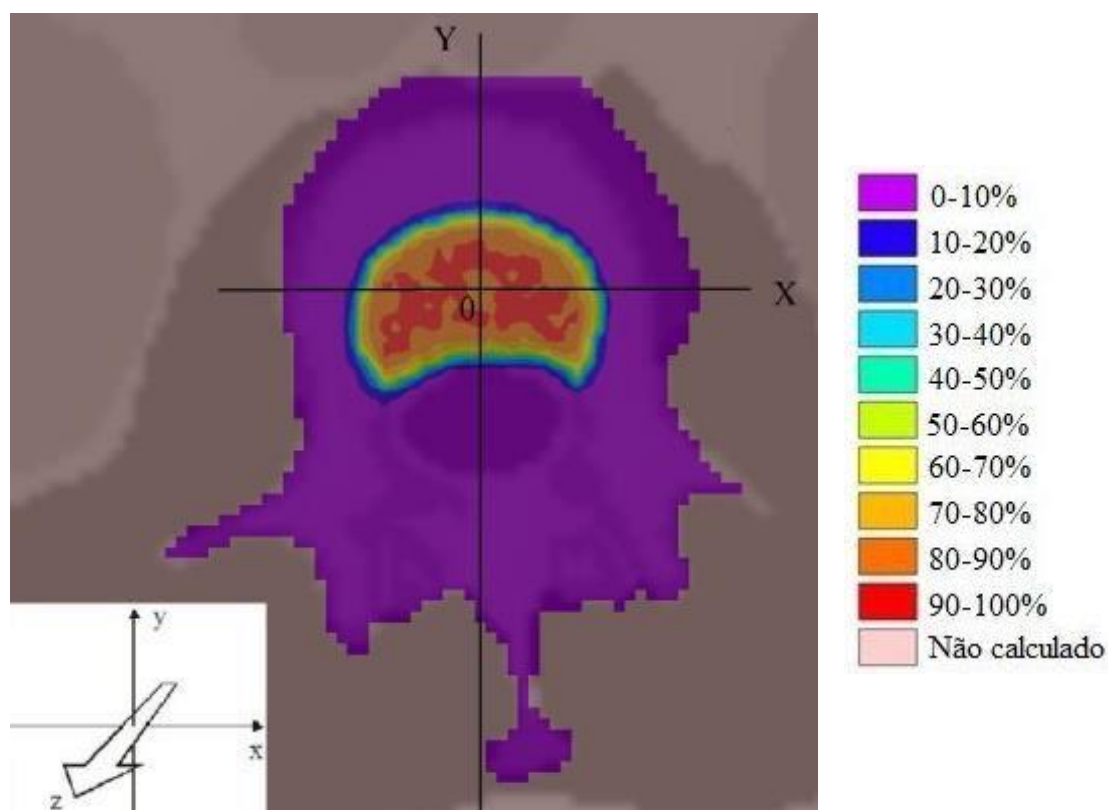


Figura 1.5 Distribuição de dose produzida pelo cimento ósseo radioativo posicionado ao lado da coluna vertebral(DONANZAM B. A., 2012).

Nesse modelo de fantoma de vértebra, elaborado computacionalmente nos códigos MCNP5 e SISCODES, o cimento radioativo acoplado com ^{166}Ho apresenta um melhor desempenho terapêutico em razão da diminuição da dose na medula espinhal em comparação com protocolo de RT megavoltagem, como apresentado na Figura 1.5 (DONANZAM, 2012). A simulação foi feita considerando 1 mg do cimento com uma atividade específica de 32,5 MBq de ^{166}Ho e para obter uma BED no tumor de 72 Gy é necessário que o cimento de ^{166}Ho alcance uma atividade específica de 24,9 MBq.

A Tabela 1.1 resume comparativamente as vantagens dosimétricas do uso do cimento radioativo, já que teoricamente a dose na medula espinhal é 10 vezes menor em comparação com a radioterapia de megavoltagem externa garantindo uma redução de dose na medula e diminuindo o comprometimento neurológico. Também é relativamente fácil observar que o fracionamento no caso da terapia com a *Radiovertebroplastia* acontece em um período de 7 dias, o que tecnicamente nos termos dosimétricos corresponderia a um tratamento hipofracionado.

Tabela 1.1 Doses e BED para diferentes técnicas de radioterapia e ^{166}Ho Radiovertebroplastia.

Tipo de radioterapia	Dose vert (Gy)	Fr/dose (Gy)	BED vert (Gy10)	Dose medesp (Gy)	BED medesp (Gy2)
Convencional	60,0	30x 2,0	72,0	60,0	120,0
RTE met. Vertebral	30,0	10x 3,0	39,0	30,0	75,0
RC met. Vertebral	16,0	1x 16,0	41,6	10,0	60,0
^{166}Ho RVT/ 32,5MBq	72,8	até 7d	102,0	6,4	7,5
^{166}Ho RVT/24,9MBq	55,6	até 7d	72,0	4,9	5,5

Legenda: Radiovertebroplastia = RVT; Radiocirurgia = RC; Radioterapia megavoltagem externa = RTE; Fracionamento = Fr; medula espinhal = medesp.; vertebra = vert.; metástases = met.

1.10. Considerações

Pesquisas em situações clínicas oncológicas de pacientes com metástases ósseas ainda continuam sendo necessárias no intuito de melhorar a resposta dos cuidados paliativos. Embora o uso de medicamentos para tratar a dor torna-se eficaz, as terapias de radiação são usualmente aplicadas devido a disponibilidade dos recursos e a presença de uma resposta paliativa favorável. No caso dos pacientes oncológicos, com metástases ósseas no corpo da vértebra, terapias de radiação otimizadas por procedimentos como IMRT e ^{153}Sm -EDTMP (*ethylene diamine tetramethylene phosphonate*) injetado na forma sistêmica têm ampliado a resposta clínica ao tratamento.

Nossa proposta de um cimento ósseo radioativo tem mostrado vantagens significativas em termos dosimétricos. Entretanto, o produto carece de avaliação clínica. Pesquisas atuais no grupo do NRI abordam a otimização dos componentes do cimento para aumento da bioatividade, diminuição da citotoxicidade e ampliação da produção de poros para melhorar a osteocondutividade e a adesão do complexo celular nos tecidos ósseos. As metástases ósseas induzem a transtornos fisiológicos, imunológicos, estruturais e neurológicos, *in situ*. Uma possibilidade apresentada é a radioterapia produzida pelos radioisótopos incorporados na HAp do cimento ósseo radioativo, estabelecido *in situ*. Posterior a total deposição da energia ionizante, um cimento com características do tecido trabécular pode auxiliar na recuperação da homeostase das células ósseas naturais, podendo auxiliar no processo de restauração natural dos ossos deteriorados. Além disso, a incorporação de possíveis componentes bioquímicos de sinalização que permitam corrigir o desbalanço celular do osso podem ser também fonte de pesquisa.

1.11. Referências

- AMAR, A. P., LARSEN, D. W., ESNAASHARI, N. N., ALBUQUERQUE, F. C., LAVINE, S. D., & TEITELBAUM, G. P. (2001, November). Percutaneous Transpedicular Polymethylmethacrylate Vertebroplasty for the Treatment of Spinal Compression Fractures. *Neurosurgery*, 49(5), 1105-1115.
- CARDOSO, E. R., ASHAMALLA, H., WENG, L., MOKHTAR, B., ALI, S., MACEDON, M., & GUIRGUIS, A. (2009). Percutaneous tumor curettage and interstitial delivery of Samarium-153 coupled with kyphoplasty for treatment of vertebral metastases. *J Neurosurg Spine*, 10, 336-342.
- CASTRO, D. G., LIMA, R. P., MAIA, M. C., NOVAES, P. R., FOGAROLI, R. C., FERRIGNO, R., SALVAJOLI, J. V. (2002). Hemangioma vertebral sintomático tratado com radioterapia exclusiva - relato de caso e revisão da literatura. *Radiologia Brasileira*, 35(3), 179-181.
- CECILIO, A. P., TAKAKURA, E. T., JUMES, J. J., DOS SANTOS, J. W., HERRERA, A. C., & VICTORINO, V. J. (2015). Breast cancer in Brazil: epidemiology and treatment challenges. *Breast Cancer: targets and therapy*, 7, 43-49.
- DALBY, M. J., DI SILVIO, L., HARPER, E., & BONFIELD, W. (2002). Increasing

- hydroxyapatite incorporation into poly(methylmetacrylate) cement increases osteoblast adhesion and response. *Biomaterials*, 23, 569-576.
- DERAMOND, H., DEPRIESTER, C., GALIBERT, P., & LE GARS, D. (1998). Percutaneous vertebroplasty with polymethylmetacrylate, technique, indications and results. *RADIOLOGIC CLINICS OF NORTH AMERICA*, 36, 533-546.
- DONANZAM, B. A. (2012). *Biocerâmicas com Ho-166 e Sm-153: síntese, caracterização e avaliação dosimétrica em Radiovertebroplastia* (Vol. Dissertação). (U. F. Gerais, Ed.) Belo Horizonte, Minas Gerais, Brasil: UFMG.
- DONANZAM, B. A., CAMPOS, T. P., DALMÁZIO, I., & VALENTE, E. S. (2013). Synthesis and characterization of calcium phosphate loaded with Ho-166 and Sm-153: a novel biomaterial for treatment of spine metastases. *J Mater Sci: Mater Med*, 24, 2873-2880.
- DOROZHKIN, S. V. (2009). Calcium orthophosphates in nature, biology and medicine. *Materials*, 2, 399-498. doi:10.3390/ma2020399
- FINLAY, I. G., MASON, M. D., & SHELLEY, M. (2005). Radioisotopes for the palliation of metastatic bone cancer: a systematic review. *Lancet Oncol*, 6, 392-400.
- FOURNEY, D. R., SCHOMER, D. F., NADER, R., CHLAN-FOURNEY, J., SUKI, D., AHRAR, K., GOKASLAN, Z. L. (2003). Percutaneous vertebroplasty and kyphoplasty for painful vertebral body fractures in cancer patients. *J Neurosurgery (Spine 1)*, 98, 21-30.
- GALIBERT, P., & DERAMOND, H. (1987). Note préliminaire sur le traitement des angiomes vertébraux par vertébroplastie acrylique percutanée. *Neurochirurgie*, 33, 166-167.
- GEORGY, B. A. (2008). Metastatic spinal Lesions: State of the art treatment options and future trends. *AJNR Am. J. Neuroradiol.*, 29, 1605-1611.
- GERZTEN, P. (2007). The role of minimally invasive techniques in the management of spine tumors: percutaneous bone cement augmentation, radiosurgery, and microendoscopic approaches. *Orthop. Clin. N. Am.*, 38, 441-450.
- GUERRA, N. B., HERNÁNDEZ, M. L., & SANTOS, R. G. (2010). Cementos Oseos Acrílicos Modificados con Hidroxiapatita/Acetato de Vinilo. Caracterización Mecánica, Termoanálisis y Bioactividad In Vitro. *Polímeros*, 20(2), 98-106.
- HARRINGTON, K. D. (1981). The use of methylmetacrylate for vertebral-body

- replacement and anterior stabilization of pathological fracture-dislocations of the spine due to metastatic malignant disease. *J. Bone Surg. Am.*, 63, 36-46.
- HIRSCH, A. E., MEDICH, D. C., ROSENSTEIN, B. S., MARTEL, C. B., & HIRSCH, J. A. (2008). Radioisotopes and vertebral augmentation: dosimetric analysis of a novel approach for the treatment malignant compression fractures. *Radioisotope dosimetry*, 87, 119-126.
- HORN, E., HENN, J., & LEMOLE, J. (2004). Thoracoscopic placement of dural-rod instrumentation in thoracic spinal trauma. *Neurosurgery*, 11, 1150-1154.
- HOSONO, N., YONENOBU, K., FUJI, T., EBARA, S., YAMASHITA, K., & ONO, K. (1995). Orthopedic Management of Spinal Metastases. *Clin Orthop Relat Res.*, 312, 148-159.
- KANCKO, T. S., SCHGAL, V., SKINNER, H. B., AL-GHAZI, M. A., RAMISINGHANI, N. S., & KEYAK, J. H. (2010). Evaluation of a radiation transport modeling method for radioactive bone cement. *Phys Med Biol*, 55, 2451-2463.
- KLIMO, P., & SCHMIDT, J. H. (2004). Surgical Management of Spinal Metastases. *The Oncologist*, 9, 188-196.
- MACEDO, R. D. (2005). *Radiovertebroplastia para tratamento de neoplasias malignas ósseas da coluna vertebral: avaliação da proposta e da viabilidade*. (Dissertação). Belo Horizonte - Brasil: UFMG.
- PEÑA, J., & VALLET-REGÍ, M. (2003). Hydroxyapatite, tricalcium phosphate and biphasic materials prepared by a liquid mix technique. *Journal of the European Ceramic Society*, 23, 1687-1696.
- RYU, S., JIN, J.-Y., JIN, R., ROCK, J., AJLOUNI, M., MOVSAS, B., KIM, J. (2007). Partial volume tolerance of the spinal cord and complications of single-dose radiosurgery. *Cancer*, 109(3), 628-636.
- RYU, S., YIN, F., ROCK, J., ZHU, J., CHU, A., & KAGAN, E. (2003). Image-guided and intensity-modulated radiosurgery for patients with spinal metastasis. *Cancer*, 97(8), 2013-2018.
- SILVEIRA, M. F. (2007). *Estudos para a viabilidade da técnica de radioosteoplastia através de simulações computacionais radiodosimétrica e de aplicações experimentais em ossos animais in vitro* (Dissertação). (UFMG, Ed.) Belo Horizonte, Minas Gerais, Brasil: UFMG.

- TURNER, T. M., URBAN, R. M., SINGH, K., HALL, D. J., RENNER, S. M., LIM, T.-H., AN, H. S. (2008). Vertebroplasty comparing injectable calcium phosphate cement compared with polymethylmetacrylate in a unique canine vertebral body large effect model. *The spine journal*, 8, 482-487.
- VAN DER LINDEN, Y. M., DIJKSTRA, S. D., VONK, E. A., MARIJNEN, C. M., & LEER, J. W. (January de 2005). Prediction of survival in patients with metastases in the spinal column. *Cancer*, 103(2), 320-328.
- VIRTO, M. R., FRUTOS, P., TORRADO, S., & FRUTOS, G. (2003). Gentamicin release from modified acrylic bone cements with lactose and hydroxypropylmethylcellulose. *Biomaterials*, 24, 79-87.
- WEILL, A., CHIRAS, J., SIMON, J., ROSE, M., SOLA-MARTÍNEZ, T., & ENKAOUA, E. (1996). Spinal Metastases: Indications for and Results of Percutaneous Injection of Acrylic Surgical Cement. *Radiology*, 199(1), 241-247

CAPÍTULO 2

2. Radioactive cement of PMMA and HAp-¹⁵³Sm, ¹⁶⁶Ho, or ¹⁸⁸Re for bone metastasis treatment.

ABSTRACT

Polymethylmetacrylate (PMMA) is a compound used in the industry and since the 80's was also been employed in dental and biomedical areas as a constituent of bone cements. The hydroxyapatite (HAp) is a bioceramic produced naturally in the bones. These two components are fundamental constituents in the preparation of bone cements. The artificial synthesis of HAp's can be made by sol-gel method. The biofosfanates has also been used in dental implants and nuclear medicine, as radiopharmaceutical or palliative systemic treatment of pain reduction in bone metastasis with ¹⁵³Sm-EDTMP. The vertebroplasty and cifoplastia are techniques used in orthopedics based on bone cement, being minimally invasive procedures with low-risk of infections, applied in osteoporosis and fractures of high impact. Recently, the NRI – Núcleo de Radiações Ionizantes at UFMG proposed a composite of M- HAp with a metallic nuclide M embedded in HAp matrix. After irradiated, M-HAP is added to PMMA compounding a radioactive bone cement that can retrieve the bone body stabilization, pasting microfractures, recomposing the anatomy and the functionality of the affected parts by the compression of the bone metastases, with possible reduction of pain by quickly radiation-induced decompression. Computational dosimetric models, synthesis and characterization of these bioceramics incorporating Re-188, Ho-166 or Sm-153 have pointed out benefits that may become a promising of an alternative to conventional radiotherapies, mainly because it holds the absorbed dose in bone structure sparing health tissue, as example in the body of the vertebra saving the spinal cord. This article presents a review on this topic.

Keywords: Radioactive bone cement, PMMA, HAp, Vertebroplasty, Kyphoplasty, Radioisotopes.

2.1. Introduction

At the present time, there are few clinical procedures to meet the countless cases of cancer in advanced stages with confirmed and widespread metastases. These represent critical clinical situations where the disease spreads from *in situ* for loco-regional sites, toward the entire human body, becoming systemic and affecting organs and skeleton. At that stage, medical science does not bring hope to the patients, and death can happen weeks or months after confirmed a diagnosis of disseminated metastasis, as a consequence of the morbidity of this disease. Bone involvement by micro tumors produces trauma that generate huge intensity of pain. In most cases the pain is severe due to several secondary metastatic processes produced by the micro-fractures in the bone structure, being recommended by clinical staff introducing palliative measures for pain reduction. In this clinical picture, it is understandable that the disease has already progressed to a stage of irreversibility and it is not likely a full recovery of the patient. Morphine is of the common use, among other medications; even if such drug doesn't act on recovering induced compression fractures produced by cancerous tumors metastatic (HORN, HENN, & LEMOLE, 2004).

There are possible interventions by the radiation therapy (RT), chemotherapy or surgical procedures. Although there is a great limitation of beam portals and of bone target volume at RT. Teletherapy brings deleterious effects because it is inevitable the exposition of other vital organs or regions of the body to ionizing radiation; especially considering the clinical condition and the patient's weakened immune system.

In the 80th, Harrington K.D. proposed the use of polymerized methyl methacrylate for stabilization of vertebral bodies with fractures or dislocations induced by bone metastases. Metastasis induces an increase in the internal pressure of the vertebral body and compromise the patient care (HARRINGTON, 1981). A solution was presented for pain reduction but the exothermal effects provided by the polymerization of methyl methacrylate became a part of the side effects of the procedure (HARRINGTON, 1981; GEORGY, 2008). In accordance to Harrington, on the post-surgery of 13 to 14 patients, an improvement in pain was observed with the stabilization of the spine with the use of methyl methacrylate. However, external radiation therapy was held in addition. The source of radiation was external to the body and the restorative cement was used only to improve

stability of the vertebral body. The clinical benefits with the use of PMMA extended from 13 to 45 months the postoperative procedure. In the 90th, this cement was used as a mechanism for the stabilization of the vertebral bodies. In cases of bone metastasis, the irradiation therapy provided by linear accelerators complements the treatment using Intensity Modulation Radiation Therapy (IMRT). IMRT proposes dose reduction in adjacent tissues (RYU, *et al.*, 2003); however, it involves greater complexity including multiple fields to limit the prescribed dose at the target volume. In other procedures, the use of radioisotopes as Rhenium-186 or Stroncium-89, were considered with intravenous application providing an imparted absorbed dose in bone structure covering a broader systemic distribution, but with a clinical effect in favor of pain reduction. However, the restorative cement of the vertebral bodies was still the option held (HIRSCH, ROSENSTEIN, MEDICH, MARTEL, & HIRSCH, 2009).

In 1987, the vertebroplasty and kyphoplasty were introduced. Those techniques considered using the restore bone cement based on the volume of the affected vertebral bodies and the metastasis-type classification, well documented in the literature. It is worth mention that Harrington K.D introduced this classification in the early 80's (GALIBERT & DERAMOND, 1987; CARDOSO, *et al.*, 2009).

Equal to the palliative IMRT, the association of radiation therapy with vertebroplasty or kyphoplasty procedures had the goal of reducing the symptoms of the bone metastases. In the early 90th, the Sm-153-EDTMP systemic therapy was investigated. The intravenous use of Sr-89 and Re-186 produced a toxic effect holding high spinal cord neurological deficits due to an effect of demyelination (VIÑA, 2005).

In 2006, a new material was introduced by the NRI research group-*Núcleo de Radiações Ionizantes* at UFMG, namely Radioactive Bone Composite including polymethylmethacrylate (PMMA) and an aggregate of hydroxyapatite incorporating a radioactive metal in its structure (CAMPOS PI 0605721-7 A2, 2006; DONANZAM, CAMPOS, DALMÁZIO, & VALENTE, 2013; DONANZAM B. A., 2012; MACEDO, 2005). Despite all the research and investment in the radioactive cement in the NRI/UFMG, it is being a challenge the improvement of biocomposite affinity on the bone structure, the expansion of the absorbed dose distribution in situ, and the generation of

knowledge in the properties of the radioactive cement and its interactions with the metastasis-bone interface.

The present review addresses these issues and describes this possible radiotherapeutic treatment represented by the interstitial insertion of an amount of radioactive cement within a bone structure, in particular in the thoracic vertebrae body. The cement contains a ceramic composite that maintains a radioisotope beta-emitter inserted into its amorphous structure. It can hold a spatial distribution such that ionizing radiation is spread and absorbed into the desired metastatic lesions, preserving the healthy adjacent tissues, avoiding possible invasive surgical procedures, and reducing indiscriminate radiation exposures (GERSZTEN, 2007).

2.2. Some cancer epidemiological data in Brazil

Cancer data on a global scale, according to *Globocan 2018*, report that in the world about of 18 million people per year get sick because of cancer, holding the larger impact on women with breast cancer (24.2%), colon and rectum (9.5%), lung (8.4%), uteri cervix (6.6%); and, on men, with prostate (13.5%), colon and rectum (10.0%), liver (6.3%), lung (14.5%), stomach (7.2%); among others (SCHILITZ, DE LIMA, ANDRADE, OLIVEIRA, & SANTOS, 2015). Our country is no stranger to this problem since the incidence of breast cancer has reached 29.5%, with 59,700 new cases in 2018-2019 (FERLAY, SOERJOTAMARAM, ERVIK, FORMAN, & BRAY, 2012). Breast cancer has produced the greatest female cancer mortality in Brazil for several decades, with the incidence increasing significantly every year. Statistics have shown that, in 1986 when the Sistema Único de Saúde-SUS was established, 12.8% of women died due to cancer that year, and breast cancer was the leading cause of these deaths. In 1998, the total number of cases of breast cancer was about 32,000 whose 66% of women died. At 2014, the southeastern region of the country showed the highest number of registered cases followed by the Northeast and South of which 60% of deaths occurred due to breast cancer (CECILIO, et al., 2015). Studies showed that the common standard metastatic conditions are the visceral (liver, lung or pleura and breast) but in smaller proportion there is bone metastases, and consequently the possibility of application of percutaneous technique with bone cement.

Regarding the cancer incidence, it is urgent to develop protocols for addressing the

problems that affect patients with disseminated cancer in order to expand the action of the *SUS* in whole country. Since breast cancer is the most likely to manifest metastasis both in thoracic region as in other parts of the body, new treatment methods need to expand, improve and be disseminated to increase the quality of life of patients and achieve a complete remission, even in clinical unfavorable situations. Even in regions with lower concentration of population, the numbers of cases are in smaller proportion, but they are still having a high impact and increasing incidence (CECILIO, et al., 2015). In addition, it is desirable the development and application of therapies that produce a lower operational cost, being minimal invasive, in order to reduce the risk of infections for patients whom in most cases are immune depleted.

The study of cements for treatments of bone metastases contains a number of clinical and technical knowledge that must be considered and detailed, at the time that new protocols are developed in the frame of the innovation of palliative treatments; in which the use of radioactive bone cement is promising.

2.3. Anatomic classification and structural mechanical functions of the bone tissue

When James Weinstein in 1989 established an anatomical classification of the regions of the vertebral body, it was possible to identify the most frequent metastases types in each of the regions and thus specify the most difficult to treat by their proximity to the spinal cord. This anatomical distribution basically presents four regions as shows in Figure 2.1(B), in which regions III and IV, laid down in front of the spine, are those that attend a percutaneous procedure by inserting a bone acrylic (GEORGY, 2008; GERSZTEN, 2007; KLIMO, MEIC, & SCHMIDT, 2004). Those two regions due to your nature have the greatest tendency to collapse as a result of the metastases because those support a greater natural compression of the skeletal structure. In the long bones, abnormalities (tumors or metastases) are frequent in the metaphyseal region. Such tissue is a kind of intermediary tissue between the spongy tissue (epiphyses) and mature or osteolytic tissue (diaphysis).

The mechanical properties maintain an important role in the study of the skeletal system. Understanding your conformation and type of structures that are part of your composition are keys to propose possible substitute materials. Such material must have greater affinity for bone tissue, represented by the fibrils of collagen, which is the

substance that composes most of the bone tissue, and the other substances as apatite carbonate crystals and all proteins that are not collagens.

2.4. Bone diseases, types of metastasis

There are different bone neoplasms that degenerate the bone tissue being classified as benign or malignant. Sarcomas are malignant neoplasms that show in different regions of the bone tissue. However, the most relevant anomalies are especially those produced by the metastasis that represents the dissemination process of different cancer cells, via vascular or lymphatic systems, toward the bone bodies, where the clonogenic process is kept inside the bone. Bone metastasis is present in 80% of the loco-regional breast carcinoma (DE PRÓSPERO, 2001).

2.5. Bone cement, structure and composition

Several biomaterials have been proposed for the replacement of bone tissue or for the reconstitution of parts of them that are missing. Such material is able to add and paste parts of the structural bone. The fractures can be filled by acrylic PMMA cement, or even can be recomposed with biocompatible substances implanted as bioceramics matrix of calcified phosphates (ONG & CHAN, 1999). Such bioceramics participate in the processes of adsorption and reabsorption of calcium, which manifest in biological phenomena such as the osteogenesis present in the regeneration of bone tissue in destroyed regions (ONG & CHAN, 1999). There are several studies in bisphosphonates, among which we can highlight the hydroxyapatite (HAp). HAP presents itself in the natural bone with 69% of mass weight. Crystals of HAp are also distributed in the fiber matrix of collagen, which represents 20% of the bone tissue (GERSZTEN, 2007). Since this substance is a natural bone constituent, HAp mixed with PMMA was proposed as biomaterial, reaching a great response of osteoblasts adhesion (ANSELME, 2000; DALBY, SILVIO, HARPER, & BONFIELD, 2002).

2.6. Therapeutic treatment and percutaneous procedures

The vertebroplasty is a percutaneous minimally invasive procedure developed for surgery in spinal bone (HORN, HENN, & LEMOLE, 2004). The procedure is performed

by inserting acrylic in the fracture of the vertebral body. Such acrylic was developed and described for the first time in France in 1987 (GALIBERT & DERAMOND, 1987; GERSZTEN, 2007). This procedure makes use of a larger gauge needle to puncture the fractured vertebral body, where it is inserted the bone cement, stabilizing and reinforcing the bone structure to recover its original configuration. The technique was first used in the treatment of vertebral hemangiomas and subsequent in fractures of compression in osteolytic metastases and osteoporosis (KLIMO, MEIC, & SCHMIDT, 2004). The technique has also been used for the treatment of osteoporosis and pathologic fractures by compression. In the United States, the most of the applications are related to osteoporosis. The literature reports a satisfactory rate of 90% pain reduction in metastatic sites. Besides, the percutaneous kyphoplasty procedure differentiates from the vertebroplasty technique. In Kyphoplasty, a balloon is inserted into the collapsed vertebral body, and the balloon is inflated prior to insertion of the bone cement (GEORGY, 2008). In this case, the bone cement is contained internally by the surface of the balloon. Figures 2.1(A) and 2.1(C) illustrates some associated instruments to Vertebroplasty.

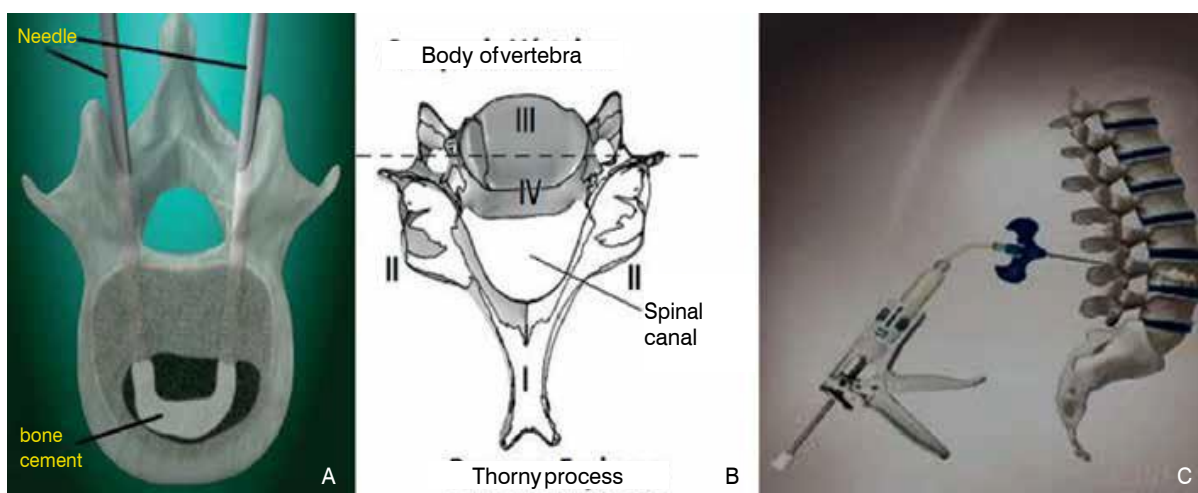


Figure 2.1 Minimal invasive procedures: anatomical position of vertebrae. (A) Vertebroplasty; (B) anatomical regions of the vertebrae according to Harrington; (C) Kit and Vertebroplasty simulation (GEORGY, 2008).

Both techniques, using polymethylmethacrylate (PMMA), improve the stability of the vertebra and attempt to retrieve the original anatomical nature. The indications of vertebroplasty and kyphoplasty are to the treatment of tumors in the spine bone and the thoracic pain reduction from fractures of the lumbar vertebral bodies in patients with cancer. The contra indications are the epidural compression of the nervous system and the

absence of recognition of symptomatic sites. Other contraindications are on coagulopathy and local infections (HAREL & ANGELOV, 2010). One of the possible failures of these techniques that make use of restorative cements is the cement extravasation, although it is an unlikely phenomenon.

The treatments are completed with teletherapy in the metastatic lesions that can be prescribed by IMRT (Intensity Modulated Radiotherapy). These procedures provide a single high dose application, assuming a no-split dose-protocol with absorbed doses limited. This procedure is scheduled after surgical removal of the tumor or metastatic lesions. The IMRT is radiotherapy where there are a suitable modulation of beam-intensities and the full covering of the target region, accompanied by the reduction of dose in the surrounding healthy tissues. Some anatomical and physiological unique aspects of the vertebral body are of relevance (RYU, et al., 2003). The RT procedure's restriction is on the low dose tolerance of the spinal cord to a no-fractionated regime. In fact, the recommended dose on the body of the vertebra must be greater than the tolerance dose of marrow, which produces a greater commitment for late neuro effects due to demyelination of the tissues of the nervous system, since its radiosensibility.

Systemic therapies are part of combined procedures for treatment of metastases. Chemotherapy, combined or mono, involves a set of drugs that depend on the histology of the tumor and of its chemical-sensibility. In general, the drugs used in prostate or breast metastasis are cytotoxic agents with low specificity. The bisphosphonates are used as pain reductions in cases of acute and moderate pain, contributing in the resorption of bone tissue removed by osteoclasts, and shrinking the tumors associated with osteolysis (DOROZHKIN, 2009). Studies in bisphosphonates have shown a significant rate decrease of fractures of the skeletal system. The systemic drugs with intravenous administration containing Strontium-89 and Rhenium-186 may be used as systemic radiation therapy of the spine, being an alternative to treat pain (FINLAY, MASON, & SHELLEY, 2005).

In 2008, Sm-153-EDTMP was incorporated into kyphoplasty (CARDOSO, et al., 2009; ASHAMALLA, et al., 2009); however, limited into a balloon. Consequently, the applied dosimetry was negligible (HIRSCH, MEDICH, ROSENSTEIN, MARTEL, & HIRSCH, 2008) (HIRSCH, MEDICH, ROSENSTEIN, MARTEL, & HIRSCH, 2008). At the kyphoplasty percutaneous procedure; the ¹⁵³Sm-EDTMP was incorporated with the

PMMA. The EDTMP is a bisphosphonate that carries the Sm-153 radioisotope by coordinating connection forming a complex (CARDOSO, et al., 2009; ASHAMALLA, et al., 2009). The advantage of using a radioisotope is in optimizing the distribution of the effective dose, which may provide the prescribed dose predefined in other radiation therapies. The β -emitters P-32, Y-90, Ho-166 are included on the radioisotope group useful for these palliative treatments. In addition, those beta-particles emitters hold lower range in trabecular tissue; and, consequently, the spatial dose distribution is contained in the bone region, unlike with Tc-99, which is a gamma emitter (HIRSCH, MEDICH, ROSENSTEIN, MARTEL, & HIRSCH, 2008).

2.7. Radioactive material production, vertebral model and computational dosimetry.

Studies conducted in the laboratory NRI-*Nucleo de Radiações Ionizantes*, by Drs. Rodrigo D'alessandro de Macedo, Márcia Flavia Silveira, Blanda Alves Donanzam, and Dr. Ilza Dálmazio, together with the present authors, provided the developed of the radioactive cement PMMA+M-HAp, being M a β -emitter radioisotope ligand to the matrix of hydroxyapatite, and so providing a radioactive cement. The synthesis of the bioceramic crystals of hydroxyapatite linked to the cold metal (cold = non-radioactive) was done using sol-gel technique (CAMPOS PI 0605721-7 A2, 2006; DONANZAM, CAMPOS, DALMÁZIO, & VALENTE, 2013; DONANZAM B. A., 2012; MACEDO, 2005). Initially, the cement was developed containing small amount of mass of HAp in relation to the mass of the PMMA (CAMPOS Nº PI 0605721-7 A2, 2006). In these conditions, the material presented a very rapid polymerization. In addition, the biomechanical properties match with those of the compact bone. Such inorganic structure hinders the calcium trades by absorption and reabsorption present in the process of restoration of natural injured bone. The M-HAp crystals exposed to thermal and epithermal neutron fluxes, about 2.6×10^{12} and 2.8×10^{11} neutron \times cm⁻² \times s⁻¹, respectively, in an irradiation time of 8 h, provided specific mass activities more than enough to control bone metastasis. The ¹⁸⁸Re, ¹⁶⁶Ho and ¹⁵³Sm nuclides were chosen, mainly due to the easiness of the chemical synthesis, the low cost of the reagents, as well as the radiodosimetric advantages produced by β -emitters. There were good spatial dose distributions in the vertebrae body and a rapid accumulation of dose, due to the short half-lives of nuclides; as well a negligible dose on spinal cord (DONANZAM, CAMPOS, DALMÁZIO, & VALENTE, 2013; DONANZAM B. A., 2012).

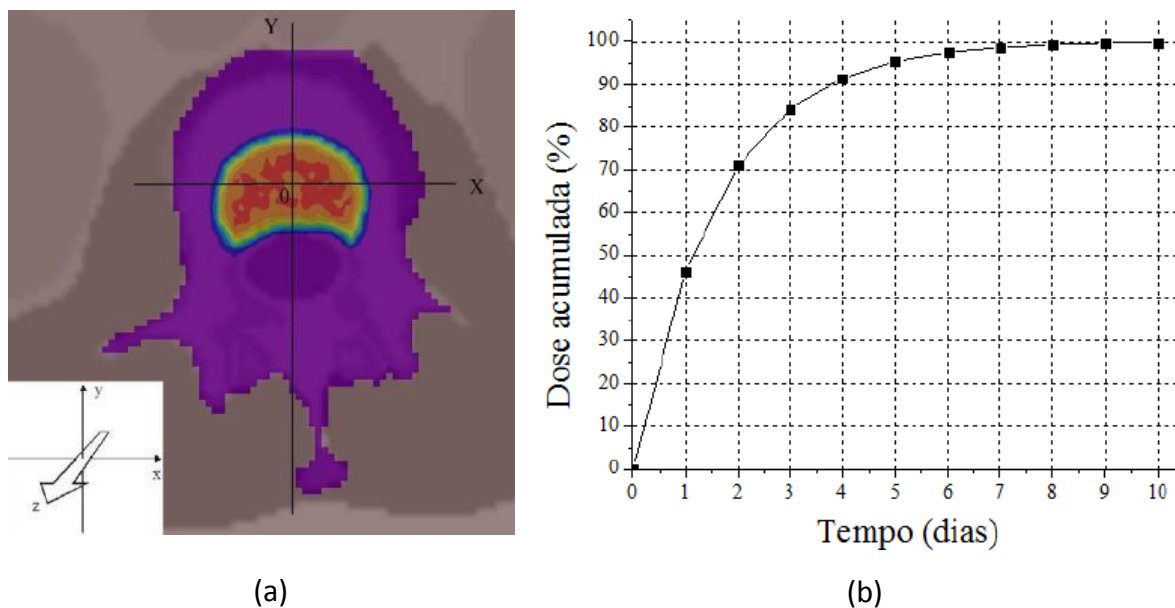


Figure 2.2 Computational model with MCNP5/Siscodes - BED. (A) vertebral model of the spine and isodose distribution. (B) accumulated dose curve for cement bound with Ho-166 (DONANZAM B. A., 2012).

The dosimetry of bone cements was demonstrated by studies in computational models (DONANZAM, CAMPOS, DALMÁZIO, & VALENTE, 2013; DONANZAM B. A., 2012). In Figure 2.2, the employed computational model of the spinal cord is depicted. The model was developed with the aid of the SISCODES program and the transport of particles was made in code Monte Carlo N-Particle version 5 (MCNP5). The absorbed dose and the BED (Biological Effective Dose) in the body of the vertebrae and spinal cord have been assessed (ANSELME, 2000; DALBY, SILVIO, HARPER, & BONFIELD, 2002). A HAp+¹⁶⁶Ho-HAp+PMMA cement, containing one milligram of ¹⁶⁶Ho-HAp, provided a BED of 102 Gy10, considering an activity of 32.5 MBq. In this procedure, there was a 10-folds reduction in spinal cord dose compared to an external beam radiotherapy procedure using IMRT. In the Figure 2.2(a) shows to the bone cement implanted at vertebral body.

Figure 2.2(b) depicts a representation of the accumulated absorbed dose in function of time produced by the proposal radioactive concrete with Ho-166, whose total dose reaches 100% after a period of 10 days. On ongoing research, the bone cement is being synthesized with Sm-152 and activated in Sm-153. The half-lives of Ho-166 is 26.8 h and Sm-153 46.50 h, and both are beta emitters. The specific activity obtained for M-HAp, irradiated in the IPR1/ CDTN reactor, was 32.5 MBq×mg⁻¹ to Ho-166 is 14.5 MBq×mg⁻¹ to Sm-153.

The larger half-life of Sm-153 can encourage management of distribution to this radiopharmaceutical to the hospitals, improving the cost-benefit ratio.

2.8. Final remarks

Radioactive bone cement offers promising features for the treatment of bone metastasis in situ. However, finding the optimum conditions of application represents a challenge. Possible biomedical studies must be developed involving radio-toxicity, cytotoxicity, dosimetry, radiobiology, clinical response, among others. In an application, one can expect a good viscosity, a suitable curing time, high porosity after curing, and permeability to bone cells that progressively are able to regrow after the end of the radiation exposure. The cement must reach the regions of metastatic lesions that usually found in the trabecular bone, where the fractures are not of high impact. In these cases, the pain is associated with the compression of the existing micro tumors and presence of possible microfractures (FINLAY, MASON, & SHELLEY, 2005).

The affected bone tissue has natural porous and have less resistant than compact one, showing constant regeneration. In these sites, other natural biological features are present, such as medullar cell diffusions, angiogenesis and revascularization (LEGEROS, LIN, ROHANIZADEH, MIJARES, & LEGEROS, 2003; GUEDE, GONZÁLEZ, & CAEIRO, 2013; CAIERO, GONZÁLEZ, & GUEDE, 2013). The future goal has been to transform the radioactive cement post-exposure more nature with characteristics of the porous bone tissue. The procedure should be optimizing avoiding unwanted effects such as thermal necrosis, produced by polymerization of PMMA where local temperatures can reach up to 110 °C, and chemical necrosis, produced by excess of chemicals that induce polymerization. The ideal is to have a composite that deals with the metastasis in situ and produces a porous matrix that does not stop the natural bone regeneration processes.

2.9. References

- ANSELME, K. (2000). Osteoblast adhesion on biomaterials. *Biomaterials*, 21, 667-681.
- ASHAMALLA, H., CARDOSO, E., MACEDON, M., GUIRGUIS, A., WENG, L., ALI, S., PANIGRAHI, N. (2009). Phase I trial of vertebral intracavitary cement and Samarium (VICS): Novel technique for treatment of painful vertebral

- mastatasis. *Int. J. Radiation Oncology Biol Phys*, 75, 836-842.
- CAIERO, J. R., GONZÁLEZ, P., & GUEDE, D. (2013). Biomechanics and Bone (& II): Trials in different hierarchical levels of bone and alternative tools for the determination of bone strength. *Rev. Osteoporos. Metab. Miner.*, 5(2), 99-108.
- CAMPOS, T. P., & MACEDO, R. D. (2006). *Brasil Patente Nº PI 0605721-7 A2*.
Fonte: <http://www.inpi.gov.br>
- CARDOSO, E. R., ASHAMALLA, H., WENG, L., MOKHTAR, B., ALI, S., MACEDON, M., & GUIRGUIS, A. (2009). Percutaneous tumor curettage and interstitial delivery of Samarium-153 coupled with kyphoplasty for treatment of vertebral metastases. *J Neurosurg Spine*, 10, 336-342.
- CECILIO, A. P., TAKAKURA, E. T., JUMES, J. J., DOS SANTOS, J. W., HERRERA, A. C., & VICTORINO, V. J. (2015). Breast cancer in Brazil: epidemiology and treatment challenges. *Breast Cancer: targets and therapy*, 7, 43-49.
- DALBY, M. J., SILVIO, L. D., HARPER, E. J., & BONFIELD, W. (2002). Increasing hydroxyapatite incorporation into poly(methylmethacrylate) cement increases osteoblast adhesion and response. *Biomaterials*, 23, 569-576.
- DE PRÓSPERO, J. D. (2001). *Tumores Ósseos*. São Paulo - Brazil: Roca.
- DONANZAM, B. A. (2012). *Biocerâmicas com Ho-166 e Sm-153: síntese, caracterização e avaliação dosimétrica em Radiovertebroplastia* (Dissertação). (UFMG, Ed.) Belo Horizonte, Minas Gerais, Brasil: UFMG.
- DONANZAM, B. A., CAMPOS, T. P., DALMÁZIO, I., & VALENTE, E. S. (2013). Synthesis and characterization of calcium phosphate loaded with Ho-166 and Sm-153: a novel biomaterial for treatment of spine metastases. *J Mater Sci: Mater Med*, 24, 2873-2880.
- DOROZHKIN, S. V. (2009). Calcium orthophosphates in nature, biology and medicine. *Materials*, 2, 399-498. doi:10.3390/ma2020399
- FERLAY, J., SOERJOTAMARAM, I., ERVIK, M., FORMAN, D., & BRAY, F. (2012). *Globocan, 2012: Estimated câncer incidence, mortality and prevalence worldwide in 2012*. Fonte: International Agency For Research on Cancer: <http://globocan.iarc.fr/>
- FINLAY, I. G., MASON, M. D., & SHELLEY, M. (2005). Radioisotopes for the palliation of metastatic bone cancer: a systematic review. *Lancet Oncol*, 6, 392-400.

- GALIBERT, P., & DERAMOND, H. (1987). Note preliminaire sur le traitement des angiomes vertebraux par vertebroplastie acrylique percutanee. *Neurochirurgie*, 33, 166-167.
- GEORGY, B. A. (2008). Metastatic spinal Lesions: State of the art treatment options and future trends. *AJNR Am. J. Neuroradiol.*, 29, 1605-1611.
- GERSZTEN, P. (2007). The role of minimally invasive techniques in the management of spine tumors: percutaneous bone cement augmentation, radiosurgery, and microendoscopic approaches. *Orthop. Clin. N. Am.*, 38, 441-450.
- GUEDE, D., GONZÁLEZ, P., & CAEIRO, J. R. (2013). Biomechanics and Bone (I): Basic concepts and classical mechanical trials. *Rev. Osteoporos. Metab. Miner.*, 5(1), 43-50.
- HAREL, R., & ANGELOV, L. (2010). Spine metastases: Current treatments and future directions. *European Journal of Cancer*, 46, 2696-2707.
- HARRINGTON, K. D. (1981). The use of methylmetacrylate for vertebral-body replacement and anterior stabilization of pathological fracture-dislocations of the spine due to metastatic malignant disease. *J. Bone Surg. Am.*, 63, 36-46.
- HIRSCH, A. E., MEDICH, D. C., ROSENSTEIN, B. S., MARTEL, C. B., & HIRSCH, J. A. (2008). Radioisotopes and vertebral augmentation: dosimetric analysis of a novel approach for the treatment malignant compression fractures. *Radioisotope dosimetry*, 87, 119-126.
- HIRSCH, A. E., ROSENSTEIN, B. S., MEDICH, D. C., MARTEL, C. B., & HIRSCH, J. A. (2009). Polymethymetacrylate and Radioisotopes in Vertebral Augmentation: An Explanation of Underlying Principles. *Pain Physician J.*, 12, 887-891.
- HORN, E., HENN, J., & LEMOLE, J. (2004). Thoracoscopic placement of dural-rod instrumentation in thoracic spinal trauma. *Neurosurgery*, 11, 1150-1154.
- KLIMO, P., MEIC, J. R., & SCHMIDT, H. (2004). Surgical Management of Spinal Metastases. *The Oncologist*, 9, 188-196.
- LEGEROS, R. Z., LIN, S., ROHANIZADEH, R., MIJARES, D., & LEGEROS, J. P. (2003). Biphasic calcium phosphate bioceramics: preparation, properties and applications. *J. Mater. Sci. Mater. Med.*, 14(3), 201-209
- MACEDO, R. D. (2005). *Radiovertebroplastia para tratamento de neoplasias malignas ósseas da coluna vertebral: avaliação da proposta e da viabilidade.*

(Dissertação). Belo Horizonte - Brasil: UFMG.

- ONG, J. L., & CHAN, D. C. (1999). Hydroxyapatite and their use as coatings in dental implants: a review. *Critical reviews in biomedical engineering*, 28(5), 667-707.
- RYU, S., YIN, F., ROCK, J., ZHU, J., CHU, A., & KAGAN, E. (2003). Image-guided and intensity-modulated radiosurgery for patients with spinal metastasis. *Cancer*, 97(8), 2013-2018.
- SCHILITZ, A. O., DE LIMA, F. C., ANDRADE, J. H., OLIVEIRA, J. F., & SANTOS, M. O. (2015). *Estimativa 2016: Incidência de câncer no Brasil*. Rio de Janeiro: INCA.
- VIÑA, J. C. (2005). Metastatic bone pain management with radioactive isotopes. *Braz. Arch. Biol. Technol.*, 48(2), 127-133.
- WEINER, S., & WAGNER, H. D. (1998). The material bone: structure-mechanical function relations. *Annu. Rev. Mater.: Sci.*, 28, 271-298

CAPITULO 3

3. Physical distribution and radiological contrast of cements implanted in vitro vertebrae

ABSTRACT

Vertebroplasty and Kyphoplasty have been studied for several years as percutaneous procedures for treatment of bone fractures, osteoporosis and other abnormalities in the skeletal system. Currently, these procedures have already been established as effective minimally invasive surgical procedures very promising in orthopedics and traumatology. Those procedures are guided by fluoroscopy using radiopaque substances such as barium sulfate BaSO_4 . The improvements of the radiological contrast at the image are still necessary. In present study, we addressed the benefits of HAp as radiopaque element in the bone cement and the possibility of removing barium sulfate to reduce the toxicity of the material.

Keywords: Bond cement, PMMA-Hydroxyapatite, Radiological contrast.

3.1. Introduction

A procedure was developed and first described in France in 1987 known as Vertebroplasty used as a percutaneous technique by means of an acrylic injected with a syringe into the fractured vertebra body. In the surgical context to this procedure, it is a minimally invasive technique for ambulatory nature. The technique was initially implemented for the treatment of vertebral hemangiomas and later was applied for decompression of fractures of osteolytic metastases and osteoporosis. Another percutaneous technique was introduced with use of PMMA (polymethylmethacrylate with chemical nomenclature $[\text{CH}_2\text{C}(\text{CH}_3)(\text{CO}_2\text{CH}_3)]_n$) as bone cement to join the fractured bone parts. In addition, it has been inserted into a balloon that it is inflated in order to restore the anatomical structure of the vertebra. Such percutaneous technique is known as Kyphoplasty. One of the major problems of the percutaneous techniques is the possible extravasations of cement outside the bone region where it aims to be located. One solution to this undesirable event is the decompression of the vertebra by re-intervention by surgery (CHEN, *et al.*, 2011; HENDRICKSON, SHEHATA, & KIRCHNER, 1976; GERSZTEN, 2007). These percutaneous procedures are complementary to therapeutic treatments within tumor control (KANEKO, *et al.*, 2010). In most cases patients have advanced metastatic disease stage and the radiation therapy is palliative. Some studies have proposed IMRT (Intensity Modulated Radiotherapy) with IGRT (Image-Guided Radiotherapy) as therapeutic treatments with less neurological impact on the marrow. Although demyelinating phenomenon of nerve tissues may occur since such structures are highly radiosensitive; it presents in lesser extension with IMRT and IGRT (EMAMI, *et al.*, 1991; RYU, *et al.*, 2007; YAMADA, *et al.*, 2008; RYU, *et al.*, 2003). At 2006, other options have been proposed in the field of radiation therapy based on the idealization of radioactive bone cement by research group (CAMPOS PI 0605721-7 A2, 2006). Such radioactive cement was addressed to treat bone metastases dealing with the elimination of the clonogenic properties of the cancer cells together with the reinforcement of the bone structure. At 2009, it has been followed by the use of Quadramet ($^{153}\text{Sm-EDTMP}$) administered percutaneously in the affected region by means of protocol Kyphoplasty (Kyphon) (ASHAMALLA, *et al.*, 2009).

There are a number of bisphosphonates considered bioceramics which have already been studied. Among those that can highlight is the Hydroxyapatite (HAp with chemical

nomenclature [$\text{Ca}_5(\text{PO}_4)_3(\text{OH})$]), contains 69% of its composition equivalent to naturally bone and the 20% of collagen matrices fibers as connective tissue. Therefore, since HAp is part of the nature of the bone, it has already been proposed to be mixed with the PMMA reaching optimal adhesion's response of osteoblasts in the biomaterial (DOROZHKIN, 2009; HIRSCH, ROSENSTEIN, MEDICH, MARTEL, & HIRSCH, 2009; DOROZHKIN, 2010).

Considering the cement implant, the improvement of the radiological contrast at the image is still necessary. In present study, it addressed the benefits of HAp as radiopaque element in the bone cement and the possibility of removing barium sulfate to reduce the toxicity of the material. Radiological images from X-ray and Ultrasonography are evaluated in cement implants in vertebrae.

3.2. Methods

3.2.1. In vitro anatomical sample preparation.

The separation of a section of a pig vertebral column, in a special cut provided by a meat market, was performed in vitro embed in an equivalent muscle tissue, maintaining anatomically its structure without considering distinct anthropometric characteristics of the model. The structure was immediately cooled to $-18\text{ }^\circ\text{C}$ to reduce the effect of decomposition.

3.2.2. Synthesis of the composite.

The composite was prepared in cold based on PMMA, HAp, barium sulfate so that the dilution held excess water as dissolvent. The solution in deionized water was done primarily to modulate the phases of the acrylic in order to increase the polymerization time by mean of stirring of the mixture. Both PMMA as the instruments in the mixture were also cooled due to polymerizing effect that is proportional to the temperature increase. The HAp was synthesized by the sol-gel method according to sol-gel technique (CAMPOS PI 0605721-7 A2, 2006; LEGEROS, LIN, ROHANIZADEH, MIJARES & LEGEROS, 2003) after to mix the components the solution was left for 24 hours in a closed beaker to force the precipitate's product, the nucleation and formation of colloids. The compounds

used for the synthesis of HAp were 3.937 g of $\text{Ca}(\text{NO}_3)_2 \cdot \text{H}_2\text{O}$, 0.69 mL of H_3PO_4 , 2 mL of CH_3OH and water as solvent in excess. Subsequently the sample was heated in an oven ramped from room temperature to 100 °C for 22 hours as follows: from room temperature to 80 °C at a rate of $0.306 \text{ }^\circ\text{C}\cdot\text{min}^{-1}$, then an isotherm 360 minutes, subsequently to 100 °C a ramp at the rate of $0.333 \text{ }^\circ\text{C}\cdot\text{min}^{-1}$ and finally an isotherm 720 minutes. The next day, the sample was heated

from room temperature to 720 °C at a rate of $6 \text{ }^\circ\text{C}\cdot\text{min}^{-1}$, then 60 min isotherm. The HAp powder is macerated and mixed in different proportions with the MMA (Methyl Ethyl Methacrylate ($\text{C}_5\text{H}_8\text{O}_2$)) to produce 1 g of bone cement in a binary system (1-x)MMA-xHAp, where [x] is the concentration of HAp in the mixture as shown in Table 3.1. The concentrations (1) and (2) were presented in this preparation only.

Table 3.1 Concentrations [x] bone cement to produce 1 g of the binary system (1-x)PMMA-xHAp

•Nº	•Concentration [x]	•MMA ($\text{C}_5\text{H}_8\text{O}_2$)	•HAp($\text{Ca}_5(\text{PO}_4)_3(\text{OH})$)
•1	•0,00000	•1,00000	•0,00000
•2	•0,50000	•0,16620	•0,83380

3.2.3. Cement injection.

The cement was injected into vertebral models designed in the laboratory drilling the vertebral body with an incline 45° to the midsagittal plane simulating needle Vertebroplasty kit.

3.2.4. Radiological contrast.

The X-ray equipment used was the BR 100, a transportable model with performance 100 mA and 90 kV. The BR 100 is composed with an X-ray tube sealed and linked to a telescope that is connected to the apparatus column than have an arm which allows depending on the movement necessary adjustment of the distance between tube and film that is studied radiographically. It also has a command table with the control elements necessary for desired voltage and current intensity. According to the radiological techniques, exposure time of 0.50 s, current of 70 mA, voltage of 60 kV and FFD (*Focal*

Film Distance) of 85 cm were applied in thoracic vertebrae. After the development processing, films were digitized to study the radiological contrast in each of the vertebrae that was implanted the bone cement. Contrast was evaluated in different points.

3.2.5. Ultrasonography images.

The GE Healthcare ultrasound equipment LOGIQe REF. 5199704 made in China in 2008 was used for image guided in the Vertebroplasty simulating procedure with the pig vertebral column. One 12L-RS probe was used in B-cine mode with a signal of 12 MHz and with a maximum depth of 7 cm for the configuration abdominal type examination in addition before to the application of the contact gel for pig column model in vitro. In the second image signal was 10 MHz and the depth of field of ultrasound was defined to 4 cm.

3.3. Results

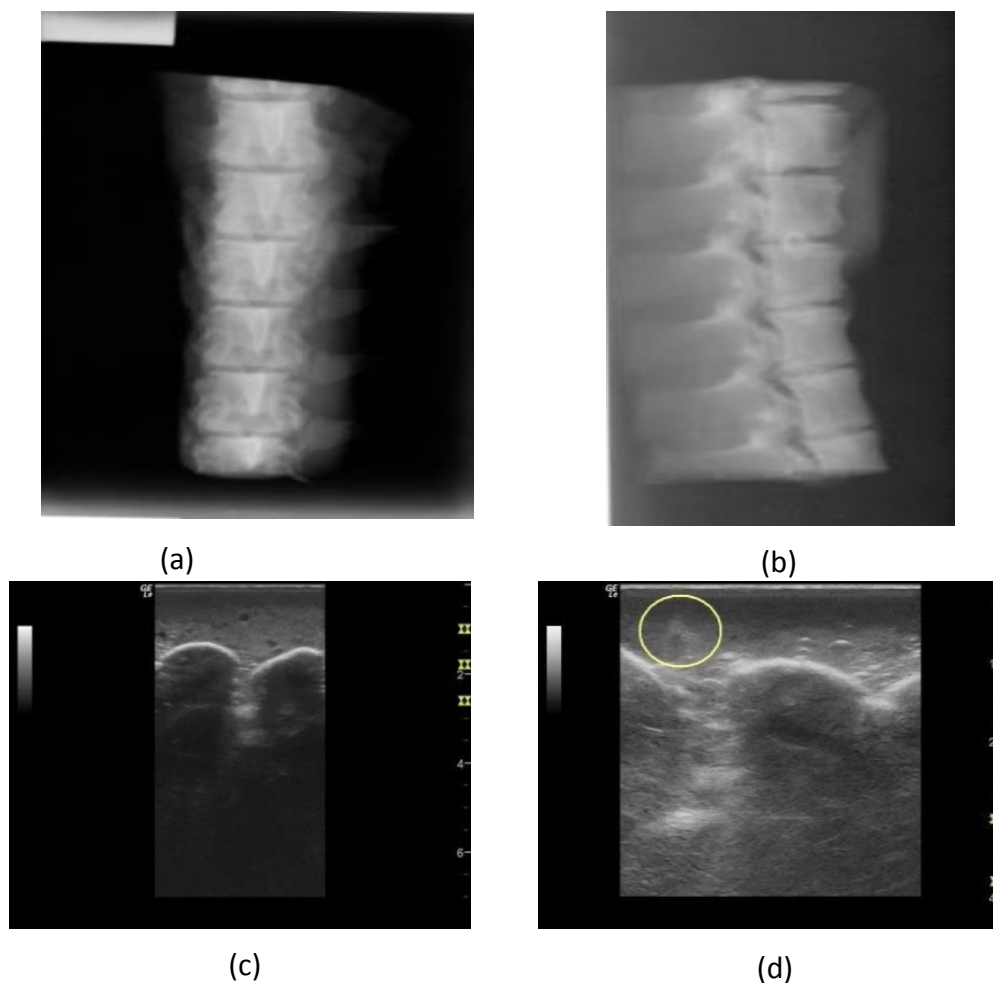


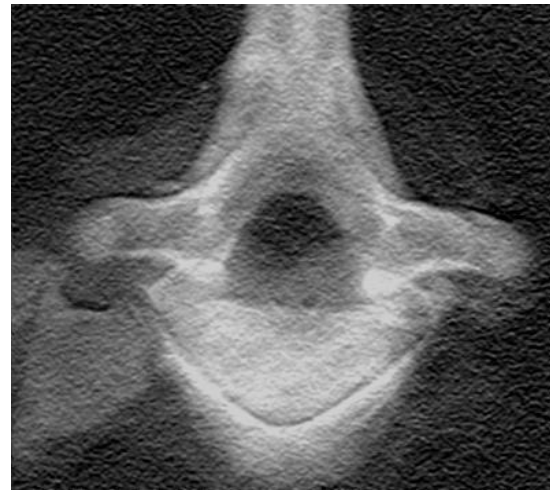
Figure 3.1 X-ray and ultrasound images in vitro from vertebrae model is presented. In (a) antero-posterior-AP incidence plane (b) lateral incidence plane (c) and (d),

there are ultrasound images; and, (d), a dynamic anomaly shows the insertion of the needle.

The images of the phantom taken with x-ray have good contrast even though the parts are embedded in a tissue simulating equivalent soft tissue. According to Fig 3.1(a), an shown on anteroposterior incidence plane of the phantom, in which the X-ray beam had to overcome apart phantom also the styrofoam lid container 2 cm that contains. The polystyrene and the surrounding soft equivalent tissue have a lower attenuation coefficient than to bone tissues. In Fig. 3.1(b), a lateral incidence image was shooting. The x-rays had to overcome two lids that are part of styrofoam container with 2 cm every one, maintaining good contrast. In Fig 3.1(c) and Fig. 3.1(d), images provided by ultrasound equipment, simulating the lumbar puncture protocol, are presented. A good contrast of the spinous processes, transverse and upper and lower joints, is observed. Just as the needle is guided by the spinous processes in the lumbar puncture for patients in gestation, it is possible to do the same in Vertebroplasty, with the difficulty of invading the field temporarily while the needle is inserted into the body of the vertebra. However, to control the flow of cement during insertion fluoroscopy is necessary.



(a)



(b)



Figure 3.2 Radiological images of four vertebral models. In (a) the vertebrae have molten lead (b) PMMA injected. (c) PMMA + 10% BaSO₄ were injected. (d) $x = 0.5$ of the bone cement.

The following images as shown in Fig. 3.2 were taken from four vertebral bodies. In Fig. 3.2(a), one of them is observed with an inlay of a small mass of lead in the linear shape that will be used as reference point to evaluate the radiological contrast of the other three images. In Fig. 3.2(b), a vertebral body with a poorly differentiated image is observed corresponding to the perforation made to the vertebral body in which PMMA was injected. In Fig. 3.2(c), it was injected PMMA with 10% BaSO₄ and no abnormalities indicating that the cement was largely diffused in bone piece. In Fig. 3.2(d), polymerizing bone cement (1-x) PMMA-xHAp with a concentration [x], $x = 0.5$ HAp in the mix was injected. As in Fig. 3.2(c) the cement is well spread in the bone piece and with better contrasts which identifiable in the area of the perforation of the vertebral body. An interesting aspect was that, despite BaSO₄ suppress in the bone cement, this still shows a good radiological contrast.

The physical distribution of this biomaterial was observed through X-ray images after application of the cements in liquid phase. It has been spread 5 up to 20 mm into the vertebrae from the inject point. It demonstrated that such biomaterial can be incorporated adequately and a large amount of the cold cement can be well distributed in the vertebral structure. The spatial distribution of cement in central regions of each vertebral body is

optimal relationship in the spongy tissue. Radiological response of the cement was demonstrated on the radiological films

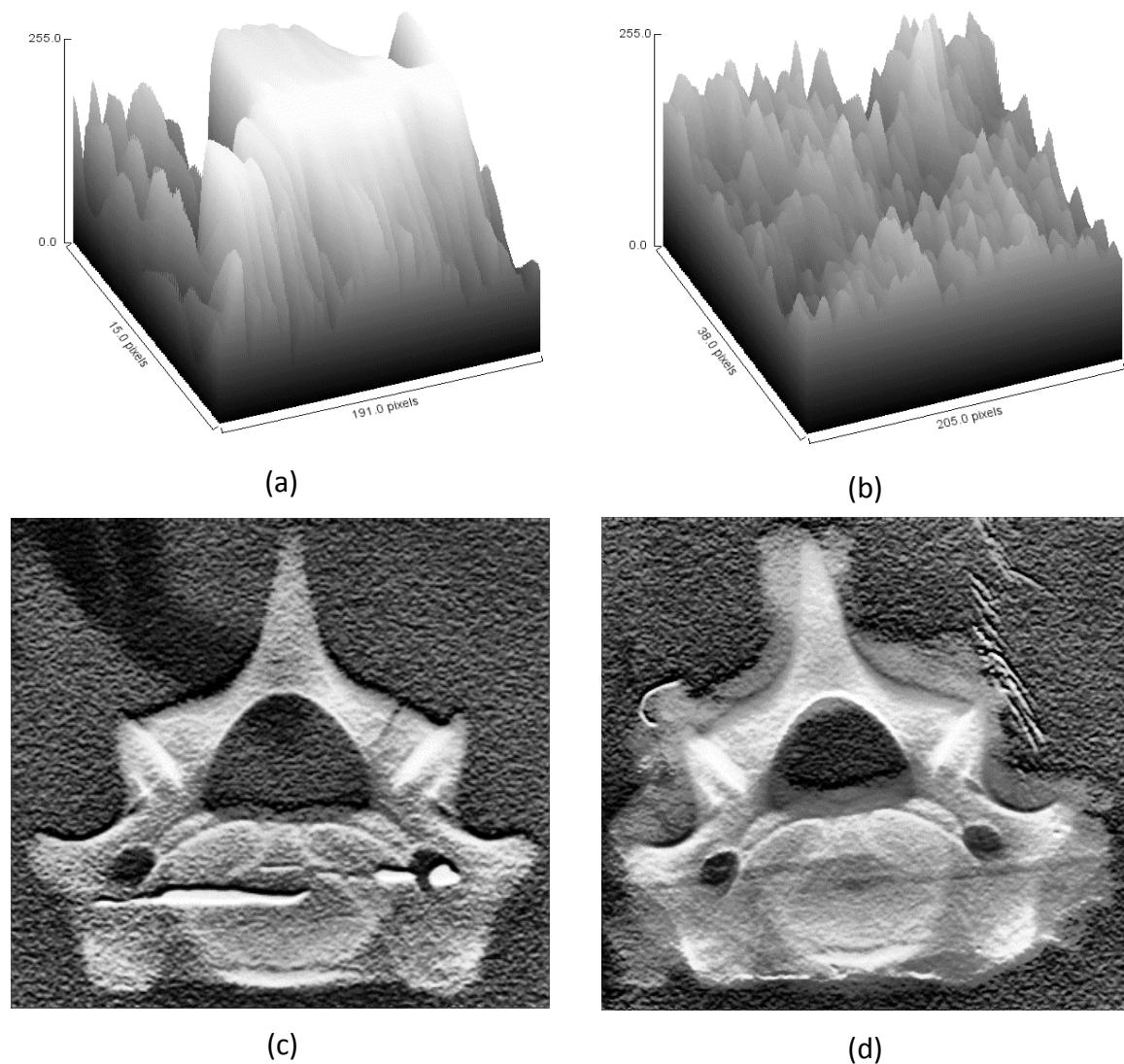


Figure 3.3 Contrast Analysis with ImageJ free software. In (a) and (c) implant's surface plot and the vertebra image has molten lead, respectively. In (b) and (d) hole's surface plot and the vertebra image has a hole, respectively

Fig. 3.3 shows the incorporation of the bone implant in one of the vertebrae and the treatment of the image as a function of the perforation made in the region of the vertebral body and its subsequent implantation. Figs 3.3 (c) and 3.3 (d) show the changes produced in terms of the incorporation of the implant in the bone piece. Fig 3.3 (a) and Fig 3.3 (b) show the region of the perforation and its implant on a plane. It is easy to notice that the image of the implant reaches its maximum in the scale of gray levels close to 255.

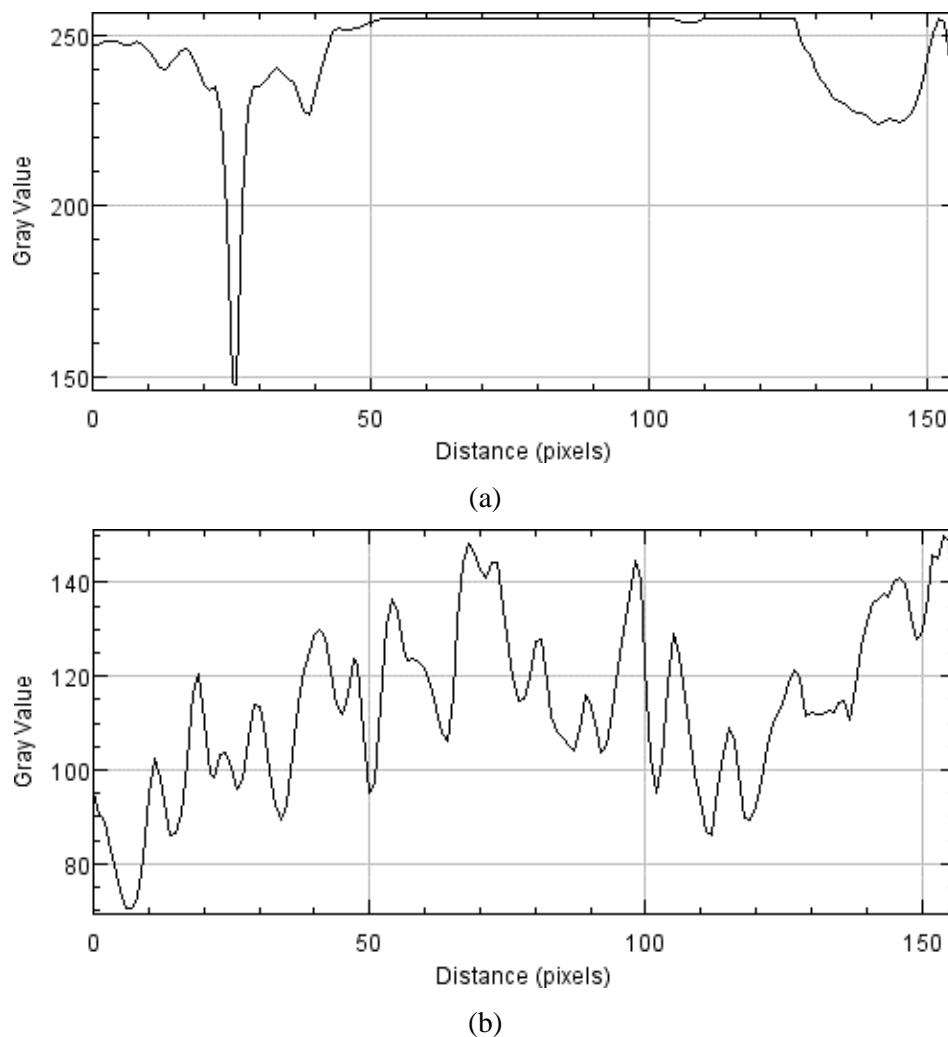
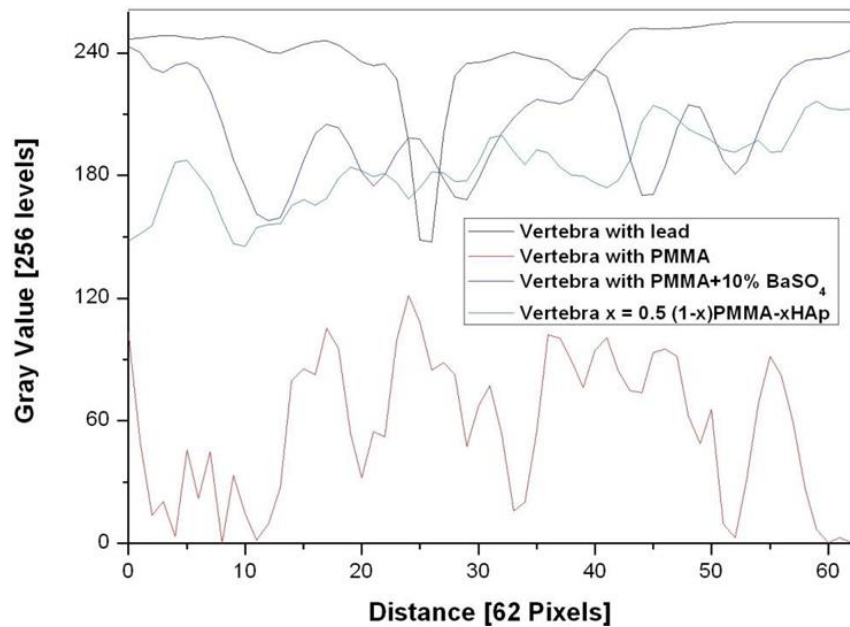


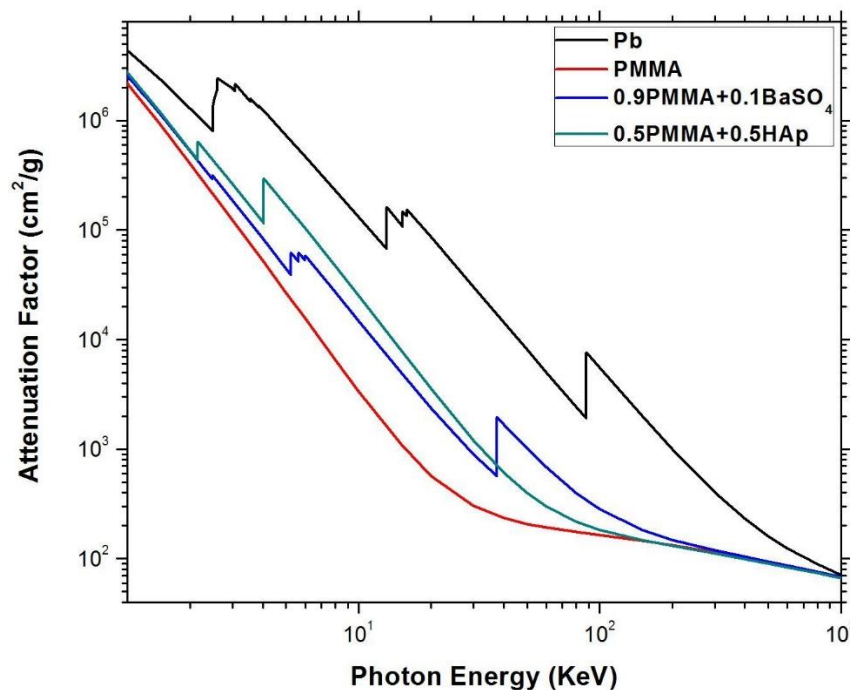
Figure 3.4 Plot profile of a vertebra in the implant region. (a) Vertebra with lead molten.
(b) Vertebra's image with hole

The radiological contrast is defined as a difference of two points in gray level of the image of 8-bits. On a scale of 256 levels, black represents zero and white 255 as showed in Fig. 3.4 for lead implant. The maximum differentiation is obtained between these two integer values, which physically corresponds the attenuation of the interaction of radiation with tissue (SELETCHI & DULIU, 2007). The lead implant on vertebrae, at the same pixel distance between 62 pixels as images' ROI (Region of Interest), generated the greatest possible contrast between the implant and the background (Fig 3.5). The Gray levels found in Fig. 3.5(a) for the two (PMMA + 10% BaSO₄ and (1-x) PMMA-xHAp with x = 0.5 samples are quite similar. At the last, the gray levels for PMMA without contrast exhibit less difference with the image background. The qualitative analysis carried out inferred about the attenuation of the x-ray field according to each one of the implants used in the

experiment. The attenuation is greater for constituents with high atomic numbers such as lead Pb defining this as a positive control in the experiment. In the case of the $(1-x)$ PMMA- x HAp system with $x = 0.5$ compared to other substances, the attenuation factor corresponds to a linear combination of the attenuation factors of its fundamental elements.



(a)



(b)

Figure 3.5 (a) Analysis of profiles plots for different implants to a length equivalent. (b) Attenuation factor for all implants download from NIST, online free XCOM (<https://physics.nist.gov/PhysRefData/Xcom/html/xcom1.html>)

Figure 3.5 (b) shows the attenuation spectrum of for photons with energy in the diagnostic range. It is evident in this energy range corresponding to the X-ray field used in the experiments that lead is the substance that most attenuates. Likewise, the bone cement proposed as an implant has an attenuation factor close to the PMMA with the contrast agent.

3.4. Conclusions

The spatial distribution of this material was observed through radiological images obtained after cement application showing the possibility of incorporating adequate amount of cement mass in the bone structure. It guaranteed the radiopaque nature of the bone cement. After cross cutting in some of the vertebrae, it was observed that the compound was solidified after being injected. Also, the spreading of the material in bone tissue was larger in the spongy bone tissue. A pair of punctures on the lumbar vertebrae can reduce the unwanted effect of extravasation due to the *in-situ* decompression.

Since these compounds are used for the purpose of be absorbed and reabsorbed bone tissues, it is very important to reduce toxicity suppressing as much as possible the substances which are not completely biocompatible with organic tissues, as radiopaque compounds used in medical imaging, without affecting significantly their action. All biological effects that may be induced by the excess of HAp must be considered in order to calculate the proportions of HAp in the cement. In addition, the desirable porosity for migration of bone cells is required. Also, porosity is essential to spread the cement and facilitate the join of fractured pieces, as the case is required.

Percutaneous column procedures guided by fluoroscopy have been already proposed. One of the major problems in radioactive cements is directly related to vertebrae dose because dose must be planned with high precision to avoid negative responses subsequent to radiotherapeutic treatments. In the Ultrasound image the commercial teams gradually have improved their services and today are already possible to reconstruct live images in 3D which is known as the 4D mode. Thus, fluoroscopic image remains needed to avoid extravasation of the cement outside the vertebral body.

3.5. References

- ASHAMALLA, H., CARDOSO, E., MACEDON, M., GUIRGUIS, A., WENG, L., ALI, S., PANIGRAHI, N. (2009). Phase I trial of vertebral intracavitary cement and Samarium (VICS): Novel technique for treatment of painful vertebral metastasis. *Int.J. Radiation Oncology Biol Phys*, 75, 836-842.
- CAMPOS, T. P., & MACEDO, R. D. (2006). Brasil Patente Nº PI 0605721-7 A2. Fonte: <http://www.inpi.gov.br>
- CHEN, J., WANG, Y., CHEN, X., REN, L., LAI, C., HE, W., & ZHANG, Q. (2011). A simple sol-gel technique for synthesis of nanostructured hydroxyapatite, tricalcium phosphate and biphasic powders. *Materials Letters*, 65, 1923-1926.
- DOROZHKIN, S. V. (2009). Calcium orthophosphates in nature, biology and medicine. *Materials*, 2, 399-498. doi:10.3390/ma2020399
- DOROZHKIN, S. V. (2010). Bioceramics of calcium orthophosphates. *Biomaterials*, 31, 1465-1485. doi:10.1016/j.biomaterials.2009.11.050
- EMAMI, B., LYMAN, J., BROWN, A., COIA, L., GOITEIN, M., MUNZENRIDER, J. E., WESSON, M. (1991). Tolerance of normal tissue to therapeutic irradiation. *Int. J. Radiation Oncology Biol. Phys.*, 21(1), 109-122.
- GERSZTEN, P. (2007). The role of minimally invasive techniques in the management of spine tumors: percutaneous bone cement augmentation, radiosurgery, and microendoscopic approaches. *Orthop. Clin. N. Am.*, 38, 441-450.
- HENDRICKSON, F. R., SHEHATA, W. M., & KIRCHNER, A. B. (1976). Radiation therapy for osseous metastasis. *J. Radiation Oncology Biol. Phys.*, 1, 275-278.
- HIRSCH, A. E., ROSENSTEIN, B. S., MEDICH, D. C., MARTEL, C. B., & HIRSCH, J. A. (2009). Polymethylmetacrylate and Radioisotopes in Vertebral Augmentation: An Explanation of Underlying Principles. *Pain Physician J.*, 12, 887-891.
- KANEKO, T. S., SCHGAL, V., SKINNER, H. B., AL-GHAZI, M. A., RAMISINGHANI, N. S., & KEYAK, J. H. (2010). Evaluation of a radiation transport modeling method for radioactive bone cement. *Phys Med Biol*, 55, 2451-2463.
- LEGEROS, R. Z., LIN, S., ROHANIZADEH, R., MIJARES, D., & LEGEROS, J. P. (2003). Biphasic calcium phosphate bioceramics: preparation, properties and applications. *J. Mater. Sci. Mater. Med.*, 14(3), 201-209.

- RYU, S., JIN, J.-Y., JIN, R., ROCK, J., AJLOUNI, M., MOVSAS, B., KIM, J. (2007). Partial volume tolerance of the spinal cord and complications of single-dose radiosurgery. *Cancer*, 109(3), 628-636.
- RYU, S., YIN, F., ROCK, J., ZHU, J., CHU, A., & KAGAN, E. (2003). Image-guided and intensity-modulated radiosurgery for patients with spinal metastasis. *Cancer*, 97(8), 2013-2018.
- SELETCHE, E. D., & DULIU, O. G. (2007). Image processing and data analysis in computed tomography. *Rom. J. Phys.*, 52(5-7), 667-675.
- YAMADA, Y., BILSKY, M. H., LOVELOCK, D. M., VENKATRAMAN, E. S., TONER, S., JOHNSON, J., FUKS, Z. (2008). High-dose, single-fraction image-guided intensity-modulated radiotherapy for metastatic spinal lesions. *Int. J. Radiation Oncology Biol. Phys.*, 71(2), 484-490. doi:10.1016/j.ijrobp.2007.11.046

CAPITULO 4

4. Hydroxyapatite influence on the thermal and mechanical properties of a possible radioactive bone cement

ABSTRACT

The main goal was to study the influence of the macroaggregate concentrations on the thermal and mechanical properties of a radioactive bone cement. The relationship of the glass transition T_g with its mechanical properties of the samples was also investigated. The bone cement as (1-x)PMMA-xHAp binary system was prepared in six distinct concentration parameter [x] at 0.0 up to 0.5. The hydroxyapatite (HAp) was synthesized using a sol-gel procedure following calcination by thermal treatment. The composite was prepared in cold based (non-radioactive) mixing PMMA (Polymethylmethacrylate) and HAp. Differential scanning calorimetry (DSC), thermogravimetric analysis (TGA) and mechanical compressive strength (CS) were used to measure the thermal and mechanical properties. The DSC and TGA thermal profiles in function to concentration parameter [x] were presented. The concentration at $x = 0.5$ or x_5 exhibited mechanical behavior similar to porous bone tissues. The CS lies in a range of 3.71 - 7.37 MPa and the glass transition temperature $T_g = 103.01$ °C. There are direct relationships between the thermoplastic properties of the PMMA-HAp and its mechanical and thermal properties as a function of the proportion of the biophosphate concentrations.

Keywords: Bone Cement, DSC, TGA, Glass Transition, Compressive Strength.

4.1. Introduction

Pathologic fractures have often occurred under normal physiologic stress in patients with spinal metastasis. The fracture occurs causing a partial or total damage of the anterior vertebral body (GEORGY, 2008). In the oncology cases, bone metastasis can significantly affect a patient's quality of life due to disabling pain, fractures or even paralysis by spinal cord compression (HAREL & ANGELOV, 2010). Radiovertebroplasty has been early suggested to be similar to Vertebroplasty; however, with the insertion in situ of a radioactive cement (CAMPOS PI 0605721-7 A2, 2006). It has already been studied by means of a computational simulation in which the dose delivered from the mixture of PMMA's bone cement and radioisotope of interest as Sm-153 or Ho-166 targeting hydroxyapatite (HAp) was spatial addressed in a vertebral phantom (DONANZAM, CAMPOS, DALMÁZIO, & VALENTE, 2013; DONANZAM B. A., 2012; MACEDO, 2005). The absorbed dose was also evaluated by MCNP5 Monte Carlo Computer Code with P-32, Ho-166, Y-90, F-18, I-125 and Tc-99m isotopes homogeneously distributed on the vertebrae. Both studies have been shown that the spreading of the spatial absorbed dose distribution is very limited to the range of the beta emitters, which favors the therapy in metastatic lesions (DONANZAM, CAMPOS, DALMÁZIO, & VALENTE, 2013; DONANZAM B. A., 2012; MACEDO, 2005; HIRSCH, ROSENSTEIN, MEDICH, MARTEL, & HIRSCH, 2009; HIRSCH, MEDICH, ROSENSTEIN, MARTEL, & HIRSCH, 2008). Nuclear characterization of the HAp doped with Sm-152 and Ho-165, their decay processes, radionuclide contaminants and the activation process in a research reactor have been addressed, demonstrated the viability of producing radioactive cement in a low-flux reactor-type. Although the nuclear proprieties of the HAp-¹⁵³Sm and HAp-¹⁶⁶Ho were presented (DONANZAM, CAMPOS, DALMÁZIO, & VALENTE, 2013); thermal and mechanical properties of the composite made of PMMA- HAp were not addressed.

Thermal, morphological and mechanical properties of PMMA electrospun nanofibers were studied. DSC was carried out to determine the phase change by increasing the PMMA/NaCl solution concentration. The results showed that the T_m (melting temperature) for a first glass transition was almost 116.19 °C to 2 samples with 12.5 wt % and 15 wt% concentrations *i.e.* invariant with NaCl concentration. Nonetheless, the second glass transition temperatures were 121.58 °C to 12.5 wt% and 123.06 °C to 15 wt% for a second thermal anomalous, confirming that the crystallinity of the fibers of PMMA/NaCl increases

with concentration (AKHTAR, SULONG, KARIM, AZHARI, & RAZA, 2015; JI, MEDFORD, & ZHANG, 2009). On the other hand, higher value of the glass transition temperature T_g yields stable thermally fibers (AKHTAR, SULONG, KARIM, AZHARI, & RAZA, 2015; MATABOLA, DE VRIES, LUYT, & KUMAR, 2011). Also, it was reported an initial decomposition temperature of the PMMA powder at 140 °C and to PMMA/NaCl fibers 302 and 320 °C respectively. This phenomenon is due to the sub-products during the thermal degradation process (AKHTAR, SULONG, KARIM, AZHARI, & RAZA, 2015; KANIAPPAN & LATHA, 2011). Other studies on TG-DTA were developed in HAp to know the decomposition process attributed to nitrates and urea, thus this being a largest weight loss. It is important to note that the methods of synthesis of HAp in both works are different. On the other hand, many positive aspects achieved when heat treatment at 800 °C was included (BEZZI, *et al.*, 2003). Another author presents an exothermic peak due to the combustion of organic components around 300 °C to results with TG-DTA. The crystallinity increased when the heat treatment is close to 700 °C (HWANG, SONG, KANG, & PARK, 2000).

The study of mechanical properties is applied only to behavior analysis in ultimate tensile strength (UTS) nanofibers, which was developed in the range 1 – 3 MPa. The modulus of the parallel layers in the nanofibers was studied with a value of 52.3 ± 5.2 MPa. Also, when the layers are arranged in cross, the modulus was 26.1 ± 4.0 MPa (AKHTAR, SULONG, KARIM, AZHARI, & RAZA, 2015; MATTHEWS, WNEK, SIMPSON, & BOWLIN, 2002). Based on previous work, Akhtar *et al.* conclude that the nanofibers PMMA/NaCl, with optimal mechanical behavior, can be used for applications in cell growth that are deposited on these PMMA nanofiber's looms for biomedical and pharmaceutical areas (AKHTAR, SULONG, KARIM, AZHARI, & RAZA, 2015). Others studies on morphological and mechanics of composite bone cement present compression properties than achieve values 71 MPa with an amount high of pores and length higher to 100 μm (PUSKA, MORITZ, AHO, & VALLITU, 2016).

There were studies where basic concepts of biomechanics and some bone properties were reviewed (GUEDE, GONZÁLEZ, & CAIERO, 2013), in which the biomechanical characteristics of the porous tissues could be appreciated (CAIERO, GONZÁLEZ, & GUEDE, 2013). In this review, the stress vs deformation profiles in an elastic region and a

plastic region can be classified. It should note that there are many mechanical characteristics to study, but for practical purposes, the previous review remains useful for understanding such properties in the bone or bone substitute materials. Resistance values for cortical bone ranging from 167 - 213 MPa and Young's modulus ranging from 14.7 - 34.3 GPa. For spongy bone, the resistance varies from 1.5 - 9.3 MPa and the Young's modulus between 10 - 1058 MPa are presented (CAIERO, GONZÁLEZ, & GUEDE, 2013). Such data can be addressed to qualify synthetic biomaterials as bone substitute in comparison to natural bone.

To fulfill our research proposal, the main goal of the present paper was to study the thermal and mechanical properties of bone cements made of PMMA-HAp composite. For tissue engineering proposal, the development of a composite mimetic trabecular bone continues to be a challenge. The interest is to investigate the PMMA-HAp system that approaches in its end into the vertebrae the trabecular bone characteristics. Such system can be applied in cold condition (non-radioactive) as bone implants, as bond cements for restoration of fractured parts, or in hot condition (radioactive) as a matrix of supporting radionuclides in treatments of bone metastases PMMA-HAp-¹⁵³Sm and PMMA-HAp-¹⁶⁶Ho.

4.2. Materials and methods

4.2.1. HAp Synthesis.

The HAp was synthesized by the sol-gel method according to Donanzam *et al.*, Campos *et al.* and Legeros *et al.* (DONANZAM, CAMPOS, DALMÁZIO, & VALENTE, 2013; DONANZAM B. A., 2012; MACEDO, 2005; LEGEROS, LIN, ROHANIZADEH, MIJARES, & LEGEROS, 2003). The reagents used for the HAp synthesis were 3.937 g of calcium nitrate ($\text{Ca}(\text{NO}_3)_2 \cdot 4\text{H}_2\text{O}$), 0.69 mL of phosphoric acid (H_3PO_4), 1 up to 2 mL of methanol CH_3OH as a catalyst for starting reaction and deionized water as solvent in excess. After mixing the components, the solution was rested for 24 h in a closed beaker. Precipitation, nucleation and formation of colloids had occurred. Subsequently the sample was heated in an oven. The temperature started at room temperature ramped to 80 °C at a rate of 0.306 °C·min⁻¹, holding 360 min at the 80 °C isotherm, subsequently ramped to 100 °C at the rate of 0.333 °C·min⁻¹ holding 720 min at 100 °C isotherm. At the calcinations,

the sample was heated from room temperature to 720 °C at a rate of 6 °C·min⁻¹, following by a 60 min at 720 °C isotherm. After cooling, the HAp samples were macerated to powder.

4.2.2. PMMA-HAp composite preparation.

HAp powder was mixed in different proportions to PMMA in its powder presentation. The composite was prepared in cold based (non-radioactive) mixing PMMA ($[\text{CH}_2\text{C}(\text{CH}_3)(\text{CO}_2\text{CH}_3)]_n$), HAp $[\text{Ca}_5(\text{PO}_4)_3(\text{OH})]$. Both PMMA and the instruments were cooled previously. The mixture was stirring. PMMA-HAp system was prepared with PMMA's micro-spheres copolymer mixed to the monomer Methyl Ethyl Methacrylate (MMA). The samples were prepared in accordance with the following concentrations $[x_n]$, with $n = 1, 2, 3, 4, 5, 6$, such that $x_1 = 0.00000$, $x_2 = 0.02167$, $x_3 = 0.09062$, $x_4 = 0.16619$, $x_5 = 0.50000$ and $x_6 = 1.00000$. The x_n is a value corresponding to x in the following system $(1-x)[\text{CH}_2\text{C}(\text{CH}_3)(\text{CO}_2\text{CH}_3)]_{n-x}[\text{Ca}_5(\text{PO}_4)_3(\text{OH})]$ or $(1-x)\text{PMMA}-x\text{HAp}$.

4.2.3. Calorimetry DSC and Thermogravimetric TGA assays.

The thermal analysis was performed by using the differential scanning calorimetry DSC-60 Shimadzu; measured in two-time intervals. The measurements were carried out in dynamic N₂ atmosphere (50 ml/min) at a heat rate of 10 °C·min⁻¹ in the 30 °C – 180 °C interval and a mass of 1 up to 3 mg. The samples placed on the aluminum pan were kept in laboratory temperature and atmospheric pressure conditions. A second heating was performed at 30 °C up to 450 °C interval following the same heating rate. The thermogravimetric analysis (TGA) was performed using METTLER TGA/DSC 1 equipment. The heating rate was the same as in the DSC previously described and in temperature range of 30 °C to 750 °C, using around 3 mg of samples in alumina crucible.

4.2.4. Mechanical Assay.

The same material was prepared for the mechanical analysis, except to the concentration x_6 since this could not keep in a compact volume. The design model for fracture was a cylindrical block of 20 mm height and 10 mm diameter. A amount of 5 g of the composite $(1-x)\text{PMMA}-x\text{HAp}$ was mixed with 1.5 mL of MMA monomer and cast. The catalyst

component was introduced to start polymerization. The pieces were fractured a week after preparation. The trials were done in INSTRON 5582 equipment Series Dual Column Floor Frames. The data acquisition was performed by Bluehill© Software. The loading speed was automatically adjustable for each sample. Two blocks per concentration were exposed to compression. For each concentration x a group of two blocks was heated at the glass transition temperature found in the DSC and maintained in a 30 min isotherm. Subsequently, the mechanical compression was performed on the two blocks.

4.3. Results

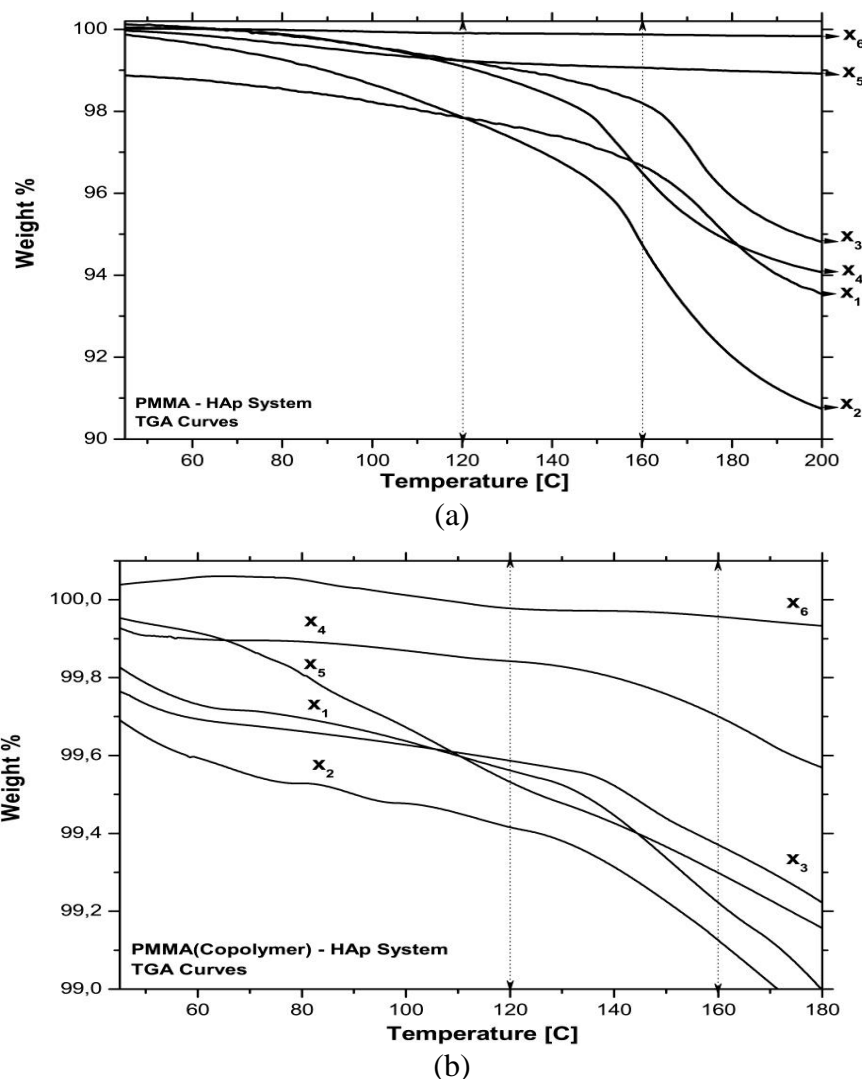


Figure 4.1 TGA heating profiles for x_i ($i=1-6$) concentrations of the $(1-x)$ PMMA- x HAp binary system in the interest temperature range between 45 – 180 °C approximately to determine system's mass loss, where (a) to PMMA(Copolymer)-HAp polymerized system, and (b) to PMMA-HAp system in powder.

TGA profiles. The TGA thermal profiles for the PMMA (copolymer)-HAp and PMMA-HAp systems were showed in Fig. 4.1. The mass in a range between 5 - 7 mg was used by TGA test. The TGA's showed a significant mass loss after 100 °C for the x_i ($i=1- 6$) concentrations that is associated with the loss of water. The maximum mass losses of 4 up to 7 % were occurring after T_g glass transition. There is no mass loss equivalent and significant to PMMA (Copolymer)-HAp Fig. 4.1(b) on the PMMA-HAp polymerized system Fig. 4.1(a) which presents less of 1 %. A possible explanation may be due to a higher water's retention and the presence of other components that have no participation in the polymerization process or a compound that was used as catalysts. In Fig. 4.1(b), a mass loss close to 4 - 7 % was due to the formation of internal pores in the system. Also, significant mass losses were observed in Figs. 4.1(a) and 4.1(b) at 110 to 160 °C intervals, above this temperature polymer melts.

DSC profiles. The DSC thermal profiles for the PMMA(copolymer)-HAp and a PMMA-HAp system in the second scanning calorimeter was showed in Fig.4.2.

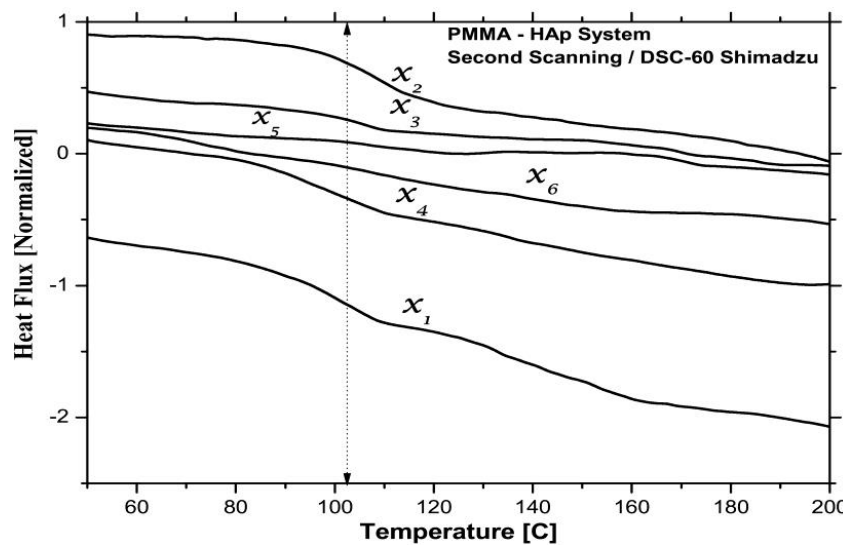


Figure 4.2 DSC heating curves for the six $[x]$ concentrations of the $(1-x)$ PMMA- x HAp binary system in the interest temperature range between 60 – 180 °C. The Heat Flux is presented in $[mJ/s]$. All curves were normalized with the maximum heat flux.

A thermal anomaly has been confirmed after the second heating for the erasure of the

thermal history and polymer stabilization for the analysis. The anomaly in DSC profiles were found in a temperature domain between 100 to 110 °C. In the Figure 4.2 showed an anomaly for the first four concentrations which held a higher proportion of PMMA weaken, with the increase in the ratio of HAp in the sample. The anomaly was observed at the first four concentrations (x_1 , x_2 , x_3 and x_4). The dotted line can guide the reader to the location on interest event described. To better understand, the phenomena occurred in the samples exposed to the heat treatment in which the baseline was corrected for each of the concentrations. The calculation T_g was made using the slope method with the help of DSC-60 Shimadzu analyzer. A relevant feature in the 100 to 110 °C domain is a possible T_g glass transition reported previously (HWANG, SONG, KANG, & PARK, 2000; MATTHEWS, WNEK, SIMPSON, & BOWLIN, 2002). PMMA(Copolymer)-HAp system in powders showed a glass transition at T_g close to 103,01 °C in average. Here the crystallization phenomena were understood as the ratio between PMMA/HAp. Indeed, the biophosphated calcium matrix should increment the crystallization level in the bone cement. Another important aspect was slightly more difficult to identify others glass transition temperature reported by in others works also. Probably due to different overlapping processes above glass transition mentioned already. In spite of this, in this second heating it can be observed that the T_g remained relatively stable between 100 – 110 °C.

Mechanical resistance. Two assays were performed. One to know the mechanical behavior of the cement as a function of the concentration of HAp. Moreover, in the other case, to know dependence on the concentration simultaneously with the test block thermally treated around to the glass transition temperature. Figures 4.3(a) and 4.3(b) depicted the profiles of the resistance to compression of the composite as a function of their x , x_i ($i=1-5$) concentrations in the PMMA-HAp system. A geometric factor was considered for each block in the group of same HAp concentration [x_n].

The Table 4.1 summarizes data strength in function of the temperature in thermal treatment and concentration of HAp in the composite. It is observed that the glass transition temperature and the weight losses were relatively stable for the concentration parameter x of 0.0 up to 0.5, thus there is confidence that the chemical and mechanical processes that were developed in each sample with distinct concentrations shall be equivalent.

Stereo surface images of PMMA-HAp samples. The Figs 4.4 shows images of the PMMA block surface without thermal treatment (x_1) (Fig 4.4(a)) and of a block with the highest concentration of HAp (x_5) with thermal treatment to T_g temperature as is presented in (Fig 4.4(b)).

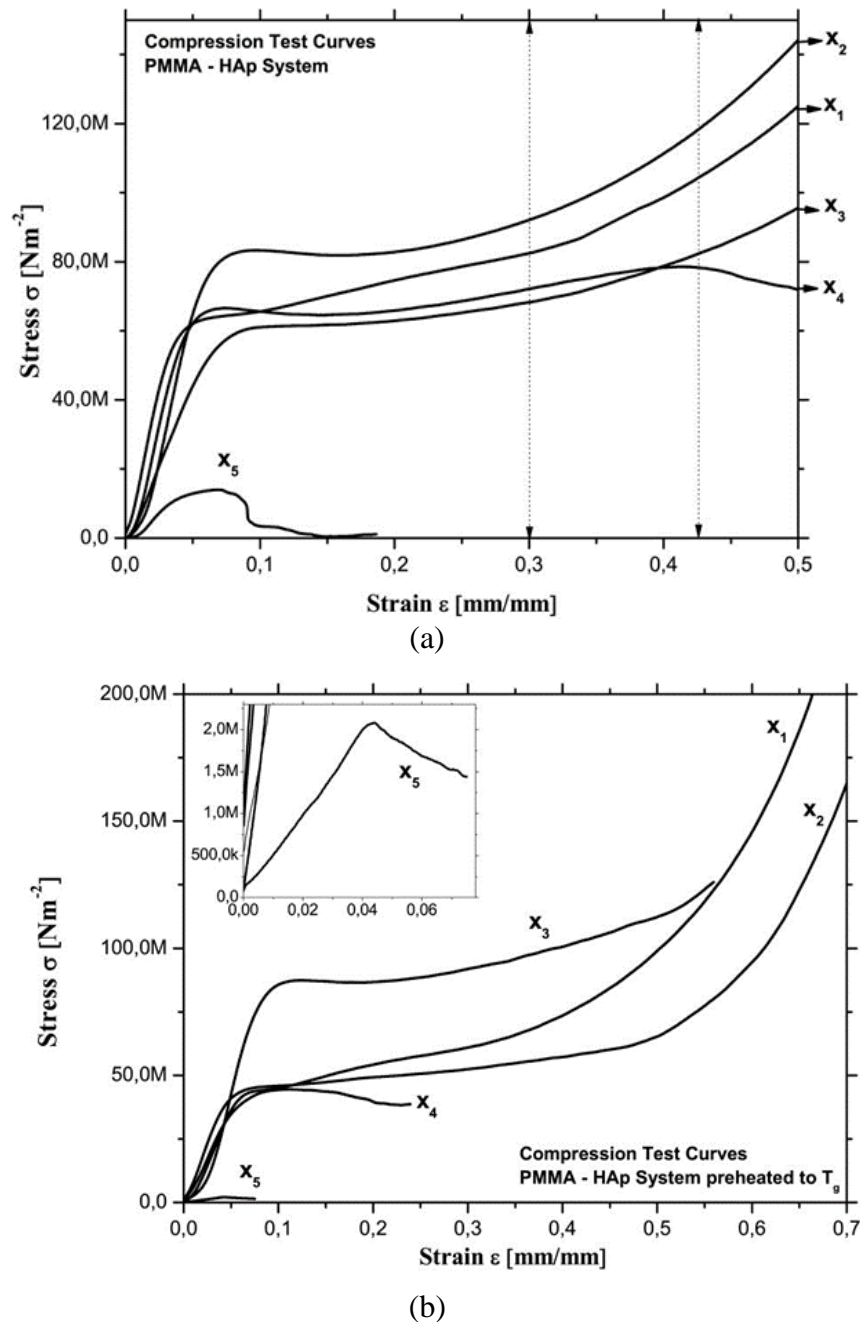


Figure 4.3 Compression profiles for the mechanical assay on the blocks with x_i ($i=1-5$) concentrations of the $(1-x)\text{PMMA}-x\text{HAp}$ binary system, where (a) PMMA-HAp polymerized system without thermal treatment with a fracture domain at 0,30 – 0,42 % compression strain; and (b) PMMA-HAp polymerized system with thermal treatment of 30 min at T_g glass transition temperature.

Table 4.1 Thermomechanical properties of (1-x)PMMA-xHAp System.

x_n	Concentration [x]	Glass Transition T_g [°C]	TGA Mass Loss [%]	Compression CS [MPa]	CS with thermal treatment [MPa]
x1	0.00000	101.78	4.02	64.44	84.00
x2	0.02167	104.34	6.80	60.45	82.77
x3	0.09062	103.65	4.33	87.60	70.13
x4	0.16619	98.08	4.89	41.40	70.07
x5	0.50000	107.23	< 1	19.50	3.71 – 7.37
x6	1.00000	-----	< 1	-----	-----
*	Cortical or compact bone			167 – 213	-----
**	Trabeculae or Spongy Bone			1.5 – 9.3	-----

* and ** cited by Caeiro *et al.* (CAIERO, GONZÁLEZ, & GUEDE, 2013); CS— Compressive Strength;

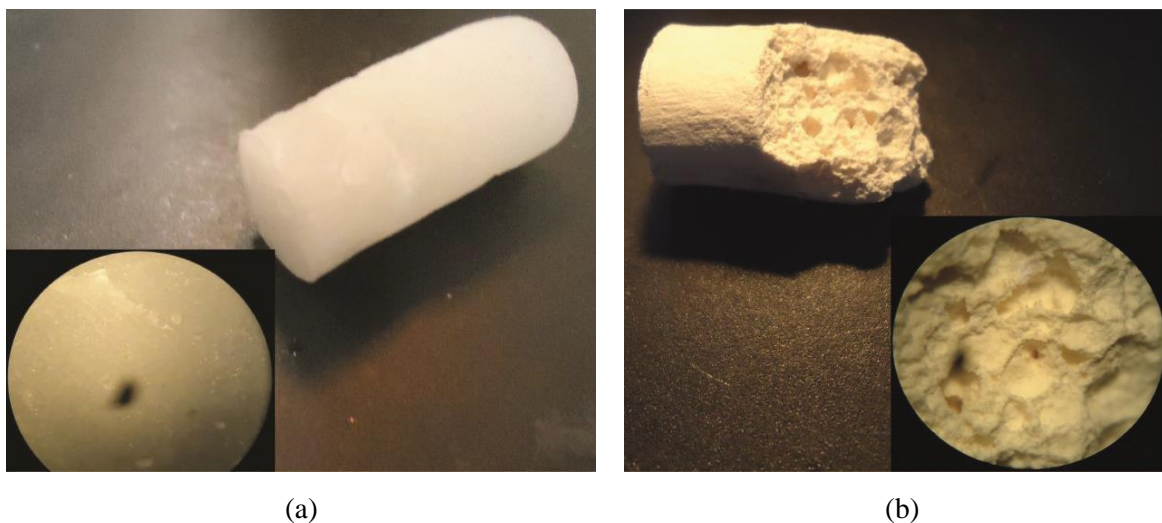


Figure 4.4 Stereoscopic images of the block surfaces, where (a) to PMMA only or x_1 concentration without thermal treatment; (b) to x_5 concentration parameter with thermal treatment for 30 min at the T_g glass transition temperature.

4.4. Discussion

The PMMA-HAp binary system in study has been the basis of various commercial bone cements. The PMMA provided two liquid and powder presentations whose moisture yields

the polymerization process aggregating the monomers and PMMA microparticles. At our PMMA-HAp composite preparation, the water solution modulated the phases of the acrylic resulting in an increase in the polymerization time (PT). The instrumentation and material cooling procedure also increased the PT due to the reduction of the intensity of the polymerizing effect that is proportional to the room temperature.

Our research team is committed to design a system that potentates mineralization processes in situ, especially those associated with spongy bone tissue. The production of pores in situ after implantation is a difficult task since at natural scale pore generations have a high degree of randomness. The pore generation was understood as spontaneous defect in the material. The pores should be connected or have thin walls in which fluid can be diffused, allowing the plasma and bone narrow diffusions, in which angiogenesis and other vascularization processes be performed facilitating all the natural biological processes. It is important to emphasize that all the thermal profiles were normalized with the maximum thermal power to evaluate how the present anomalies behave as a function of the concentration of HAp in the cement. Another important aspect of the DSC analysis of our systems was to confirm the existence of a T_g glass transition in the temperature interval that has already been mentioned by other researchers (HWANG, SONG, KANG, & PARK, 2000), which shall bring to the question how the mechanical properties of the composite is when it has been treated thermally.

The second-weight loss step in TGA analysis (Fig. 4.1(b)) suggest the possibility of increasing the polymorphic characteristics of the system and in turn promoting more defects associated with its porosity. Some reactions with gas-releasing may start after the glass transition where the polymer chains interact with $(OH)^-$, with groups producing water vapor and CO_2 . These low weight losses depicted in Fig. 4.1(a) confirm that calcium matrices are only in the heterogeneous phase in the system which reduces the gas-releasing process due to the interaction of the $(OH)^-$ groups and the polymer. The polymerized blend in Fig. 4.1(b) remains a much more intricate heterogeneous composite between calcium matrices and polymer chains.

Considering the mechanical resistance depicted in Fig. 4.3(a), the region between the dotted lines shows a tentative of defining the strain domain where the fracture of the material occurred. In principle, the modulus of compressive strength decreases with

increasing concentration of HAp. In the Fig. 4.3(b), one can observe that the plastic region is smaller for the concentrations x_4 and x_5 , whereby it becomes clear that the material is more fragile. It is important to recall that the blocks were heated to the glass transition temperature in order to respond the question of how is the mechanical feature of the material after glass-transition temperature treatment. The Compressive Strength (CS) for the block of x_1 concentration parameter was one-third of the CS mean values to human cortical bone; while it was 15-fold for x_1 and 4-fold for x_5 higher to mean value to the human spongy bone. For the blocks with thermal treatment, the CS presents close to 30 % higher that without thermal treatment; although, for the concentration x_5 the CS values is in the range of the spongy bone tissue. It is easy to observe in Fig. 4.4 that the outset of the defect formation in Fig. 4.4(b) could fit the intention of the in-situ pore generation. Subsequent studies will enclose both transport phenomena and rheological analyzes.

4.5. Conclusion

In this study, it was possible to establish a direct relationship between the thermoplastic properties of the PMMA-HAp polymer and its mechanical and thermal property changes as a function of the proportion of the concentration of the biophosphate matrix. The HAp concentration in the composite can be used to optimize its mechanical qualities for the purpose of a desired biomedical application. The biomechanical results for the concentration x_5 present Compressive Strength values between 3.71 – 7.37 MPa that are very close to the porous bone presented by Caeiro *et. al* (CAIERO, GONZÁLEZ, & GUEDE, 2013) with values between 1.5 – 9.3 MPa according to Table 4.1. The greatest innovation reached in this work was to improve bone cement syntheses through the biochemical properties use to increase the porosity of the material reaching a range such that the bone's marrow diffusion is feasible in the implant. An increase in the HAp's amorphous polycrystalline structure favors the segregation interactions in different segments of the PMMA polymer with hydrophobic nature similar to the reactions of amphiphilic molecules with water. The pores' size is such that are perceptible to the human eye very close to those found in trabecular bone tissue itself. This phenomenon was optimized with the thermal treatment carried out in the samples at the glass transition temperature close to 107 °C presented by the polymer and which was characterized by the colorimetric technique used, on the other hand, the possible dehydration reactions that occurred in the material potentiated the formation of more pores and larger size due to the

release of water and CO₂ in the heterogeneous mixture.

4.6. References

- AKHTAR, M. N., SULONG, A. B., KARIM, S. A., AZHARI, C. H., & RAZA, M. R. (2015). Evaluation of thermal, morphological and mechanical properties of PMMA/NaCl/DMF electrospun nanofibers: an investigation through surface methodology approach. *Iran Polym. J.*, 24, 1025-1038.
- BEZZI, G., CELOTTI, G., LANDI, E., LA TORETTA, T. G., SOPYAN, I., & TAMPIERI, A. (2003). A novel sol-gel technique for hydroxyapatite preparation. *Materials Chemistry and Physics*, 78, 816-824.
- CAIERO, J. R., GONZÁLEZ, P., & GUEDE, D. (2013). Biomechanics and Bone (& II): Trials in different hierarchical levels of bone and alternative tools for the determination of bone strength. *Rev. Osteoporos. Metab. Miner.*, 5(2), 99-108.
- CAMPOS, T. P., & MACEDO, R. D. (2006). *Brasil Patente nº PI 0605721-7 A2*. Obtenido de <http://www.inpi.gov.br>
- DONANZAM, B. A. (2012). *Biocerâmicas com Ho-166 e Sm-153: síntese, caracterização e avaliação dosimétrica em Radiovertebroplastia* (Dissertação). (UFMG, Ed.) Belo Horizonte, Minas Gerais, Brasil: UFMG.
- DONANZAM, B. A., CAMPOS, T. P., DALMÁZIO, I., & VALENTE, E. S. (2013). Synthesis and characterization of calcium phosphate loaded with Ho-166 and Sm-153: a novel biomaterial for treatment of spine metastases. *J Mater Sci: Mater Med*, 24, 2873-2880.
- GEORGY, B. A. (2008). Metastatic spinal Lesions: State of the art treatment options and future trends. *AJNR Am. J. Neuroradiol.*, 29, 1605-1611.
- GUEDE, D., GONZÁLEZ, P., & CAEIRO, J. R. (2013). Biomechanics and Bone (I): Basic concepts and classical mechanical trials. *Rev. Osteoporos. Metab. Miner.*, 5(1), 43-50.
- HAREL, R., & ANGELOV, L. (2010). Spine metastases: Current treatments and future directions. *European Journal of Cancer*, 46, 2696-2707.
- HIRSCH, A. E., MEDICH, D. C., ROSENSTEIN, B. S., MARTEL, C. B., & HIRSCH, J. A. (2008). Radioisotopes and vertebral augmentation: dosimetric analysis of a novel approach for the treatment malignant compression fractures. *Radioisotope*

dosimetry, 87, 119-126.

- HIRSCH, A. E., ROSENSTEIN, B. S., MEDICH, D. C., MARTEL, C. B., & HIRSCH, J. A. (2009). Polymethymetacrylate and Radioisotopes in Vertebral Augmentation: An Explanation of Underlying Principles. *Pain Physician J.*, 12, 887-891.
- HWANG, K., SONG, J., KANG, B., & PARK, Y. (2000). Sol-gel derived hydroxyapatite films on alumina substrates. *Surfaces and Coatings Technology*, 123, 252-255.
- JI, L., MEDFORD, A. J., & ZHANG, X. (2009). Electrospun polyacrylonitrile/zinc chloride composite nanofibers and their response to hydrogen sulfide. *Polymer*, 50, 605-612.
- KANIAPPAN, K., & LATHA, S. (2011). Certain investigation on the formulation and characterization of PS/PMMA blends. *Int. J. Chem. Technol. Res.*, 3, 708-717.
- LEGEROS, R. Z., LIN, S., ROHANIZADEH, R., MIJARES, D., & LEGEROS, J. P. (2003). Biphasic calcium phosphate bioceramics: preparation, properties and applications. *J. Mater. Sci. Mater. Med.*, 14(3), 201-209.
- MACEDO, R. D. (2005). *Radiovertebroplastia para tratamento de neoplasias malignas ósseas da coluna vertebral: avaliação da proposta e da viabilidade*. (Dissertação). Belo Horizonte - Brasil: UFMG.
- MATABOLA, K. P., DE VRIES, A. R., LUYT, A. S., & KUMAR, R. (2011). Studies on single polymer composites of poly(methyl methacrylate) reinforced with electrospun nanofibers with a focus on their dynamic mechanical properties. *Express Polym. Lett.*, 5, 635-642.
- MATTHEWS, J. A., WNEK, G. E., SIMPSON, D. G., & BOWLIN, G. L. (2002). Electrospinning of collagen nanofibers. *Biomacromolecules*, 3, 232-238.
- PUSKA, M., MORITZ, N., AHO, A. J., & VALLITU, P. K. (2016). Morphological and mechanical characterization of composite bone cement containing polymethylmethacrylate matrix functionalized with trimethoxysilyl and bioactive glass. *J. Mech. Behav. Biom. Mat.*, 59, 11-20

CAPITULO 5

5. Influence of HAp on the polymerization processes of a possible radioactive bone cement.

ABSTRACT

Polymethylmethacrylate PMMA is an acrylic that has been already proposed as a composite to adhere together the fractured bone structures. Subsequently, augmentation bone cements have incorporated Calcium Biphosphates as vital part of its components to increase the biocompatibility with osseous tissues. Minimally invasive percutaneous techniques such as Vertebroplasty and Kyphoplasty have been developed to reduce surgical impact on patients, but in turn have been reported undesirable effects as extravasations of the cement outside of the planning target volume due to the compression of the internal bone fluids or other tissues. An in-situ variable that helps favoring of the PMMA polymerization process is the temperature; however, heat may bring deleterious effects. On the methodology, an assay was addressed varying the Hydroxyapatite HAp concentration in the bone cement. Also, the cement processing was modified by setting water as a vehicle for particle dispersion. The ratios of HAp/PMMA concentrations were: 0.00000, 0.02167, 0.09062, 0.16619 and 0.50000 mixed in PMMA and liquid catalyst and monomer. The thermal profiles were measured during polymerization and analyzed. Nuclear magnetic resonance NMR analysis was carried out on the polymerization process in an aqueous state to monitor the H-H₂O proton signal. As results, an increasing in the cement hardness time was found in the proportion of the HAp- concentration. The highest τ polymerization time was found for the x₅ concentration and the signal from the water trapped in the HAp amorphous lattice was determined around ~5 ppm in the ¹H NMR spectra.

Keywords: PMMA-Hydroxyapatite system, thermal profile, proton H-H₂O signal NMR

5.1. Introduction

There is currently a high number of bone cements applied to minimally invasive surgical procedures. Most of these bone cements are based on poly-acrylic substances such as Poly (Methyl Methacrylate) also known as: PMMA, diffused in biophosphate compounds' matrix such as Hydroxyapatite (HAp). The cement presents biomechanical properties similar to porous bone tissues and present biocompatibility (HIRSCH, ROSENSTEIN, MEDICH, MARTEL & HIRSCH, 2009; LEGEROS, LIN, ROHANIZADEH, MIJARES & LEGEROS, 2003; KLIMO & SCHMIDT, 2004). Orthopedic procedures such as Vertebroplasty and Kyphoplasty are widely used, although they continue to present certain limitations in relation to problems associated with extravasation due to the unbalance between internal and external pressure during the development of the procedure. Other manifestations at the cellular level are present, such as: thermal necrosis due to the energy release during polymerization, chemical necrosis due to the excesses of residual monomers, poor adhesion to the cement-bone interface, among others. The goal of the use of these cements is to join the fractured parts and recover their mechanical stability (GEORGY, 2008; GERSZTEN, 2007; GUERRA, HERNÁNDEZ, & SANTOS, 2010). Therefore, it is highly essential that its biomechanical properties are close to the osteolytic bone. In the case of Kyphoplasty, it is also desired to anatomically recover the structure and make a therapeutic contribution in reducing pain (GEORGY & WONG, 2007).

It is essential to have the chemical understanding of the polymeric structures that are formed in order to solve the problems presented by the bone cement implants, found in the biomedical applications. Many studies of biopolymer characterization have been developed in recent years using techniques of Nuclear Magnetic Resonance (NMR) and Mass Spectrometry (MS) (MIRAU, 2005; MONTAUDO, 2002). The conjugation of both techniques has revealed the naturalization of polymer chains, their component groups and/or end-groups than kinetically interacting among them (GIORDANENGO, *et al.*, 2009). The kinetic' study in the aqueous state of the bone cement components based on PMMA-HAp allows to understand the structural dynamics of these compounds that with other techniques such as XRD (*X-Ray Diffraction*) or FTIR Spectroscopy (*Fourier-transform Infrared Spectroscopy*) is not easy to observe due to the complexity of the polymer chains and to the HAp polycrystallinity (FADLI, AKBAR, PUTRI, PRATIWI, &

MUHARA, 2014; YUKSELA, BAYKARA, SHIRINZADE, & SUZEN, 2011).

The copolymer blocks that are randomly distributed in the PMMA are structurally dependent on parameters such as: molecular weight distribution, chemical nature of the functional groups and end-groups, the randomness of the copolymers and the balance between the hydrophobic and hydrophilic segments. Those are the essential aspects in the study of these bioactive glasses (HAMLEY, 2005). On the other hand, the analyses of the branches and/or end-groups provide vital information to greatly understand the polymerization processes of the material. In the case of PMMA, these end-groups are associated with the initiators of the polymerization. Polymerization processes giving rise to secondary reactions, involving residual reagents which do not interact with the primary polymerization reactions and produce homopolymers, further to the same existing copolymers. The NMR is an analytical technique that allows the structural characterization of the polymers in the aqueous phase and their possible coupling. However, there are two fundamental problems in the use of this technique for the analysis of these materials. The first one is due to sensitivity because it is very low compared to other analytical techniques. Second, the analysis of the ^1H spectrum is very complicated due to signal overlap. One way of reducing the drawbacks of sensitivity in the analysis of the ^1H NMR spectrum is obtained by using the ^{13}C NMR spectrum. However, when the purification of the sample is not optimal, due to the presence of impurities, monomers or residual initiators where it is necessary to overcome this difficulty using multidimensional NMR experiments (RINALDI, 2004). Characterization studies made by R. Giordanengo *et al.* (GIORDANENGO, *et al.*, 2009), in which the copolymeric system MAA- MMA and the NMR techniques conjugated with MS and MS/MS spectrometry were used, found a reason for the removal of water and methanol-associated units of MAA in the co- oligomeric branches of the main chain. The random nature of this copolymer, based on typical dissociation reactions, reveals how extremely useful is the application of the NMR spectrum and MS spectrometry techniques.

In addition, the Hydroxyapatite HAp has been investigated extensively. This substance is naturally found in the bony tissues. A large number of studies have shown hygroscopic characteristics in this substance that manifests water absorption probably by the dipolar coupling detected by Klimavicius *et al.* (KOLMAS, *et al.*, 2011; KLIMAVICIUS, KAREIVA, & BALEVICIUS, 2014). In this work, the NMR spectrum shows a significant

signal of the hydroxyl groups (OH). In spite of this, it is feasible to appreciate a less intense, but very close signal in the chemical shift. It may make reference to the presence of the water in the polycrystalline lattice. The analysis described by this author suggests formation of dipole moments in the HAp lattice (by couplings possibly depending on internuclear distances between the ^1H of the OH^- and ^{31}P) and as consequence dipole-dipole interactions between the HAp and the H_2O , thus revealing the possible reason for its hygroscopic nature, since the dipole water feature favors this type of interactions (KLIMAVICIUS, KAREIVA, & BALEVICIUS, 2014).

One of the key aspects to develop optimal bone cement is directly related to the most adequate proportions of HAp in relation to PMMA since during the mixing of these two compounds it is clear that a process of diffusion and auto-diffusion occurs. Already, in some experiments, the polymerization process provides the peaks of maximum temperature. It has been reported peaks reaching almost $60\text{ }^\circ\text{C}$ (COSTA & CAMPOS, 2008).

Our hypothesis is based on taking advantage of the HAp's hygroscopic nature to reduce the exothermic effects in the polymer. The segregation between the polymer segments and the water trapped in the HAp lattice will increase in the polymerization time. Diffusion between the two basic components of the PMMA-HAp cement is slower, *i.e.*, the polymerization time can be extended, thus the energy dissipation in the form of heat is higher due to segregation reactions between copolymeric segments and water trapped in the HAp lattice. Macroaggregate may present a lower heating on a macroscopic scale.

The goal to synthesize this bone cement is to orthopedic use; however, it could also be used to hold and transport radioactive sources, such as: ^{153}Sm and/or ^{166}Ho . It allows oncological treatments, *in situ*, in patients with advanced metastatic state (DONANZAM, CAMPOS, DALMÁZIO, & VALENTE, 2013; DONANZAM B. A., 2012; MACEDO, 2005). Therefore, it is imperative that this material acquires optimum porous properties in order to be introduced into bone regions where metastases are present. A greater presence of HAp in the cement improves the formation of pores that are not present in the PMMA (LEGEROS, LIN, ROHANIZADEH, MIJARES, & LEGEROS, 2003).

5.2. Materials and Methods

5.2.1. Bone cement synthesis.

HAp Synthesis. The HAp was synthesized by the sol-gel method according to Donanzam *et al*, and Legeros *et. al* (DONANZAM, CAMPOS, DALMÁZIO, & VALENTE, 2013; LEGEROS, LIN, ROHANIZADEH, MIJARES, & LEGEROS, 2003; CAMPOS PI 0605721-7 A2, 2006). The reagents used for the HAp synthesis were 3.937 g of calcium nitrate ($\text{Ca}(\text{NO}_3)_2 \cdot 4\text{H}_2\text{O}$), 0.69 mL of phosphoric acid (H_3PO_4), 1 up to 2 mL of methanol CH_3OH as a catalyst for starting reaction and deionized water as solvent in excess. After mixing the components, the solution was rested for 24 h in a closed beaker. Precipitation, nucleation and formation of colloids had occurred. Subsequently the sample was heated in an oven. The temperature started at room temperature ramped to 80 °C at a rate of 0.306 °C·min⁻¹, holding 360 min at the 80 °C isotherm, subsequently ramped to 100 °C at the rate of 0.333 °C·min⁻¹ holding 720 min at 100 °C isotherm. At the calcinations, the sample was heated from room temperature to 720 °C at a rate of 6 °C·min⁻¹, following by a 60 min at 720 °C isotherm. After cooling, the HAp samples were macerated to powder.

PMMA-HAp composite preparation. HAp powder was mixed in different proportions to PMMA in its powder presentation. The composite was prepared in cold based (non-radioactive) mixing PMMA ($[\text{CH}_2\text{C}(\text{CH}_3)(\text{CO}_2\text{CH}_3)]_n$), HAp [$\text{Ca}_5(\text{PO}_4)_3(\text{OH})$]. Both PMMA and the instruments were cooled previously. The mixture was stirring. PMMA-HAp system was prepared with PMMA's micro-spheres copolymer mixed to the monomer Methyl Ethyl Methacrylate (MMA). Acetone was used in other mixtures as the catalyst in the polymerization process and the dissolution medium of the system.

Sample discrimination. The samples were prepared in accordance with the following concentrations [x_n , with $n = 1, 2, 3, 4, 5, 6$], such that $x_1 = 0.00000$, $x_2 = 0.02167$, $x_3 = 0.09062$, $x_4 = 0.16619$, $x_5 = 0.50000$ and $x_6 = 1.00000$. The x_n is a value corresponding to x in the following system $(1-x)[\text{CH}_2\text{C}(\text{CH}_3)(\text{CO}_2\text{CH}_3)]_n - x[\text{Ca}_5(\text{PO}_4)_3(\text{OH})]$ or $(1-x)\text{PMMA} - x\text{HAp}$.

5.2.2. Macroaggregate thermology

Low-resolution thermology experiments were performed using a TD-880 ICEL digital thermometer with K-type thermocouples and an accuracy of 0.1 °C. The energy release as the heat of the bone cement was monitored during its period of polymerization using an RS232 Data logger data acquisition and a communication interface. The thermology of the samples, x_n of $n = 1$ to 5, were analyzed. Each powder sample had a total mass of 2.5 grams and was mixed with its monomer in excess, about 3 mL per sample. The mixtures were made in a sterile silicone mold to facilitate the unmold of the cement from the vessel after the experiment was developed. The design of the specimens was defined by a cylindrical geometric factor where L represents the height of the cylinder and D the diameter. In the cement aqueous phase, the thermocouple was introduced in the center of the cylinder to guarantee the greatest possible thermal contact.

5.3. Results and Discussion

In Figure 5.1(a), the thermograms showed a critical maximum temperature of T_c , in which the cement begins its cooling process by heat transfer to the medium. The peak temperature basically indicated the presence of an exothermic process in which thermal energy from the polymerization, based on PMMA's chemical reactions, has been released macroscopically. It can easily be seen that this exothermic peak has two tendencies. The first is associated with the no-linear dependence of the energy transferred to the mold in function to the macroaggregate HAp concentrations, since T_c begins to decrease with the increase in the HAp concentration on the system. And the other characteristic is due to the time shift of the exothermic peak in function of the increase of the HAp in the system. At the same starting time in which the components are mixed, the chemical potentials related to the bonds, forming the polymer chains, are activated by the chemical mediators in which the monomer is dissolved. These chemical reactions can be studied by kinetic parameters that help determining the activation energy of the polymerization process. In our experiment, there was no such control of these kinetic factors, but qualitatively it is possible to make an approximation based on the fact that the chemical energy of the bonds in the polymer must be proportional to the thermal energy absorbed by the external medium to the cement. It is not possible to assure that the thermal conductivity factor κ' in this process is equal to the cooling produced by the absorption of heat by thermal contact

with an external source as basically described by Newton's cooling law. But it is useful to make an approximation by making use of this natural law in order to approach the finding of the time τ , in which most of the chemical reactions in the polymer have occurred, as shown in Fig. 5.1(b), and described by the following equations:

$$y = A + B \cdot \exp(\kappa'' \cdot t) \quad (1)$$

in which y is temperature, in °C, A and B are constants, κ'' is the thermal conductivity factor, and t is the time from starting to τ (polymerization time in which T_c occurs) applied to the polymerization process. And,

$$y = C + D \cdot \exp(-\kappa' \cdot t) \quad (2)$$

in which y is temperature, in °C, C and D are constants, κ' is the thermal conductivity factor, t is the time from τ (critical temperature T_c) to the cooling time (room temperature).

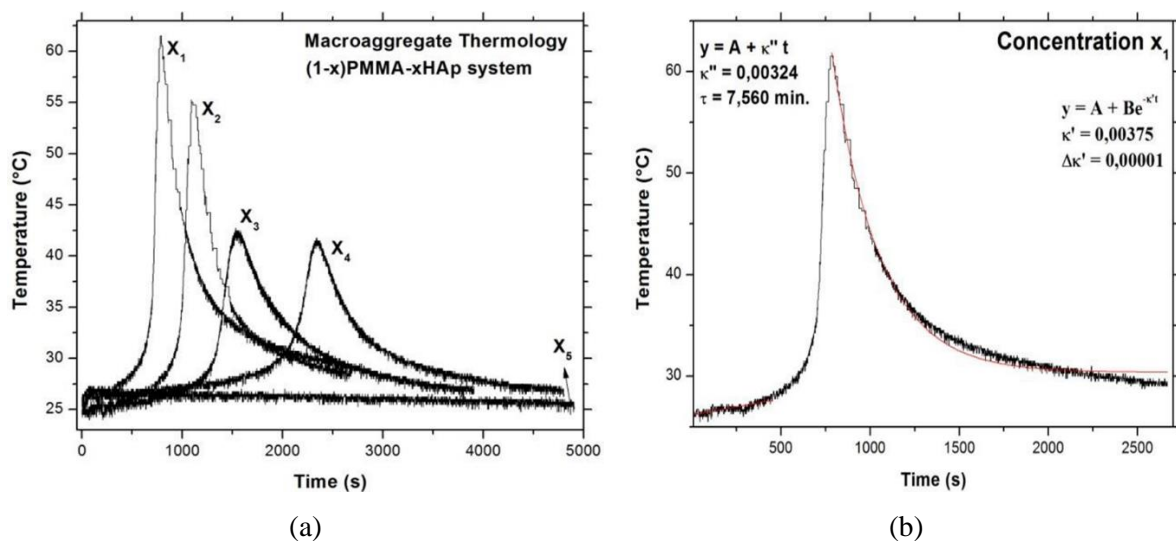


Figure 5.1 Shows the change in temperature as a function of time for each of the samples. Macroaggregate thermology in the bone cement. (a) Thermal profiles varying x_n in the (1- x)PMMA-xHAp system. (b) Fit exponential curve for the x_1 concentration.

The adopted empirical model was based on a hollow cylinder, where the thermocouple was concentric to the main axis of the cylinder. The heat transfer occurs radially. In the Table 5.1, the different critical temperatures are presented and in particular an increase of

the polymerization time can be observed as the concentration of the HAp in the cement increases, being maximum for the concentration x_5 . The τ time for the biomedical application is the limit of time in which the cement presents some fluidity or malleability. The clinical practice indicates that after this time the moisture could no longer be injected because it has reached maximum stiffness.

Table 5.1 Viscous phase polymerization time of the cement based in the (1-x)PMMA- xHAp system are numbered with Roman numerals.

x_n	T_c [°C]	Factor κ' [W·m ⁻¹ ·K ⁻¹]	Polymerization Time τ [min]	Factor κ'' [W·m ⁻¹ ·K ⁻¹]	Macroaggregate Mass [g]	L [mm]	D [mm]
x1	61.50	0.00375	7.560	0.00324	4.05260	45.40	10.70
x2	55.25	0.00399	11.666	0.00283	4.28560	41.95	10.80
x3	42.75	0.00188	17.059	0.00214	4.22150	36.80	10.95
x4	41.75	0.00124	27.159	0.00222	4.29452	36.05	10.60
x5	27.25	-----	undetermined	-----	2.93200	22.55	11.05

diameter of the contact area $d = 2.65$ mm.

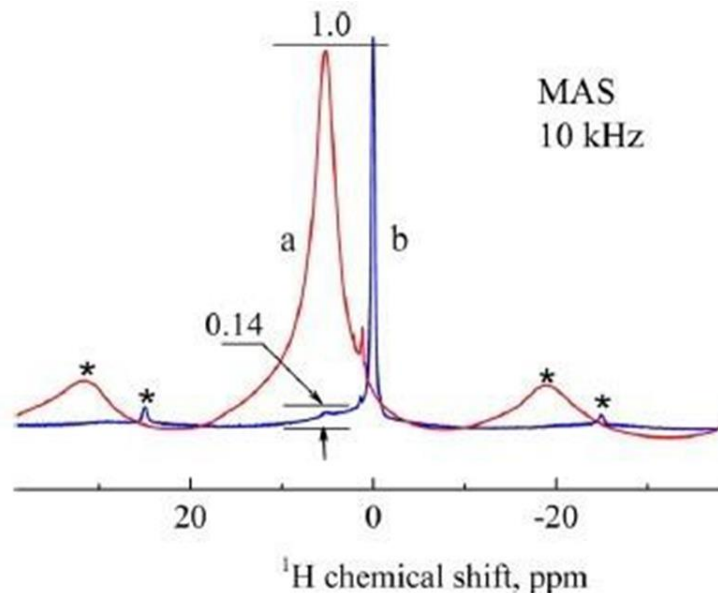


Figure 5.2 ¹H MAS NMR spectra of ACP-CaHA (red) and nanostructured CaHA (blue). Taken from the reference (KLIMAVICIUS et al. 2014).

In Fig 5.2, the ¹H MAS NMR spectra of HAp is presented. One of them was amorphous and the other nanostructured, besides both were analyzed by NMR. In essence in this figure, it is shown that near the signal of the hydroxyl structural groups there is a much

smaller signal associated with the water trapped in the nanostructured network of HAp ~ 5 ppm. For the amorphous HAp the signal of the absorbed water is much greater than the hydroxyl groups. The presence of water in the HAp favors the segregation between the two components due to the hydrophobic nature of PMMA. A higher concentration of HAp would be translated as a temporary inhibitor of the polymerization of the segments. This result is in line with the increase in the polymerization time found in the thermograms.

5.4. Conclusion

Bone cements based on PMMA-HAp have been used for different biomedical applications including bone restoration. The nature of the material plays an important role in the different potential applications of this cement. For oncological and radiotherapeutic use *in situ* it is essential that the living tissues can diffuse through this material. Accordingly, it is imperative that it holds large porous and that its polymerization time be clinically practical, *i.e.* relative to the time of the clinical procedure, about 20 to 30 minutes. Nuclear coupling between the phosphorus atoms ^{31}P with OH groups (Hydroxyl) produces dipole moments in the HAp that facilitate the dipole-dipole interaction with the water molecules, which generates a gradual absorption of water in the amorphous polycrystalline lattice.

5.5. References

- CAMPOS, T. P., & MACEDO, R. D. (2006). *Brasil Patente nº PI 0605721-7 A2*.
Obtido de <http://www.inpi.gov.br>
- COSTA, I. T., & CAMPOS, T. R. (2008). Investigação do perfil térmico de cimento ósseo para radiovertebroplastia. *Congresso Brasileiro de Engenharia Biomédica*. Salvador- BA.
- DONANZAM, B. A. (2012). *Biocerâmicas com Ho-166 e Sm-153: síntese, caracterização e avaliação dosimétrica em Radiovertebroplastia* (Dissertação). (UFMG, Ed.) Belo Horizonte, Minas Gerais, Brasil: UFMG.
- DONANZAM, B. A., CAMPOS, T. P., DALMÁZIO, I., & VALENTE, E. S. (2013). Synthesis and characterization of calcium phosphate loaded with Ho-166 and Sm-153: a novel biomaterial for treatment of spine metastases. *J Mater Sci: Mater Med*, 24, 2873-2880.

- FADLI, A., AKBAR, F., PUTRI, P., PRATIWI, D. I., & MUHARA, I. (2014). Hydroxyapatite Powder Prepared by Low Temperature Hydrothermal Method from Sea Shells. *The 1st Conference on Ocean, Mechanical and Aerospace*, (págs. 24-29)
- GEORGY, B. A. (2008). Metastatic spinal Lesions: State of the art treatment options and future trends. *AJNR Am. J. Neuroradiol.*, 29, 1605-1611.
- GEORGY, B. A., & WONG, W. (2007). Plasma-mediated radiofrequency ablation assisted percutaneous cement injection for treating advanced malignant vertebral compression fractures. *Am. J. Neuroradiol.*, 28(4), 700-705.
- GERSZTEN, P. (2007). The role of minimally invasive techniques in the management of spine tumors: percutaneous bone cement augmentation, radiosurgery, and microendoscopic approaches. *Orthop. Clin. N. Am.*, 38, 441-450.
- GIORDANENGO, R., VIEL, S., HIDALGO, M., ALLARD-BRETON, B., THÉVAND, A., & CHARLES, L. (2009). Structural characterization of a poly(methacrylic acid)- poly(methyl methacrylate) copolymer by nuclear magnetic resonance and mass spectrometry. *Analytica Chemical Acta*, 654, 49-58.
- GUERRA, N. B., HERNÁNDEZ, M. L., & SANTOS, R. G. (2010). Acrylic bone cement modified whit hydroxyapatite/vinyl acetate. Mechanical, thermoanalytical characterization and in vitro bioactivity. *Polímeros*, 98-106.
- HAMLEY, I. W. (2005). *Block Copolymers in Solution: Fundamentals and Applications*. Reading, UK: John Wiley & Sons.
- HIRSCH, A. E., ROSENSTEIN, B. S., MEDICH, D. C., MARTEL, C. B., & HIRSCH, J. A. (2009). Polymethymetacrylate and Radioisotopes in Vertebral Augmentation: An Explanation of Underlying Principles. *Pain Physician J.*, 12, 887-891.
- KLIMAVICIUS, V., KAREIVA, A., & BALEVICIUS, V. (2014). Solid-State NMR Study of Hydroxyapatite Containing Amorphous Phosphate Phase and Nanostructured Hydroxyapatite: Cut-Off Averaging of CP-MAS Kinetics and Size Profiles of Spin Clusters. *J. Phys. Chem.*, 118, 28914-28921.
- KLIMO, P., & SCHMIDT, J. H. (2004). Surgical Management of Spinal Metastases. *The Oncologist*, 9, 188-196.
- KOLMAS, J., JAKLEWICZ, A., ZIMA, A., BÚCKO, M., PASZKIEWICZ, Z., LIS, J., KOŁODZIEJSKI, W. (2011). Incorporation of Carbonate and Magnesium Ions

- into Synthetic Hydroxyapatite: The Effect on Physicochemical Properties. *J. Mol. Struct.*, 987, 40-50.
- LEGEROS, R. Z., LIN, S., ROHANIZADEH, R., MIJARES, D., & LEGEROS, J. P. (2003). Biphasic calcium phosphate bioceramics: preparation, properties and applications. *J. Mater. Sci. Mater. Med.*, 14(3), 201-209.
- MACEDO, R. D. (2005). *Radiovertebroplastia para tratamento de neoplasias malignas ósseas da coluna vertebral: avaliação da proposta e da viabilidade*. (Dissertação). Belo Horizonte - Brasil: UFMG
- MIRAU, P. A. (2005). *A practical Guide to Understanding the NMR of Polymers*. Hoboken, USA: John Wiley & Sons.
- MONTAUDO, M. S. (2002). Mass spectra of copolymers. *Mass Spectrom. Rev.*, 21, 108-144.
- RINALDI, P. L. (2004). Three-dimensional solution NMR spectroscopy of complex structures and mixtures. *Analyst Journal*, 129, 687-699.
- YUKSELA, N., BAYKARA, M., SHIRINZADE, H., & SUZEN, S. (2011). Investigation of triacetin effect on indomethacin release from poly(methyl methacrylate) microspheres: Evaluation of interactions using FT-IR and NMR spectroscopies. *International Journal of Pharmaceutics*, 404, 102-109

CAPITULO 6

6. Computational dosimetric evaluation using a radioactive bone cement based on PMMA+HAp with optimal radiological contrast

ABSTRACT

Background: Breast cancer is a disease that affects a large part of the Brazilian female population. In many cases, patients suffer from bone metastasis in the thorax, spinal column and abdominal region. Especially, those metastases developed in the spinal column can produce potential fractures with neurological compromise or reduction of the life's quality of the patient due to chronic pain. Radiovertebroplasty is a treatment that has emerged as an alternative to control bone metastasis with low therapeutic response to conventional treatments such as conformal radiotherapy or Intense Modulated Radiation Therapy - IMRT. **Methods:** In this study, dosimetry in situ of three predominantly negative β -emission sources such as ^{90}Y , ^{166}Ho and ^{153}Sm coupled to a radioactive bone cement (RB cement) based on PMMA+HAp in a 1:1 ratio have been evaluated. Additionally, their radiological response has been quantified by calculating the contrast compared to a lead implant in an experimental vertebral model. Based on radiological images of the vertebra, digitized models were constructed in the code MCNPx. Doses were evaluated in the axial plane (XY) of the implants of the radioactive bone cement simulating the metastasis. The organ at risk (OAR) was the spinal cord. The implant itself on the vertebra was the prescribed tumor volume (PTV). The Sm-153, Ho-166 and Y-90 nuclides were considered distributed in the PTV. **Results:** A therapeutic dose in the implant provided by the radioactive bone cement reached levels above 90% of the volume at 72 Gy for a specific activity of 3 GBq or $\sim 70\text{mCi}$ for the Y-90 coupled to the cement. The source of Ho-166 produces a lower dose than Y-90 but higher than in Sm-153. The spatial dose distribution from radionuclide implants was better than IMRT, with a significant dose reduction in the spinal cord. Beta emitting from Y-90 have a greater range. **Conclusions:** The radioactive cement in a Y-90 implant can potentially favor optimal tumor control and lower side effects in OARs.

Keywords: RB Cement, PMMA, HAp, Radiovertebroplasty, MCNP, Bone Metastasis.

6.1. Introduction

Radiovertebroplasty is a treatment that has emerged as an alternative to control bone metastases with low therapeutic response to conventional treatments such as conformal radiotherapy or IMRT (Intensity Modulated Radiotherapy) (Montaño & Campos, 2019). The use of bone cements based on PMMA (Polymethylmetacrylate) and biophosphates play an important role in the restoration of collapsed vertebrae due to the compression provided by metastases development (Horn, Henn, & Lemole, 2004). In many cases, the aim is the palliative pain reduction (Harrington, 1981; Georgy, 2008; Finlay, Mason, & Shelley, 2005). Despite the fact that the IMRT produces a significant dose sparing in the organs at risk, it remains high for the oncological patient that may develop myelopathies in a long term and have gradual neurological compromise (Ryu, *et al.*, 2003). The administration of systemic $^{153}\text{Sm-EDTMP}$ (Samarium-153-ethylene diamine tetramethylene phosphonate) has produced satisfactory pain reduction in a good number of patients; although, imaging studies performed in a certain population of cancer patients showed regional and in situ recurrences, 3 up to 6 months after treatment (Ashamalla, *et al.*, 2009; de la Calle, González-González, Fornés, & Martínez-Calderón, 2006).

The NRI/UFMG – Research group of Federal University of Minas Gerais proposed and patented the radioactive cement for bone metastasis treatment (Brasil Patente Nº PI 0605721-7 B1, 2006). Hirsch *et. al* (Hirsch, Medich, Rosenstein, Marcel, & Hirsch, 2008) also have explored this ideas, they modeled the dose, the dose rate and the BED in a vertebral bone tissue due to a beta radioactive sources distribution coupled to a PMMA implant in a spherical shape of 1 mm radius. The most important finding in this work was the evaluation of the BED, proposed by Dale (Dale, 1985), correlated to the linear quadratic model (LQ) for a specific α/β cellular response, in which absorbed dose was calculated by Monte Carlo code MCNP v.5, applied to some β^- -emitters such as P-32, Y-90 and Ho-166.

In the radiotherapeutic field, seeds based on I-125 and Pd-103 have been proposed as radioactive sources of interstitial use for prostate cancer. One of the greatest advantages of using this Brachytherapy technique is the facility to deposit the greatest amount of absorbed dose in the tumor, which is known as in situ procedure (Trinidade, Christóvão,

Trinidade, Falcão, & Campos, 2012). Computational simulations performed on highly differentiated tissues using the MCNP-5 (Monte Carlo N-particle V.5) and SISCODES (Computational System for Neutron and Photon Dosimetry by Stochastic Methods) showed a significant dose reduction in the pelvic region with the use of a source of Pd-103 compared to I-125 prostate implants. The study also highlights the requirement to put carefully implants according to clinical protocols (Trinidade, Christóvão, Trinidade, Falcão, & Campos, 2012). Computational resources become an optimal alternative for estimating dose and other radiometric units that are often calculated using empirical dosimetric techniques for dose calculation indirectly such as Thermoluminescence dosimetry (TLD), due to chemical reactions to the polymeric degradation of radiochromic or radiographic films due to the exposure of ionizing radiation fields, among other techniques.

In 2013, Blanda *et. al* to perform neutron activation of bone cement samples based on PMMA and bioceramics in a TRIGA MARK I IPR-R1 research reactor. The characterization of the samples made in this work allowed to obtain activities per milligram in order of MBq.mg⁻¹. The analysis of the contaminants in the calcium biophosphates present in the macroaggregate was demonstrated (Donanzam, Campos, Dalmázio, & Valente, 2013; Donanzam, Bioceramics com Ho-166 e Sm-153: síntese, caracterização e avaliação dosimétrica em radiovertebroplastia., 2012). Using the LQ model and Monte Carlo MCNP v.5 and SISCODES codes, it was possible to determine dose, dose rate and BED (Biological Effectiveness Dose) for permanent implants in a lumbar tomographic vertebral model. In this study, the bone implant composed of PMMA+HAp had a β -decay source of Ho-166. The results showed a significant dose reduction in the organs at risk, especially in the spinal cord. A therapeutic control dose was equivalent to those achieved in conformal radiotherapy and in the IMRT (Donanzam, Bioceramics com Ho-166 e Sm-153: síntese, caracterização e avaliação dosimétrica em radiovertebroplastia., 2012). The activities used in the simulation were the same as those obtained in the neutron activation in the research reactor of 32.5 MBq/mg for the Ho-166.

A possible deleterious effect of the Vertebroplasty procedure is the extravasation of the bone cement outside the planned site. In some patients, extravasation produces thrombosis in the underlying vascular system. Also, the material may invade to the medullary duct

(Hirsch, Medich, Rosenstein, Marcel, & Hirsch, 2008). The use of contrast agents can also produce adverse reactions in some patients. To avoid these adverse effects, it is necessary to optimize the material distribution in the implant covering the vertebral body where the lesion is located. Higher concentrations of HAp can improve the radiological contrast since the attenuation factor is higher for the calcium atoms. Therefore, the application of the contrast agent in the implant procedure shall be reduced or discarded (Montaño, Nogueira, & Campos, Physical distribution and radiological contrast of cements implanted in vitro vertebrae., 2016). The quantification of the radiological contrast of the bone cement must be determined in samples in which the concentration in mass of the biophosphates incorporated in the cement are increased in order to find a suitable imaging. There are many ways to quantify the radiological contrast, qualitatively or quantitatively. Some authors quantify the contrast of an image by defining regions of interest. It leads to a topological analysis that can be made simple or complex depending on the resolution of the image, size and the degree of elements that compose it since they are in turn associated with the density variation of all the elements exposed to the field of radiation, in the radiological case. Currently there are several software that help in the calculation of the contrast in an image based on the gray level histograms of the image under consideration (Seletchi & Duluiu, 2007).

Suetens *et al.* (Suetens, 2009) allows visualizing conceptually and mathematically the contrast as the amplitude of the Fourier Transform (*FT*) in the domain of spatial frequency. In other words, contrast is a difference of the gray levels in a certain region of the image. In the case of a radiological image, the formation of the image and the contrast maintains a close relationship with the attenuation pattern of the object interposed between the source and the radiographic film, in addition to the quality factors of the radiographic film. Despite losing information in the scanning of a radiological image, the manipulation of its data is advantageous to comprehend quantitatively the elements that compose it.

In our study, we calculated the contrast of radiological images of the vertebrae model with bone cement implants. Subsequently, such model was used on the computational dosimetric studies, based on Monte Carlo code MCNPx. The spatial dose distributions were evaluated using three distinct radioactive sources (^{153}Sm , ^{166}Ho and ^{90}Y), with therapeutic potential in performing *Radiovertebroplasty*.

6.2. Materials and methods

6.2.1. The RB cement synthesis

HAp Synthesis. The HAp was synthesized by the sol-gel method according to Donanzan et al and Legeros *et. al* (Donanzam, Bioceramicas com Ho-166 e Sm-153: sintese, caracterização e avaliação dosimetrica em radiovertebroplastia., 2012; Donanzam, Campos, Dalmázio, & Valente, 2013; Legeros, Lin, Rohanizadeh, Mijares, & Legeros, 2003). The reagents used for the HAp synthesis were 3.937 g of calcium nitrate ($\text{Ca}(\text{NO}_3)_2 \cdot 4\text{H}_2\text{O}$), 0.69 mL of phosphoric acid (H_3PO_4), 1 up to 2 mL of methanol CH_3OH as a catalyst for starting reaction and deionized water as solvent in excess. After mixing the components, the solution was rested for 24 h in a closed beaker. Precipitation, nucleation and formation of colloids had occurred. Subsequently the sample was heated in an oven. The temperature started at room temperature ramped to 80 °C at a rate of 0.306 °C.min⁻¹, holding 360 min at the 80 °C isotherm, subsequently ramped to 100 °C at the rate of 0.333 °C•min⁻¹ holding 720 min at 100 °C isotherm. At the calcinations, the sample was heated from room temperature to 720 °C at a rate of 6 °C•min⁻¹, following by a 60 min at 720 °C isotherm. After cooling, the HAp samples were macerated to powder.

PMMA-HAp composite preparation. HAp powder was mixed in different proportions to PMMA in its powder presentation. The composite was prepared in cold based (non-radioactive) mixing PMMA ($[\text{CH}_2\text{C}(\text{CH}_3)(\text{CO}_2\text{CH}_3)]_n$), HAp [$\text{Ca}_5(\text{PO}_4)_3(\text{OH})$]. Both PMMA and the instruments were cooled previously. The mixture was stirring. PMMA-HAp system was prepared with PMMA's micro-spheres copolymer mixed to the monomer Methyl Ethyl Methacrylate (MMA). The samples were prepared in accordance with the following concentrations [x_n , with $n = 1, 2, 3, 4, 5$], such that $x_1 = 0.00000$, $x_2 = 0.02167$, $x_3 = 0.09062$, $x_4 = 0.16619$, $x_5 = 0.50000$. The x_n is a value corresponding to x in the following system $(1-x)[\text{CH}_2\text{C}(\text{CH}_3)(\text{CO}_2\text{CH}_3)]_n-x[\text{Ca}_5(\text{PO}_4)_3(\text{OH})]$ or $(1-x)\text{PMMA}-x\text{HAp}$. In the case of radioactive bone cement the proportions were given as $(1-x)\text{PMMA}-x\text{HAp}+y^A\text{MHAp}$, where M is the coupled radionuclide.

6.2.2. Radiological Analysis

In vitro anatomical sample preparation. The separation of a section of a pig vertebral

column, in a special cut provided by a meat market, was performed in vitro embed in an equivalent muscle tissue, maintaining anatomically its structure without considering distinct anthropometric characteristics of the model. The structure was immediately cooled to -18 C to reduce the effect of decomposition.

Cement injection. The cement was injected into vertebral models designed in the laboratory drilling the vertebral body with a bent 45° to the midsagittal plane simulating drilling needle Vertebroplasty kit.

Radiological contrast. The X-ray machine used was the BR 100, a transportable model with performance 100 mA and 90 kV. The BR 100 is composed with an X-ray tube sealed and linked to a telescope that is connected to the apparatus column than have an arm which allows depending on the movement necessary adjustment of the distance between tube and film that is studied radiographically. It also has a command table with the control elements necessary for desired voltage and intensity.

According to the radiological techniques, exposure time of 0.50 s, current of 70 mA, voltage of 60 kV and FFD of 85 cm were applied in thoracic vertebrae. After the development processing, films were digitized to study the radiological contrast in each of the vertebrae that was implanted the bone cement. Contrast was evaluated in ROI (Region Of Interest) for all vertebrae. The radiological density of biomaterial was addressed for evaluating the contrast response.

6.2.3. Computational vertebrae models

Images treatment. The images scanned in .jpg format were smoothed and simplified in 5 domains corresponding to the tissues of interest, such as 1. bone tissue with red bone marrow, 2. soft tissue, 3. medullary duct and spinal cord, 4. metastasis bone of mammary origin and 5. bone implant. The ImageJ software was used. The anatomical dimensions of the human vertebrae were conserved assuming a vertebral section of 10.50 x 8.80 x 2.3 cm³. The space outside the vertebra was considered as soft tissue. The size of the voxel was adjusted to the pixel dimensions of the image. The dimensions of the voxels were 0.25 x 0.25 x 0.25 mm³.

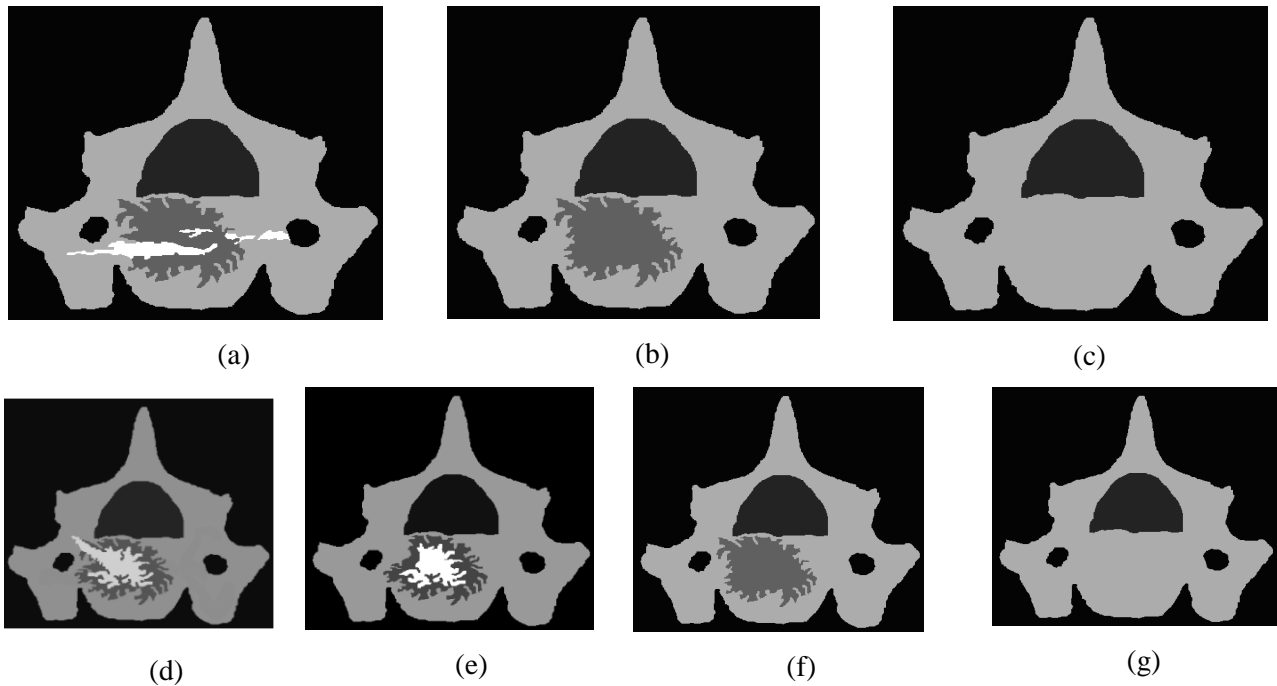


Figure 6.1 XY-planes characteristics of the vertebral models with mammary metastasis. (a) Bone Implant XY-planes for Vert. A between $z = -7$ and $z = 7$. (b) Bone Metastasis XY-planes only for Vert. A for $(-43 < z < -8)$ and $(8 < z < 43)$. (c) Bone tissue only for Vert. A $(-47 < z < -44)$ and $(44 < z < 47)$. (d) Bone Implant XY-planes for Vert. B between $z = -7$ and $z = 7$. (e) Bone Implant XY-planes for Vert. B $(-31 < z < -8)$ and $(8 < z < 31)$. (f) Bone Metastasis XY-planes only for Vert. B for $(-39 < z < -32)$ and $(32 < z < 39)$. (g) Bone tissue only for Vert. A $(-47 < z < -40)$ and $(40 < z < 47)$.

Five universes corresponding to the aforementioned tissues were considered in the context of the MCNP v.6 code (Pelowitz, MCNP6 USER'S MANUAL v.1.0, 2013; Pelowitz, MCNPX USER'S MANUAL v.2.7.0, 2011). Two different cards were defined with the purpose of introducing pores in the vertebral model, in the universe of bone tissue. Each voxel in the bone held a pore of spherical symmetry completely filled with red bone marrow and the excess defined as bone tissue. This novelty in the computational model improved the density of the bone tissue bringing it closer to the real situation. Another important model characteristic was the ability of simulating metastasis of mammary origin in the vertebral body studying the dosimetry response of possible infiltrations in the medullary duct.

The implant of the radioactive bone cement was distributed according to the

radiological image where empirically 1,2 g of the bone cement was introduced. In a second modelling, the amount of implant was increased. A greater cavity with a mass 6,77 g was simulated for the insertion of the bone implant material. The dose was evaluated in the plane of the bone implant, that is, at $z = 0$, exactly where the cement was inserted. In summary, Fig. 6.1 shows the XY-plane sections depicting the vertebral 3D models. The nomenclature *Vert. A* was adopted for the first model and *Vert B* for the second model. Both models were constructed with an array of 95 planes in the Z direction. Figures 6.1(a), 6.1(b) and 6.1(c) are the characteristic planes of the *Vert A* vertebral model. Figures 6.1(d), 6.1(e), 6.1(f) and 6.1(g) are the characteristic planes of the *Vert B* vertebral model.

TC vertebral lumbar model. A tomographic model of a lumbar section of $10.80 \times 9.24 \times 8.76 \text{ cm}^3$ composed of 45 planes in Z direction was prepared. The voxel size was $1.2 \times 1.2 \times 1.2 \text{ mm}^3$. This model was designed without bone metastasis as in the previous models but the volume studied covers a wide region with organs at risk in which it is possible to estimate the dose depending on each of the three radionuclide sources.

Specific activity required. the specific activity for 1 mg of the sources activated by Donanzam *et. al* (Donanzam, Campos, Dalmázio, & Valente, 2013) was used, for the estimation of the deposited dose in all the models.

6.3. Results

6.3.1. Radiological contrast

The digitized and smoothed radiological images were presented in Fig. 6.2. The reference image with lead implant Pb was also depicted in Fig 6.2(a). The image with PMMA implant was depicted in Fig. 6.2(b). The Fig 6.2(c) represents the implant in the proportion $0.9\text{PMMA}+0.1\text{BaSO}_4$. Fig. 2(d) represents the image with PMMA+HAp implant at 1:1 ratio. In all experiments, one gram of the respective radioactive PMMA+HAp substances were implanted.

The radiological contrast can be quantified based on the profile of gray levels for each collection of points in space (x, y), shown in Fig. 6.3. It is possible to reduce the complexity of the image analysis using a specific ROI, equivalent to all imagens. The

mathematical elements indicate that the ROI is a topologically defined area for all the points (x, y) where it is probable to find the implant which is associated with a set of intensities of grays (k_x, k_y) . Each point in our image $I(x, y) \sim \tilde{I}(k_x, k_y)$ is transformed into the space of the frequencies associated with the gray levels. On the other hand, the number of gray levels is adjusted computationally to the weight of the image determined by the configuration established in the scanning device.

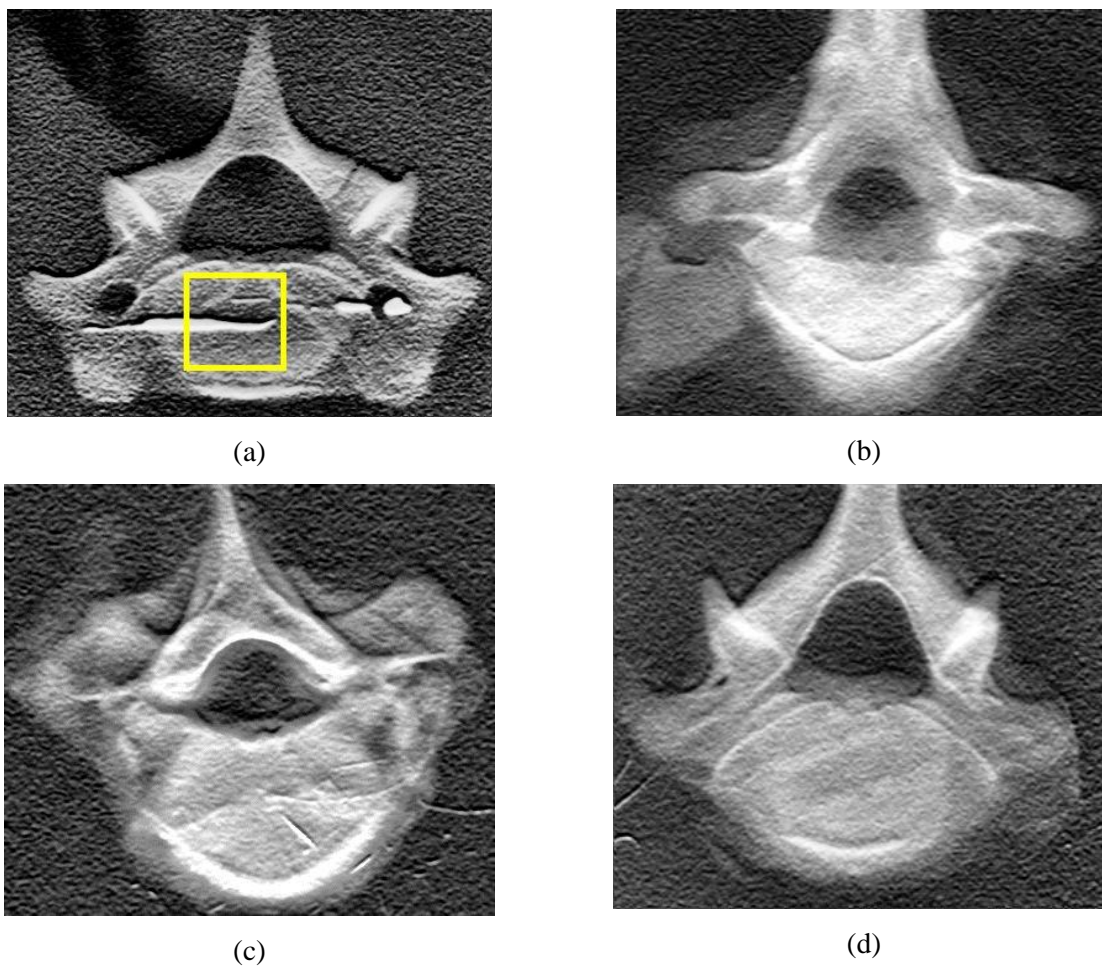


Figure 6.2 Radiological images of four vertebral models. In (a) the vertebrae have molten lead with ROI defined as 84 pxls x 80 pxls on vertebral body. (b) PMMA injected. (c) 0.9PMMA + 0.1BaSO4 were injected. (d) $x = 0.5$ concentration of the HAp for the bone cement.

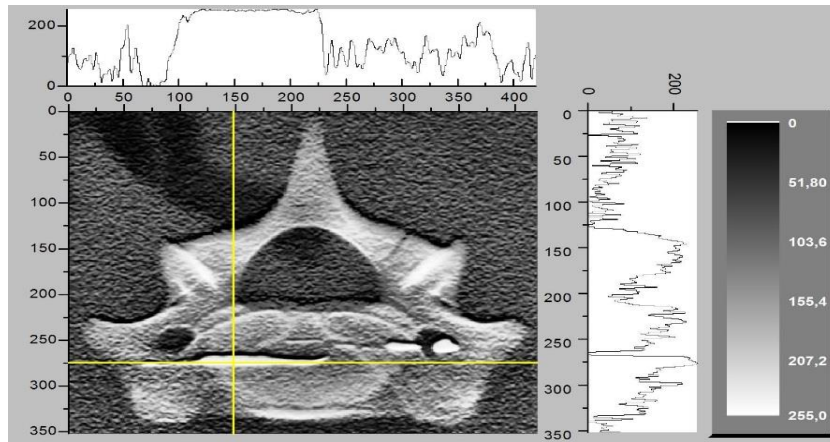
It should be noted that the user can modify the size of the image after the scanning procedure and as a consequence a significant loss of resolution would be likely. The computational size of the images was configured to 8 bits. Therefore, the images were digitally reconstructed with 256 levels of gray. If each profile in the spatial domain is

treated as a function, it could be considered bounded, monotonous and periodic. Therefore, the definition by Suetens (Suetens, 2009) for the contrast of an image would be congruent from the mathematical point of view. In this Fig 6.3. (b), (c), (d), (e) correspond to the 2D FFT (Fast Fourier Transform in 2 dimensions) of the ROI defined in Fig. 2 for each vertebra.

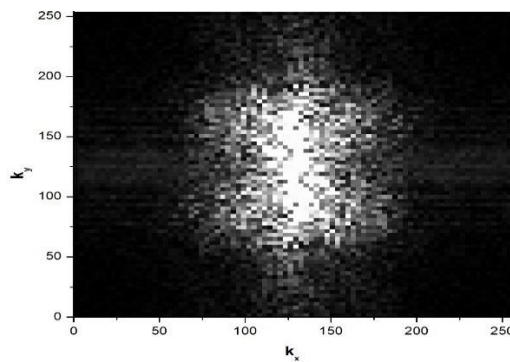
A set of matrices was generated in the calculation of the 2D FFT for each ROI. The surfaces referent to those matrices, corresponding to the amplitude in the Fourier domain of the spatial frequencies, are presented in Fig. 6.4. The surfaces represent the frequency space of the gray levels that make up the image. In this way, considering the definition of Suetens for the contrast of an image, the 2D FTT corresponds to:

$$\tilde{I}(\vec{k}) = \frac{1}{\sqrt{2\pi}} \int_{-\infty}^{+\infty} d\vec{r} e^{-i\vec{k}\cdot\vec{r}} I(\vec{r}) \quad (a)$$

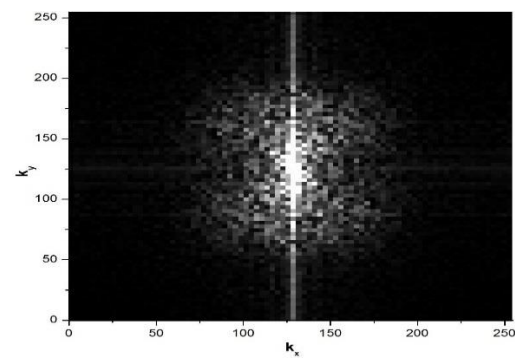
$$I(\vec{r}) = \frac{1}{\sqrt{2\pi}} \int_{-\infty}^{+\infty} d\vec{k} e^{i\vec{k}\cdot\vec{r}} \tilde{I}(\vec{k}) \quad (b)$$



(a)



(b)



(c)

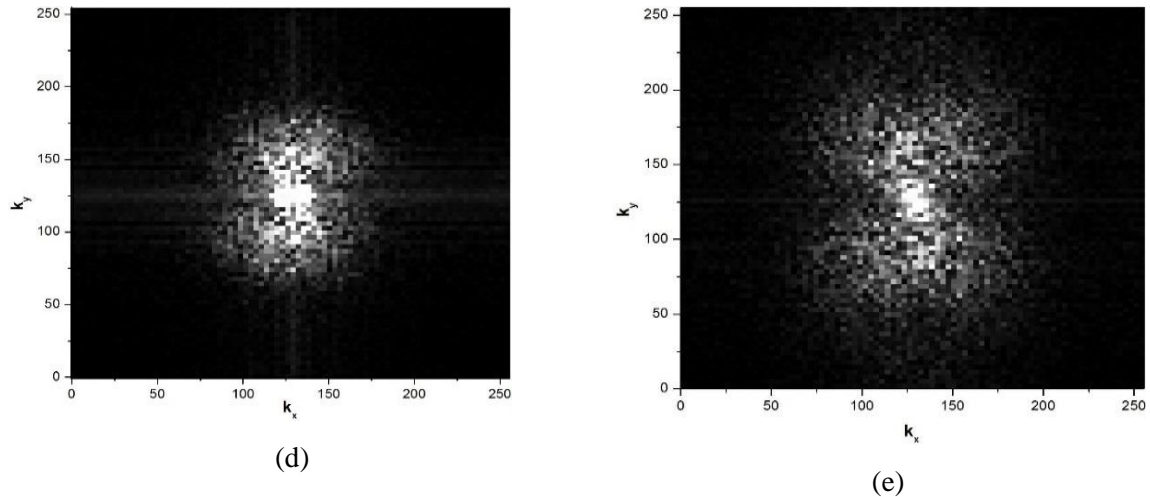


Figure 6.3 The gray-profiles in the spatial domain of the $I(x,y)$ and FFT 2D images of their respective ROIs. Example for a gray profile in (a) straight lines parallel to $x = 0$ and $y = 0$; (b) FFT 2D for ROI with the lead implant; (c) FFT 2D for ROI with PMMA implant; (d) FFT 2D for ROI with the 0.9PMMA + 0.1BaSO₄ implant; and, (e) FFT 2D for ROI with PMMA+HAp implant and 1:1 ratio.

Equation (b) represents the inverse transform which is a function associated with a profile of points in the image space, in which $\vec{r} \rightarrow (x, y)$ and $\vec{k} \rightarrow (k_x, k_y)$ where \vec{k} is the space of spatial frequencies. In addition, $I(\vec{r})$ also depends on the attenuation profile of the X-ray field that impacts the radiographic film after being attenuated by the vertebra and bone implant.

In Fig. 6.4(a), 6.4(b), 6.4(c), 6.4(d), the surfaces of the 2D FFT were obtained by the software Origin 2019b. These surfaces are defined as a subspace of points $S = S(k_x, k_y)$ in the Fourier domain. A possible approximation of these surfaces to a mathematically known surface is the Gaussian adjustment. A Gauss surface fitting the graph of the amplitude of the 2D FFT for the ROI with the lead implant, was presented in Fig 6.4(e). The software performs the best adjustment through a determined number of iterations. The Gaussian adjustment parameters could be set, reducing the standard error. Table 6.1 presents a summary of the analyzes performed for the four different types of implants used of the vertebrae studied.

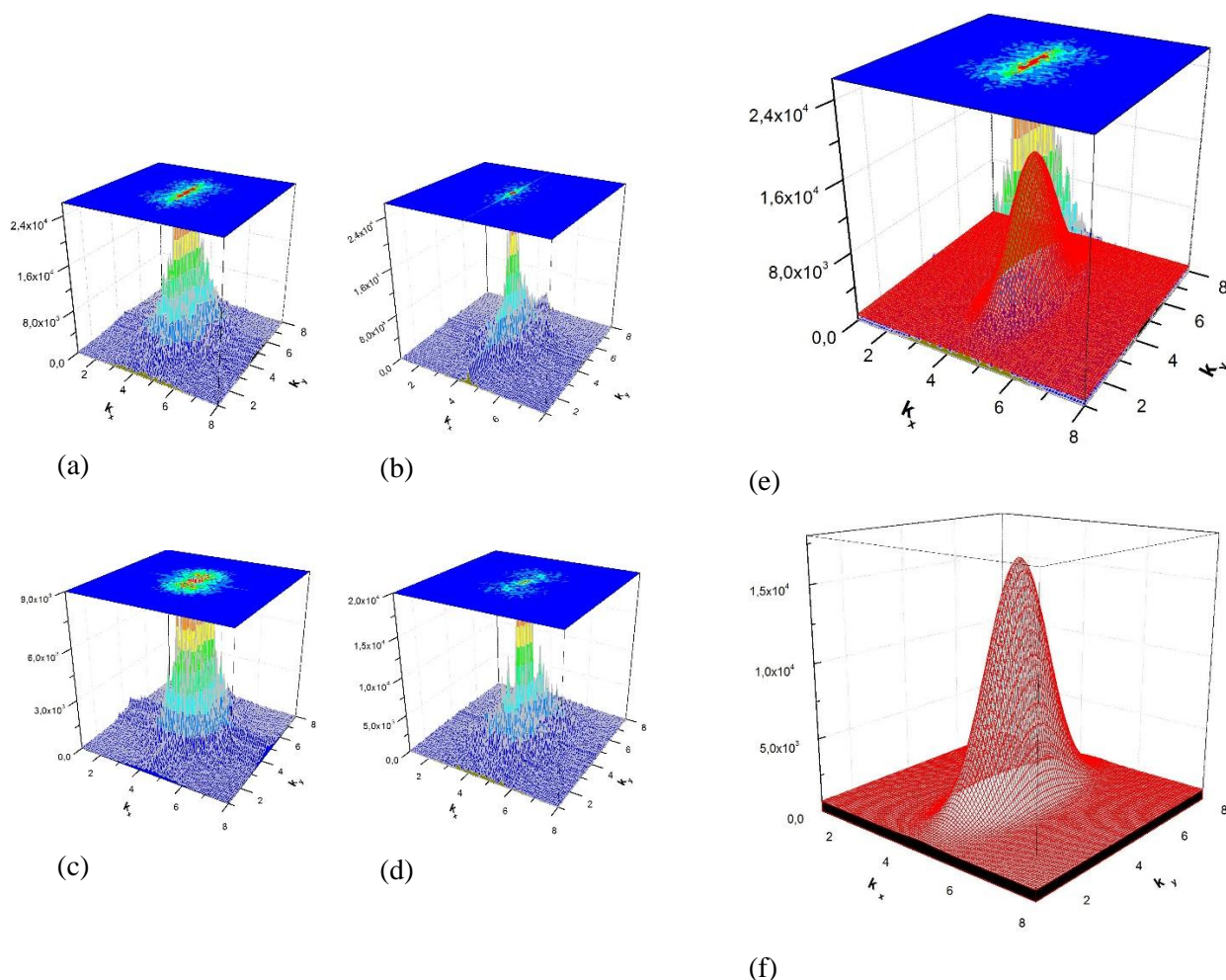


Figure 6.4 FFT 2D curves from ROIs and Gauss surface fit. (a) Plotting Surface of the FFT 2D corresponds to ROI with lead implant. (b) Plotting Surface of the FFT 2D corresponds to ROI with PMMA implant. (c) Plotting Surface of the FFT 2D corresponds to ROI with the 0.9PMMA + 0.1BaSO₄ implant. (d) Plotting Surface of the FFT 2D corresponds to ROI with PMMA+HAp implant, and 1:1 ratio. (e) Gauss surface fit for the lead implant (f) Gauss surface for case (e).

The FWHM (Full Width at Half Maximum) was calculated considering all the statistical parameters of the 2D Gaussian adjustment. This measure of the surface extension would correspond to the radiological contrast of the ROI in the image studied. The extreme values related to all the points that form the Gaussian surface of 2D adjustment were considered. The values in Table 6.1 showed a high contrast in the ROI with the Pb implant as a consequence of its high attenuation factor, thus contributing greatly to the heterogeneity of the image. Such data was taken as reference in the experiment. The contrast of the bone cement of PMMA+HAp was compared to the polymer coupled to the contrast medium

PMMA+BaSO₄. It is easy to notice that their values are very close which would indicate that the use of the contrast medium in the cement could be discarded in the practice of the Radiovertebroplasty implants.

Table 6.1 Evaluation of the Radiological Contrast by means of the FWHM due to the implants.

Testing implants	Standard Deviation σ_x	Error $\Delta\sigma_x$	Standard Desviation σ_y	Error $\Delta\sigma_y$	*SD $\sigma \Delta\sigma = \pm 0,01$	Radiological Contrast FWHM $\pm 0,02$
Lead – Pb	0,425	0,005	1,11	0,01	1,18	2,79
PMMA	0,232	0,003	0,83	0,01	0,86	2,04
0.9PMMA+0.1BaSO ₄	0,418	0,005	0,81	0,01	0,91	2,14
PMMA+HAp (1:1)	0,345	0,005	0,86	0,01	0,93	2,19

$$* \sigma^2 = \sigma_x^2 + \sigma_y^2;$$

6.3.2. Computational dosimetric evaluation of the vertebrae models.

In the previous radiological experiments, the amount of one gram for each of the substances was implanted in the four vertebrae. The dose deposited by one gram of the radioactive implant in the vertebral model was evaluated. The dose deposited was estimated for the β -emission in the vertebra model. The lead implant was assumed as the bone cement coupled with the radioactive source.

The tally *F8 was requested in the input file of the simulation referent to the energy pulses deposited by each bin. The statistical treatment allowed reducing the total variance with a high number of particles for the NPS in the INPUT file. The output file provided the total energy deposited by voxel in units of MeV. In addition, the mass and density of each voxel were presented. The energy spectrum of the beta emissions for each radionuclide was extracted from the computer tool provided by the *Nuclear Regulatory Commission of the United States* (NRC US) or freely by the National Laboratory OAK RIDGE (ORNL) through the Radiological software Toolbox (Rad Toolbox v. 3.0.0 5/1/2014).

The computer tool mentioned above stored complete information on a broad spectrum of radionuclides based on reports from the International Commission on Radiological Protection (ICRP). The beta-particle decay factor for particle for each radionuclide was expressed in particles/decay, the specific activity expressed in [Bq/mg] and the mass from voxel in grams [g]. The absorbed dose was calculated considering the total decay from the

source. The specific activity was chosen in the order of the 3 GBq to reach the range of 70-72 Gy and thus the maximum levels of tolerance to the nearest risk organ were maintained (Spinal cord). Emami *et al.* suggests that for TD 50/5 (Tolerance Dose, the probability of 50% complication within five years) shall be up 73 Gy for the spinal cord (Emami & et al., 1991).

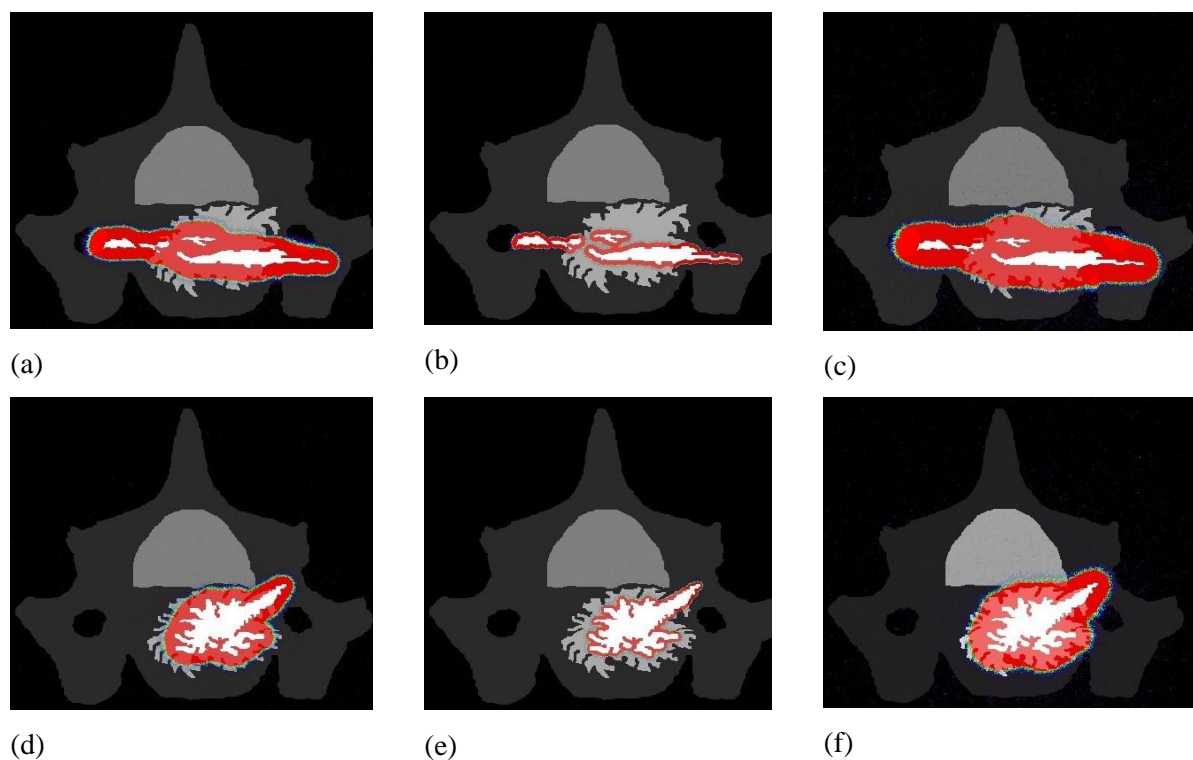
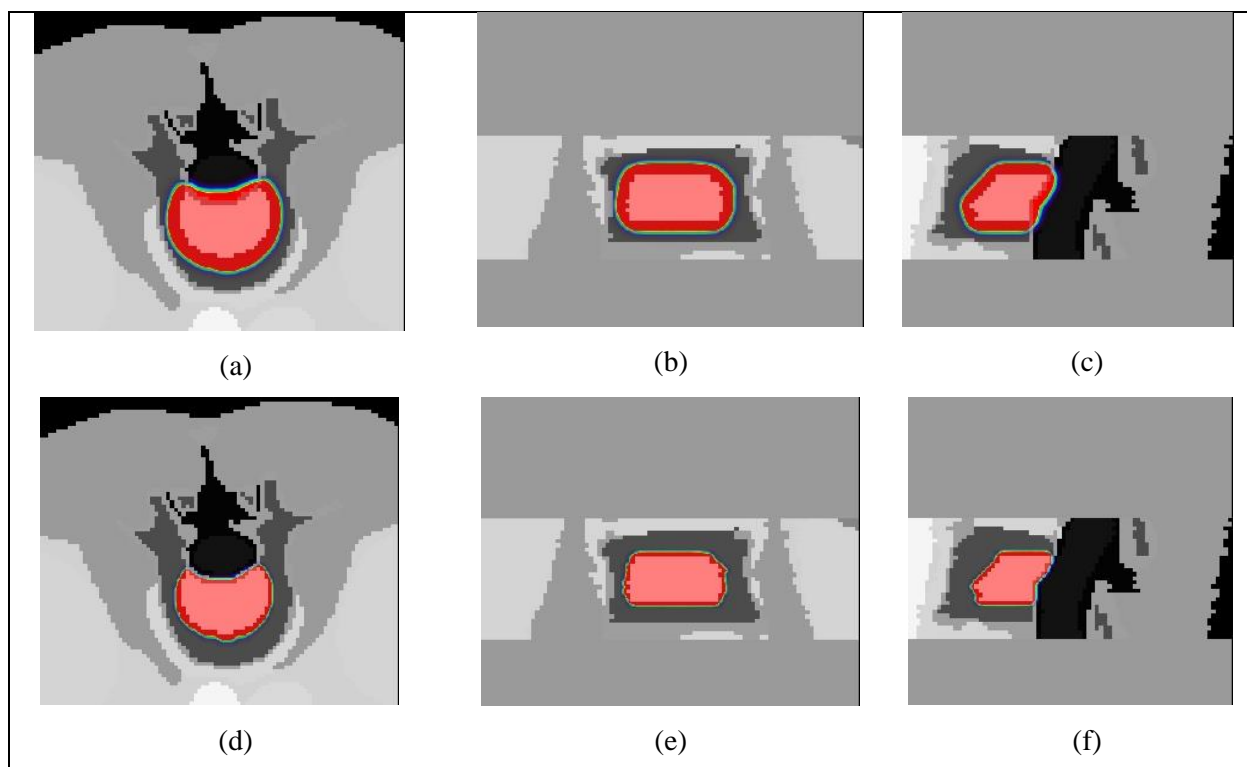


Figure 6.5 Computational dosimetric evaluating in the vertebrae models. Dose spatial distribution for Vert A model: (a) Ho-166 coupled source (b) Sm-153 coupled source (c) Y-90 coupled source. Dose spatial distribution for VertB model: (d) Ho-166 coupled source (e) Sm-153 coupled source (f) Y-90 coupled source. The dose for the β -emission for all models was limited to 72 Gy.

The model *Vert A* simulated a bone implant with a mass of 1.20 g, mimicking the radiological experiment, shown in Fig. 6.5(c) with the BC- Y^{90} (Bone Cement) shows a large spatial dose distribution, although it does not cover 100% of the metastasis' volume. In fig 6.5(a) BC- Ho^{166} presents a better performance in the spatial dose distribution with respect to BC- Sm^{153} , as shown in Fig. 6.5(b). bases on the simulations, it can be concluded that the amount of cement implanted in *Vert A* produces the undesirable therapeutic effect with respect to the dose deposition since it held a poor spatial distribution. *The Vert B* simulated a bone implant with a mass of 6.77 g being an event compared to the previous one. almost 6 times greater than the bone implant used on the others. In Fig 6.5(f) with the

BC-Y⁹⁰. a large spatial distribution was reached although the medullary canal partially presents a higher dose near the tolerance limit. In this case, the dose deposited by the implant covers almost 100% of the metastasis' volume. In Fig. 6.5(d) with the BC-Ho¹⁶⁶, the spatial dose distribution held lower cover of the PTV; although, qualitatively it is possible to affirm that the source has an acceptable therapeutic behavior. In none of the cases the use of BC-Sm¹⁵³ *in situ* reaches the full cover with a therapeutic dose that guarantees the tumor control of the metastasis. The reference dose (D_{ref}) was 72 Gy.

Also, a lumbar tomographic model was used in which the implant was located in the central space of the vertebral body. The bone cement used in these experiments was 0.9PMMA+0.1BaSO₄ coupled with the radioactive sources. The amount of implanted material was 7,52 g. The absorbed dose from the chosen sources was evaluated. The transverse, coronal and sagittal planes are presented In Fig 6.6(a), 6.6(b), 6.6(c), respectively, with their center at the origin. The BC-Ho¹⁶⁶ partially covered the volume of the vertebral body and in a lesser extension partially deposits the reference dose in the medullary duct. In Fig 6.6(d), 6.6(e), 6.6(f), the BC-Sm¹⁵³ almost completely deposits the reference dose in the implant. The probability of deposition of the maximum tolerance dose TD 50/5 of 72 Gy was too small in the spinal cord.



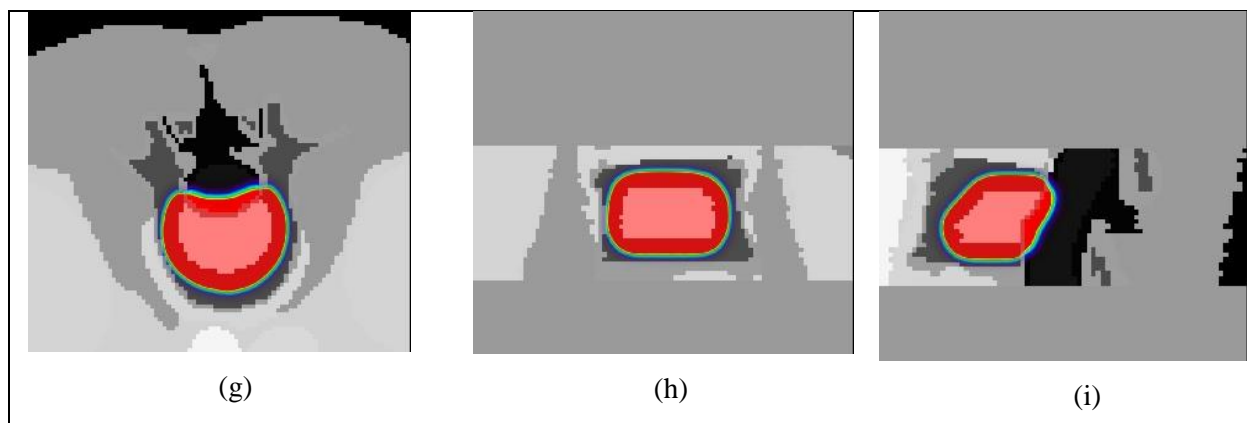


Figure 6.6 Dose spatial distribution for lumbar vertebral model. Ho-166 coupled source: (a) Transverse XY-plane (b) Coronal XZ-plane (d) Sagittal YZ-plane. Sm-153 coupled source: (a) Transverse XY-plane (b) Coronal XZ-plane (d) Sagittal YZ-plane. Y-90 coupled source: (a) Transverse XY-plane (b) Coronal XZ-plane (d) Sagittal YZ-plane.

In Fig 6.6(g), 6.6(h), 6.6(i), the BC- Y^{90} distributed in a large volume of the spinal cord increasing the risk with respect to the TD 50/5 = 72 Gy. Treatment with this source is more conservative. Thus, the possibility of finding a better therapeutic response to metastasis control grows.

The dose-volume histograms is presents in Fig.6.7. The volume affected by D_{ref} used in each organ can be compared. For both the risk organs (OAR) and for the planning target volume (PTV), the D_{ref} was set based on the maximum radiotoxicity that the spinal cord and bone tissues can receive. From the radiotherapeutic point of view, regardless of the radionuclide used, this may be acceptable for PTV if at least 90% D_{ref} is reached. The dose of 65 Gy meets the previous condition and according to Emami *et. al* (Emami & et al., 1991), TD 50/5 is 65 Gy as a reference value for the bone. In Fig. 6.7(a), only the BC- ^{90}Y implant deposited a higher dose into the spinal cord in *Vert B* model. The maximum committed volume that received the 72 Gy is less than 1.60% of the total volume of the spinal cord (OAR 1). Therefore, the toxic dose only reaches the region of the dura mater in the spinal cord, thus reducing the probability of developing myelitis.

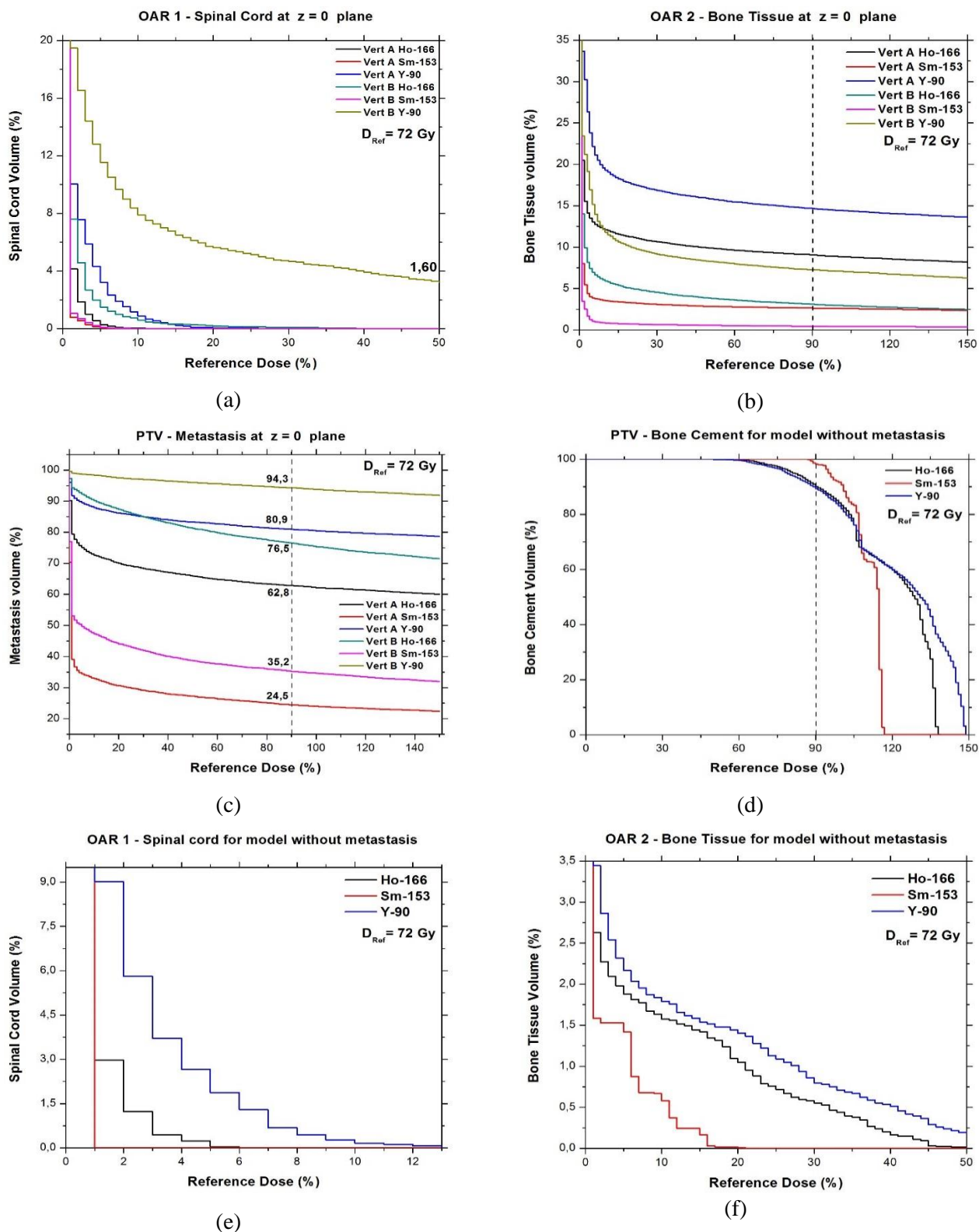


Figure 6.7 Dose-Volume Histograms for PTV and OAR in vertebral models with 90% $D_{ref}=72$ Gy. (a) OAR 1 for spinal cord at $z = 0$ in Vert. A and Vert. B (b) OAR 2 for bone tissue at $z = 0$ in Vert. A and Vert. B (c) PTV for metastasis at $z = 0$ in Vert. A and Vert. B (d) PTV for bone cement in model without metastasis (e) OAR 1 for spinal cord in model without metastasis (f) OAR 2 for bone tissue in model without metastasis.

In the case of the bone tissues that constitute the *Vert A* and *Vert B* models (OAR 2), the toxic dose is a little higher because the proximity of the implant as seen in Fig. 6.7 (b). Similarly, the committed volume for 90% D_{ref} is less than 15% of the total volume on bone tissues that constitute the vertebrae. The BC- ^{90}Y was the implant that have a larger accumulative dose in the *Vert A* model. For the vertebral model without metastasis depicting in Fig. 6.7(e) and 6.7(f), the BC- ^{90}Y remains the radionuclide with the highest dose deposited in OAR 1 and OAR 2. This is important to keep in mind since the amount of bone implant used in this computational experiment corresponds to 7.52 g. The absorbed doses were less than 90% of the D_{ref} in these simulations. Therefore, the volume committed for these radiotoxic doses is negligible, being less than 0.1%. In Fig. 6.7(c), the PTV represents the vertebral metastasis for *Vert A* and *Vert B* models. The tally for dose was calculated on the XY-plane's implant, with BC- ^{90}Y as the radionuclide. Such radionuclide held a better therapeutic effect in the *Vert. B* model since a greater spatial dose distribution was obtained, reaching up to 94.3% of the total metastasis volume for 90% D_{ref} . The PTV of Fig. 6.7(d) corresponds to the implant in the model without metastasis. The specific activity was calculated in such a way that 90% D_{ref} could be obtained with respect to 90% or more of the volume with that RB cement amount.

Table 6.2 shows the specific activities required for each β -emitter source to satisfy with the condition that 90% of volume and 90% of D_{ref} in the model without metastasis were reached. The BC- ^{90}Y was the implant that requires less specific activity to reach the desired therapeutic dose levels. The 90% D_{ref} was not reached in all cases for the OAR defined in the Table 6.2. A percentage ratio of volume that reaches a D_{ref} percentage is presents in the Table 6.2. Although ^{90}Y provided a higher dose levels in the spatial dose distribution, these remained a tolerable alternative to radiotoxicity due to the use of these radioactive sources.

Table 6.2 Therapeutic Dose Deposited and Radiotoxicity for PTV and OAR – Volume percentage estimated for 90% of the Reference Dose (72 Gy) concerning to TD 50/5 for each organ.

Tumor, Organs or Bone Cement	Specific Activity $A_0 = 3 \text{ GBq}$						Model without metastasis		
	Vert. A			Vert. B			Ho-166	Sm-153	Y-90
	Ho-166	Sm-153	Y-90	Ho-166	Sm-153	Y-90	$A_0 = 50 \text{ MBq}$	$A_0 = 72 \text{ MBq}$	$A_0 = 16,2 \text{ MBq}$
Metastasis – PTV	62,77	24,47	80,91	76,49	35,22	94,30	-----	-----	-----
Spinal Cord – OAR 1 *	0,02/10	0,01/7	0,01/30	0,01/39	0,01/9	1,80/90	0,029/5	0,000	0,058/12
Bone Tissue – OAR 2 *	9,04/90	2,62/90	14,65/90	3,09/90	0,41/90	7,26/90	0,007/55	0,007/20	0,007/68
Bone Cement – PTV	-----	-----	-----	-----	-----	-----	90,05	98,09	89,25

* % Volume/% Dose [D_{ref}]

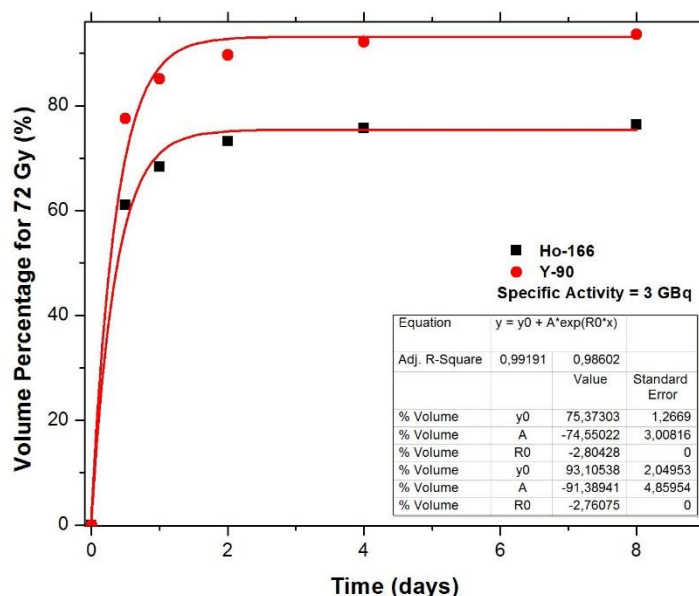


Figure 6.8 Volume Percentage with 90% of the Reference Dose as a time decay function for Ho-166 and Y-90 with a bone cement 6,77 g simulated in the Vert. B model.

Fig. 6.8 shows the proportion of the volume of the metastasis that reached the therapeutic dose planned as a function of accumulative time on the Vert. B. It is easy to notice that the ^{90}Y has a better kinetic performance compared to ^{166}Ho . Despite the aforementioned, the Ho-166 could be configured as another alternative to the minimally invasive procedures *in situ*, performed by the Radiovertebroplasty. In both cases, after 2 days, almost full therapeutic dose was achieved. The exponential fit on the graph allows predicting what would be the percentage of volume reached after the full source decay.

6.4. Discussion

One of the major problems in radioactive cements is directly related to vertebrae dose because dose must be planned with high dosimetric precision in terms of the spatial dose distribution.

The contrast calculated by the sensiometric curve using an intensifier can be compared with the mathematical calculation made directly on the digitalized images. The evaluated contrast has confirmed that a high concentration of HAp in the cement facilitates its visibility on radiological imaging. The guide image procedure by means of fluoroscopy is used for the location of the bone cement during the insertion in the Vertebroplasty. Therefore, a higher concentration of calcium atoms raises the attenuation factor of the cement. In the radiological experiments, the insertion of the bone cement was more difficult since the vertebral piece is at atmospheric pressure. In the clinical situation, the vertebrae are under compression in their usual anatomical environment; this physical characteristic has been exploited in Vertebroplasty to perform the procedure.

The radiological images facilitated the assembling a computational model that would serve as input file for the dosimetric study. Later, it was on the scope to investigate the therapeutic and radiotoxic response. The computational cost of the stochastic methods becomes extremely high due to the small size of the voxels. Such modelling depends on the physical technological resources in order to the simulations be carried out in a range of days, weeks or even months. Only the absorbed dose from β -emissions was evaluated; however, there is reliability of the results since the β -emissions in the three sources has the high percentage of emissions. In all simulations, it was confirmed that the spatial dose distribution was greater for the ^{90}Y compared to ^{166}Ho and ^{153}Sm . For therapeutic purposes, Sm-153 could be unsuitable use for the *in-situ* implant. According to graph 6.7(b), this indicates that a smaller amount of implant is not directly related to the reduced dose distribution in the organs at risk (OAR), since it depends on the spatial distribution of the implant in the vertebral body. On the other hand, the implant itself acts as an attenuation element.

The logistic procedure of Radiovertebroplasty may facilitate the management's patient. It could be done without taking into account several sections of the treatment. Radiovertebroplasty may be performed in an ambulatory since it is a minimal invasive.

6.5. Conclusion

Both BC-⁹⁰Y and BC-¹⁶⁶Ho are quite promising for their protocol implementation in the Radiovertebroplasty. In the frame of the computational dosimetry and with these studied concentrations of HAp in the RB cement, more studies are needed on the toxic response at cellular level (cytotoxicity) to evaluate the degree of acceptance of the RB cement after the source decays. According to the results found, the ¹⁵³Sm source could be more promising and in this way be in another type of minimally invasive procedures such as Radioangioplasty, which in the past was studied with other beta emission sources such as ³²P, which presents higher levels of radioactive contamination due to ¹⁵³Sm (Hehrlein, 2002). The sources with the highest dosimetric performance deposited 90% of the dose within 2 days after to be implanted, being equivalent to radiosurgery or planning for hypofractionation.

6.6. References

- Anselme, K. (2002). Osteoblast adhesion on biomaterials. *Biomaterials*, 21, 667-681.
- Ashamalla, H., Cardoso, E., Macedon, M., Guirguis, A., Weng, L., Ali, S., & Panigrahi, N. (2009). Phase I trial of vertebral intracavitary cement and Samarium (VICS): Novel technique for treatment of painful vertebral metastasis. *Int. J. Radiation Oncology Biol Phys.*, 75, 836-842.
- Campos, T. P., & D'alessandro, R. (21 de 07 de 2006). *Brasil Patente N° PI 0605721-7 B1*.
- Dale, R. G. (1985). The application of the linear-quadratic dose-effect equation to fractionated and protracted radiotherapy. *Br J Radiol.*, 58, 515-528.
- de la Calle, A. B., González-González, G., Fornés, C., & Martínez-Calderón, F. (2006). ¹⁵³Sm-EDTMP (SAMARIO) for the treatment of metastatic bone pain. *Rev. Soc. Esp. Dolor*, 3, 159-163.
- Donanzam, B. A. (2012). *Bioceramicas com Ho-166 e Sm-153: sintese, caracterização e avaliação dosimetrica em radiovertebroplastia*. Belo Horizonte, MG, Brasil: Universidade Federal de Minas Gerais.
- Donanzam, B. A., Campos, T. P., Dalmázio, I., & Valente, E. S. (2013). Synthesis and characterization of calcium phosphate loaded with Ho-166 and Sm-153: a novel

- biomaterial for treatment of spine metastases. *J Mat Sc: Mat in Med*, 24, 2873-2880.
- Emami, B., & et al. (1991). Tolerance of normal tissue to therapeutic irradiation. *Int J Radiat Oncol Biol Phys*, 21(1), 109-122.
- Finlay, I. G., Mason, M. D., & Shelley, M. (2005). Radioisotopes for the palliation of metastatic bone cancer: a systematic review. *Lancet Oncol*, 6, 392-400.
- Georgy, B. A. (2008). Metastatic Spinal Lesions: State-of-the-Art Treatment Options and Future Trends. *Am J Neuroradiol.*, 29, 1605-1611.
- Harrington, K. D. (1981). The use of methylmetacrylate for vertebral-body replacement and anterior stabilization of pathological fracture-dislocations of the spine due to metastatic malignant disease. *J Bone Joint Surg Am*, 63, 36-46.
- Hehrlein, C. (2002). Is Radioangioplasty Next? *Cardiovascular Interventions*, 57, pp. 295-296.
- Hirsch, A. E., Medich, D. C., Rosenstein, B. S., Marcel, C. B., & Hirsch, J. A. (2008). Radioisotopes and vertebral augmentation: Dosimetric analysis of a novel approach for the treatment of malignant compression fractures. *Radiotherapy and Oncology*, 87, 119-126.
- Hirsch, A. E., Rosenstein, B. S., Medich, D. C., Martel, C. B., & Hirsch, J. A. (2009). Polymethylmethacrylate and Radioisotopes in Vertebral Augmentation: An explanation of underlying principles. *Pain Physician*, 12, 887-891.
- Horn, E., Henn, J., & Lemole, J. (2004). Thoracoscopic placement of dural-rod instrumentation in thoracic spinal trauma. *Neurosurgery*, 11, 1150-1154.
- Legeros, R. Z., Lin, S., Rohanizadeh, R., Mijares, D., & Legeros, J. P. (2003). Biphasic calcium phosphate bioceramics: preparation, properties and applications. *J Mater Sci Mater Med*, 14(3), 201-209.
- Montaño, C. J., & Campos, T. P. (2019). RADIOACTIVE CEMENT OF PMMA AND HAP-Sm-153, Ho-166 OR RE-188 FOR BONE METASTASIS TREATMENT. *Acta Ortop. Bras.*, 27(1), 64-8.
- Montaño, C. J., Nogueira, L. B., & Campos, T. P. (2016). Physical distribution and radiological contrast of cements implanted in vitro vertebrae. *Physical distribution and radiological contrast of cements implanted in vitro vertebrae.*, AP-35, 4-6. Belo Horizonte, Brasil: SENCIR - Semana da Engenharia Nuclear e as Ciências das Radiações.

- Pelowitz, D. B. (2011). *MCNPX USER'S MANUAL v.2.7.0*. Report No. LA-CP-11-00438.
- Pelowitz, D. B. (2013). *MCNP6 USER'S MANUAL v.1.0*. DB, Report No. LA-CP-13-00634.
- Ryu, S., Yin, F. F., Rock, J., Zhu, J., Chu, A., & Kagan, E. (2003). Image-guided and intensity-modulated radiosurgery for patients with spinal metastasis. *97(8)*, 2013-2018.
- Seletchi, E. D., & Dului, O. G. (2007). Image processing and data analysis in computed tomography. *Rom. Journ. Phys.*, *52(5-7)*, 667-675.
- Suetens, P. (2009). *Fundamentals of Medical Imaging*. (2d ed.). Cambridge University Press.
- Trinidade, B. M., Christóvão, M. T., Trinidade, D. F., Falcão, P. L., & Campos, T. P. (2012). Comparative dosimetry of prostate brachytherapy with I-125 and Pd-103 seeds via SISCODES/MCNP. *Radiol. Bras.*, *45(5)*, 267-272.

CAPITULO 7

7. Cytotoxicity study in PBMC cultures due to exposition of a possible radioactive-bone cement based in PMMA-HAp.

ABSTRACT

Background: Radiovertebroplasty has emerged as a therapeutic alternative for the treatment of bone metastasis that present low therapeutic response or high radiological risk to conventional treatments. The radionuclides beta-sources coupled to a bone cement implanted in situ produces absorbed doses for tumor control in the same level of megavoltage radiotherapy. Such composite based on HAp (hydroxyapatite) biophosphates and Polymethylmethacrylate (PMMA) may to simulate the natural bone tissues to be restored. A broad study of the interactions of the implant bone-cement with cellular bone constituents is required. Cellular biocompatibility of PMMA have already been investigated. Cell adhesion studies in pure HAp bioceramics have also been carried out to evaluate the cell diffusion in this biological microenvironment. **Methods:** 1. Synthesis of the matrix of biophosphates and preparation of the macroaggregate RB cement in pellets of 2 mm in diameter and 1 mm in thickness. 2. Obtaining PBMC cells by centrifugation and density separation. 2. Cultive of the PBMC cells in RPMI medium modulated and no modulated by PHA.4. Study of toxicity due to cellular exposition to the cold bone cement per collection of supernatant's cells and MTT cell viability analysis at time kinetics of 24, 48 and 72 h of exposure of the cultures to the bone cement. **Results:** The morphologic analysis showed: 1. At 24h, a set of selected cell fields near the pellets with monocyte grouping and formation of a surrounding cellular halo, related to a possible aggregation response. 2. At 144h, long term cell survival. 3. No statistical significance was found for $p < 0.05$ between experimental groups exposed to the PMMA and PMMA + HAp pellets. **Conclusions:** The PBMC cells exposed to a cold RB cement based on PMMA+HAp presented morphologic elements that indicate no toxicity. It was possible to assess that there is survival and cellular aggregation near pellets, preserving their similar immune function characterized by this type of hematopoietic cells.

Keywords: RB Cement, PBMC, Metastasis, MTT viability cell, Cytotoxicity, PMMA, HAp.

7.1. Introduction

Radiovertebroplasty is a novel technique that combines an intervention for general bone modeling, similar to vertebroplasty (VT), and the use of Poly (methyl methacrylate) acrylic (PMMA), Hydroxyapatite target to radioactive and contrast agent, for the bone metastases treatment. The VT technique has been proposed mainly to help reduce pain in patients who suffer from the compression of bone pieces and possible microfractures (Macedo, 2005; Donanzam, 2012; Campos & D'alessandro, 2006). The use of bone cements in VT is addressed to the management of patients with osteoporosis and other large bone fractures. These cements were initially based on polymers such as PMMA whose main function was the union of the fractured pieces by apparent high impact traumas. In addition, the stabilization and anatomical recovery of the bone piece has been proposed in the Kyphoplasty, this technique being an improved variant of Vertebroplasty (Klimo, Meic, & Schmidt, 2004; Georgy, 2008; Harel & Angelov, 2010; Gerszten, 2007; Gerszten, et al., 2005). The use of these techniques was mainly guided to patients with neurological compromises due to spinal cord injury. Subsequently, other composites were developed to restore bone tissues, such is the case of bioceramics. Compounds based on calcium matrices such as HAp (Hydroxyapatite) were studied for purposes of clinical application, taking into account that a significant percentage of bone mineralization processes are mediated by the formation of these calcium matrices with good adhesion to tissue bone and osteoblastic cellular response (Legeros, et al., 2003; Dalby, 2002; Dalby, 2001; Vallo, 1999). Other advances in therapeutic treatment against cancer were developed. The radiotherapeutic use of ^{153}Sm -EDTMP (Samarium-153 ethylene diamine tetra methylene phosphonate) has been used for the patients' treatment with bone metastases, mainly attending to the reduction of pain. Despite the efficacy in the use of this radiopharmaceutical, there are some difficulties that have not yet been solved, such as its poor metastasis response to low-energy beta irradiation poor particle penetration in the bone metastasis, low radiopharmaceutical distribution on metastasis possibly due to intravenous drug administration. Although others studies claim that the drug does not drive to an adverse hematological response, controversies still exist regarding to cytotoxicity (de la Calle, et al., 2006).

Radiovertebroplasty proposed the use of a possible radioactive bone (RB) cement in situ performing a minimally invasive procedure. The aim of the RB cement based on PMMA-

HAp-¹⁵³Sm or PMMA-HAp-¹⁶⁶Ho is to overcome some of the drawbacks of ¹⁵³Sm-EDTMP. Synthesis and characterization studies have shown the benefits of RB cement in relation to the cost-benefit of the ¹⁵³Sm-EDTMP radiopharmaceutical. The suitable natural isotopic abundance and high neutron cross section for radioactive neutron reaction (n,γ) of both the Sm-152 and the Ho-165 nuclides in the RB cement makes them good candidates to have HAp-¹⁶⁵Ho or HAP-¹⁵³Sm activated with induction of a small number of contaminants. Such RB cement can contribute to the therapeutic absorbed dose in a predictable and reproducible way. Computational studies developed mimicking the RB material into synthetic vertebrae have shown a dose equivalent to a hypofraction protocol found in the clinical treatments often used in of the megavoltage teletherapy. Additionally, the dose absorbed by the spinal cord and other healthy tissues showed much lower than in conventional radiotherapeutic treatments (Donanzam, et al., 2013).

Other aspects related to the PMMA's polymerization in *Vertebroplasty* when the product is in excess are associated with the chemical cytotoxicity necrosis, as well as the thermal necrosis by exothermic polymerization reactions that reach temperatures up to 110 °C (Guerra, et al., 2010). Studies carried out early showed suitable biological responses to the exposure of PBMC+HAp cultures *in vitro*. One of the most important findings of this work was the increase in osteogenic potential due to exposure to HAp in cultures with red bone marrow cells. The synthesis of osteocalcins detected on the samples' surface indicating cellular activity developed in the culture (Jäger & Wilke, 2003). One of the determining factors to infer the increase in cell adhesion was associated with the surface's roughness of the bone implant. In another study with macrophages derived from activated monocytes, these showed the relationship between PMMA particle size and the phagocytic function developed by macrophages. This phagocytic function is carried out by the macrophages when the PMMA particle had a size less than 9.6 micrometers (Chikaura, et al., 2016). The inflammatory response has also been studied for cured and uncured bone implants based on PMMA showing greater inflammation in uncured cements (Ramstedt, et al., 2010).

Thus, the main goal for this paper was to evaluate the cement's cytotoxicity for higher concentration ratio of HAp in relation to PMMA in monocytes that integrate the PBMC cultures.

7.2. Materials and Methods

7.2.1. The RB cement synthesis

HAp Synthesis. The HAp was synthesized by the sol-gel method according to Donanzan *et al*, Campos *et al* and Legeros *et al* (Macedo, 2005; Donanzam, 2012; Campos & D'alessandro, 2006). The reagents used for the HAp synthesis were 3.937 g of calcium nitrate ($\text{Ca}(\text{NO}_3)_2 \cdot 4\text{H}_2\text{O}$), 0.69 mL of phosphoric acid (H_3PO_4), 1 up to 2 mL of methanol CH_3OH as a catalyst for starting reaction and deionized water as solvent in excess. After mixing the components, the solution was rested for 24 h in a closed beaker. Precipitation, nucleation and formation of colloids had occurred. Subsequently the sample was heated in an oven. The temperature started at room temperature ramped to 80 °C at a rate of 0.306 °C.min⁻¹, holding 360 min at the 80 °C isotherm, subsequently ramped to 100 °C at the rate of 0.333 °C•min⁻¹ holding 720 min at 100 °C isotherm. At the calcinations, the sample was heated from room temperature to 720 °C at a rate of 6 °C•min⁻¹, following by a 60 min at 720 °C isotherm. After cooling, the HAp samples were macerated to powder.

PMMA-HAp composite preparation. HAp powder was mixed in different proportions to PMMA in its powder presentation. The composite was prepared in cold based (non-radioactive) mixing PMMA ($[\text{CH}_2\text{C}(\text{CH}_3)(\text{CO}_2\text{CH}_3)]_n$), HAp [$\text{Ca}_5(\text{PO}_4)_3(\text{OH})$]. Both PMMA and the instruments were cooled previously. The mixture was stirring. PMMA-HAp system was prepared with PMMA's micro-spheres copolymer mixed to the monomer Methyl Ethyl Methacrylate (MMA). The samples were prepared in accordance with the following concentrations [x_n , with $n = 1$ and 5], such that $x_1 = 0.00000$ and $x_5 = 0.50000$. The x_n is a value corresponding to x in the following system $(1-x)[\text{CH}_2\text{C}(\text{CH}_3)(\text{CO}_2\text{CH}_3)]_n - x[\text{Ca}_5(\text{PO}_4)_3(\text{OH})]$ or $(1-x)\text{PMMA}-x\text{HAp}$. In the case of radioactive bone cement the proportions were given as $(1-x)\text{PMMA}-x\text{HAp}+y^{152}\text{Sm}\cdot\text{HAp}$. After the preparation of the macroaggregates, these were dissolved in the catalyst to induce the polymerization and on a mold of 3 mm in diameter by 0.5 mm in thickness, the PMMA and PMMA+HAp chip was designed in a 1:1 ratio which were then placed in the cell culture medium. Fig. 7.1 shows the design of the pellets that were thermally sterilized before their subsequent use for crops. The chips were heated to a temperature of 102 °C and maintained at this temperature for 2 hours.



Figure 7.1 Chip-shaped samples of PMMA+HAp bone cement (1:1 ratio) and PMMA

7.2.2. Toxicity experiments

7.2.2.1. Peripheral blood mononuclear cells

Maintenance of crops. Human peripheral blood mononuclear cells (PBMC) were obtained from healthy volunteers. Cell cultures were maintained in RPMI-1640 culture medium supplemented with 10% SBF and antibiotics gentamicin ($50\mu\text{g } \mu\text{L}^{-1}$) and streptomycin ($500\text{mg}\cdot\text{mL}^{-1}$) in T-25 culture beakers in a humid atmosphere containing 5% CO_2 at 37°C .

PBMC cells separating. The peripheral blood mononuclear cells of patients were separated according to the procedure described by GAZZINELLI *et al.* (Falcão, Motta, Lima, Lima, & Campos, 2015; Gazzinelli, Katz, & Rocha, 1983). The heparinized blood applied in 15 mL, siliconized tubes containing a mixture of Ficoll-diatrozate, obtained commercially, in the ratio of one-part Ficoll-diatrozate to two parts of blood. The preparation will be subjected to centrifugation for 30 min at 1400 rpm at room temperature. At the end of the centrifugation a ring of mononuclear cells obtained at the interface between Ficoll and plasma, which were removed with the aid of a Pasteur pipette and transferred to sterile 15 ml conical bottom tubes carefully. The volume should be completed for 15 mL with unsupplemented RPMI-1640 (GIBCO) solution and another centrifugation (10 min, 1200 rpm). Cells washed two more times (10 min, 1200 rpm). At the end, an aliquot of the cell suspension collected and diluted (1:20) in an Eppendorf tube containing $90\mu\text{L}$ of Türck's solution, and the number of cells determined by counting in

Neubauer's chamber with the aid of an optical microscope. The cell concentration was adjusted to a suspension containing 1.0×10^6 cells·mL⁻¹ of RPMI-1640 supplemented, under sterile conditions, in laminar flow hood.

7.2.2.2. Toxicity to cold RB cement

Sample collection. Homogenized and cell suspension aliquots from PBMC cultures collected from bottles (T-25) in triplicates. The triplicates of 500 µL aliquots were collected from the T-25 bottles and transferred to Eppendorf tubes using an automatic pipette. Eppendorf tubes identified for testing the MTT (3- (4,5 dimethylthiazol-2yl) 2,5-diphenyltetrazolium bromide). Homogenized and suspended aliquots collected from the bottles were place in culture with PHA (Phytohemagglutinin). Control and samples of RB solid cement, in cylinder-coil shape, were place in the wells, in triplicate. After kinetic period of 24, 48, 72 h after homogenized, cell aliquots were removed for the MTT assay. Also, culture supernatant was removed for cytokines assays.

Cell viability. The MTT cell viability test was based on the verification of viability and cell proliferation's quantification based on tetrazolium salt (MTT) cleavage. After incubation of cells subjected to this assay, a dye solution is formed, which is measured by ELISA reader (Enzyme-linked Immunosorbent Assay), and in this way it is possible to correlate the absorbance with the number of viable cells and to evaluate cell viability in vitro, as well as to monitor macroscopically the proliferation of cell lines. The kinetic time was quantified for PBMC culture supernatant after 24, 48, 72 and 96 h.

7.3. Results

7.3.1. ANOVA Cell viability

Fig. 7.2 shows the results of the ANOVA for 6 groups of PBMC cultures studied. There are two types of control culture: i) a control culture without exposure to the RB cement, only with PBMC cells; and ii) another culture with PBMC cells in which cell proliferation has been induced by the incorporation of PHA into the medium. The graphs were divided using a dot line by means of separate the cell viability responses without PHA on the left side and with PHA on the right side. In Fig 7.2(a), greater activity was observed, therefore

greater uptake of MTT in the PBMC culture group with PHA exposed to PMMA.

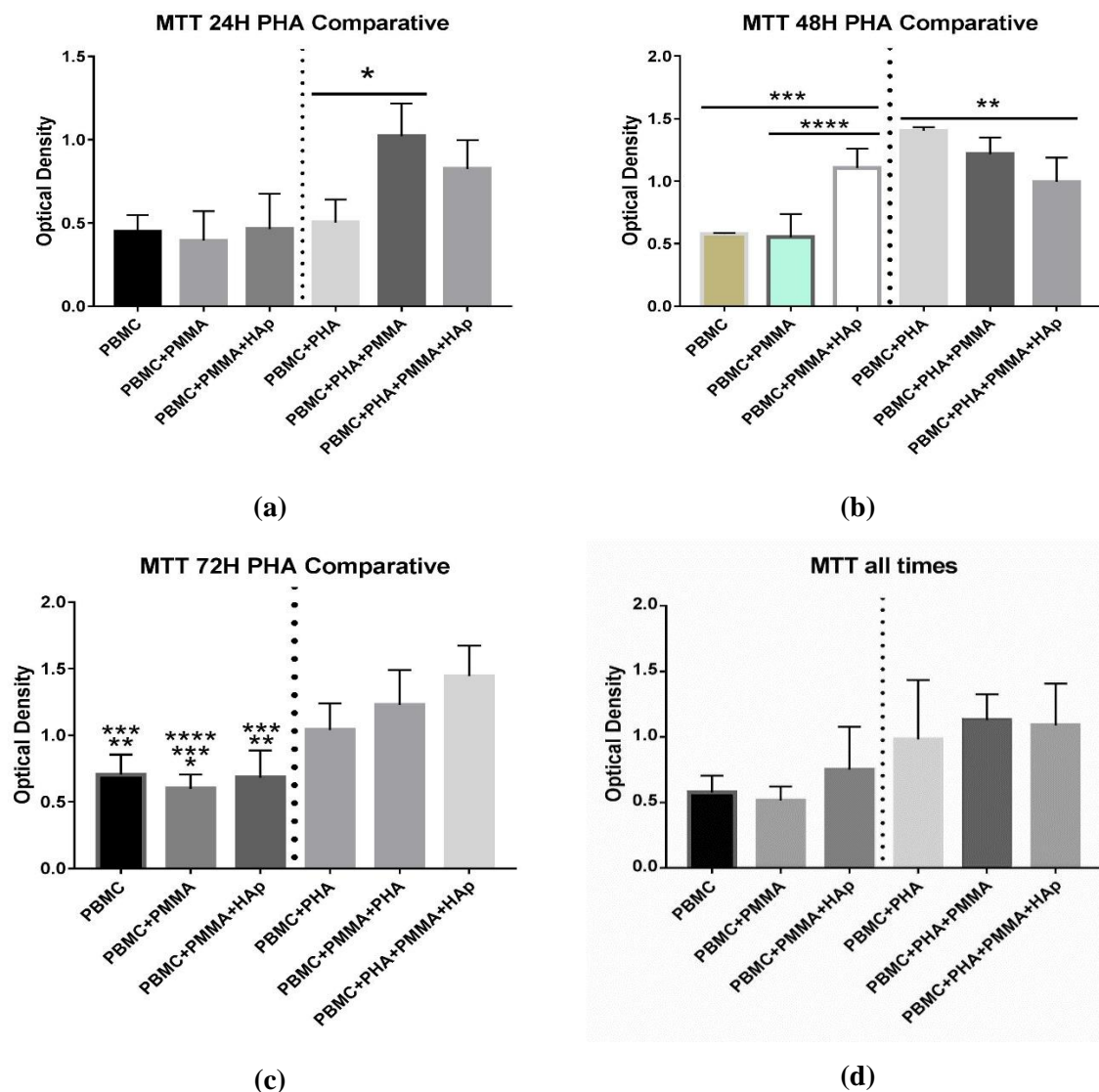


Figure 7.2 ANOVA results for the time kinetic of the diverse studied groups at (a) 24 h (b) 48 h (c) 72 h and (d) all times inter-groups.

There is statistical significance between the PBMC+PHA+PMMA and the PBMC+PHA groups. The mean value of the PBMC+PHA+PMMA group also differed with all the mean values of the cultures without PHA. In Fig. 7.2(b), the MTT uptake increased in the cultures without PHA in the PBMC+PMMA+HAp group at 48 h, showing statistical significance with the other two groups. In cultures with PHA, MTT uptake was greater in the PBMC+PHA group and its mean value was significantly higher than the PBMC+PHA+PMMA+HAp group. There was also statistical difference between the mean value of the PBMC+PHA and without PHA groups. In Fig. 7.2(c), culture media with PHA

presented higher MTT uptake than medium without PHA. No statistical difference between the undifferentiated groups by the PHA factor only showed statistical significance between the groups without PHA with those with PHA. In Fig. 7.2(d), the inter-group comparison in all times held a high standard deviation. There was no statistical significance between the PBMC in the PBMC+PMMA and PBMC+PMMA+HAp groups. Likewise, there was no statistical significance between the groups that have the PHA factor in the culture medium. For the kinetics of all the evaluated times, the culture media with the PHA factor presented higher uptake of the MTT.

7.1.1 ANOVA Cell count for cellular field

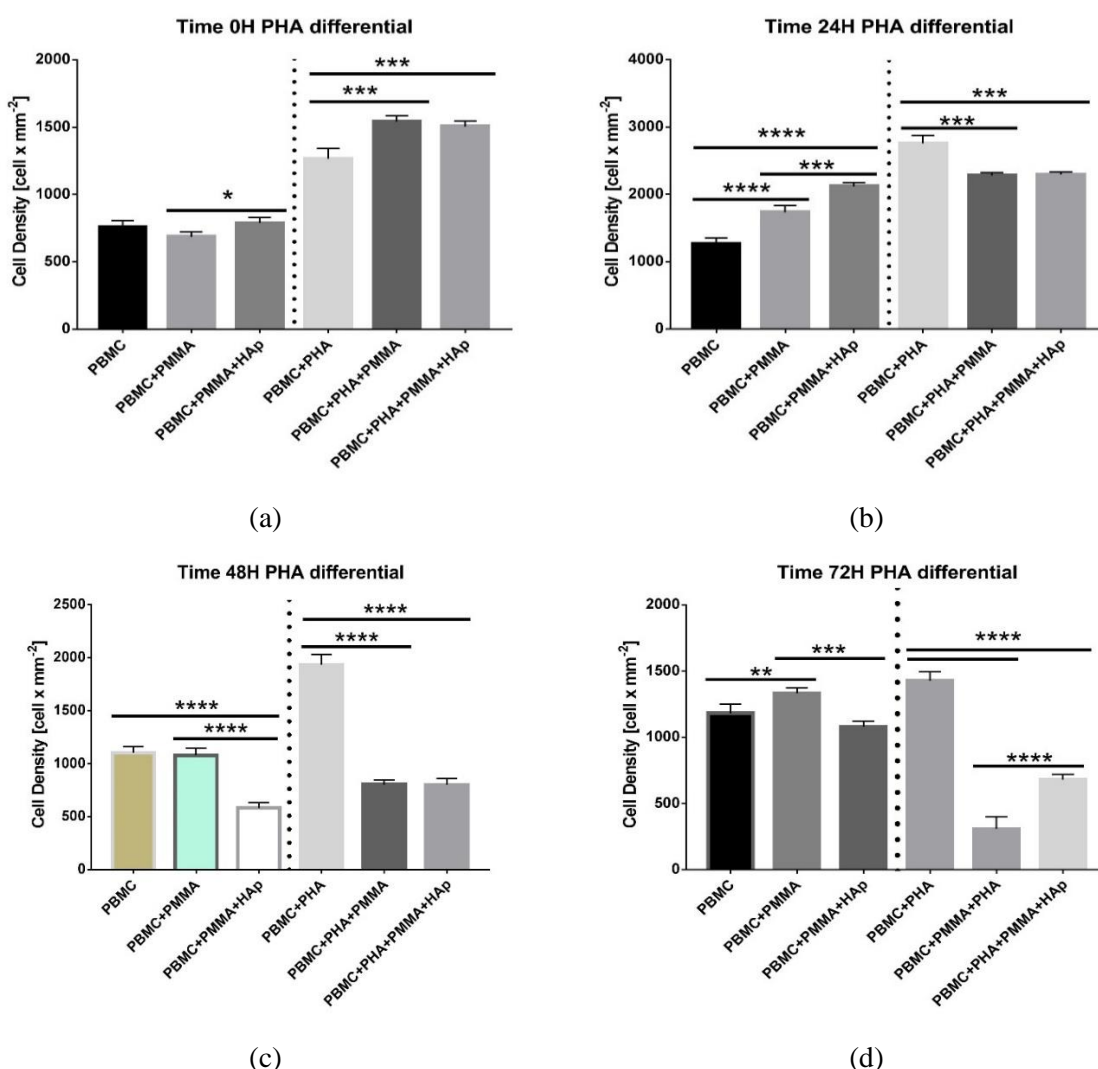


Figure 7.3 ANOVA Cell count for analysis of cellular field microphotography in kinetic time function ($500 \times 500 \mu\text{m}^2$ cellular field) at (a) 0 h (b) 24 h (c) 48 h and (d) 72 h.

In Fig. 7.3, we have studied the changes in the number of cells near the pellets made with the bone cement. An inverted Coleman microscope was used for taking the photographs, calibrated with a translucent metric rule to obtain the conversion factor of the images in pixels in function of amplified image distance at 1000 μm . Applying this correction factor, the cells were counted in a cell field of 500 x 500 μm^2 . The cell count was determined using the tools of the ImageJ-Fiji program. The photographs were taken with a lateral magnification of 40x/0.6 WD (Work Distance) 2.6 mm in four quadrants around the pellets infusing the bottom of the well and below each sample. In Fig. 7.3(a), a higher cell density per field was observed for those cultures that contain the PHA proliferation factor. The control cell number were measured at an estimated time close to zero hours. On the photographic procedure, the PHA factor in the exposed cultures induced an increase in cellular clonogenicity, increasing the proliferation and therefore its number. There was also statistical difference of those groups that are exposed to PMMA and PMMA+HAp. In Fig. 7.3(b), cultures without the PHA factor increased their cell density at 24 h. Meanwhile, cultures with the PHA factor decreased their cell density. In Fig. 7.3(c), there was a significant decrease in cell count in all PBMC cultures exposed to bone cements. The cell count decreased mainly in the culture without the PHA factor. In addition, there was statistical difference between the control groups. In Fig. 7.3(d), there was a tendency to increase cell density for groups without the PHA factor. Also, it was observed a decrease in cell density of the groups in which the culture medium contains PHA. Regarding the kinetics of time, a greater proliferative decrease of the PBMC+PHA+PMMA group was observed only at 72 h. In general, the cell density per area as a function of time remained the same in all groups or was higher than the initial cell density, so it is easy to infer that the cell viability was constant despite the exposure of the PBMC cells to the samples of bone cement.

7.4. Discussion

The MTT results infer cellular viability as a function of the time kinetics for the PBMC control culture without the PHA growth factor. The uptake activity of MTT remains stable during the 72 hours after starting the culture. The PBMC control with the proliferation factor in the culture medium showed a tendency to increase the clonogenicity due to the increase in MTT uptake. Therefore, with the previous result it is possible to confirm that

the PHA factor in the medium is a stimulant for the proliferation of monocytes in the culture. In all the cultures without the PHA factor the MTT uptake was stable according to the average values of the optical densities obtained by the reading device at 595 nm. Therefore, it is possible to infer that there is cell viability in PBMC cells exposed to bone cements. At 48 hours an increase was observed in the PBMC+PMMA+HAp group. In crops with the PHA factor, the increase in MTT uptake was significant. As a result of these experiments it can be concluded that there was cellular viability both to the PMMA exposure and to the exposure of the non-commercial cement of our interest based on PMMA+HAp in a 1:1 ratio.

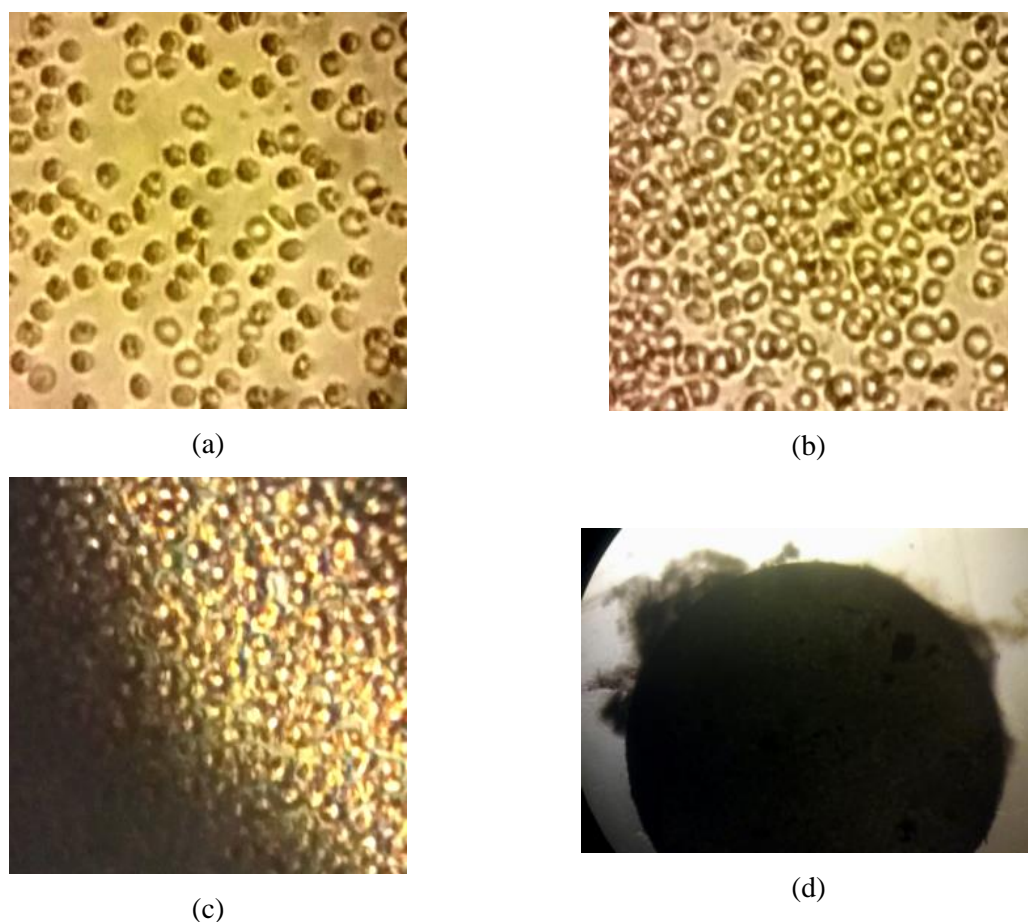


Figure 7.4 Microphotographs on cell proliferation and aggregation to bone cement samples. (a) Initial cell density at $t = 24$ hours distant from the bone implant sample. (b) Increase in cell density at $t = 24$ hours close to the chip. (c) Increase in cell density at $t = 24$ hours below of the chip. (d) Aggregation and cell adhesion detected at the chip edge at $t = 72$ hours

In the cellular count by area (Cell Density) for PBMC control culture, its value was

constant during the 72 hours of the monitoring carried out by the microphotography. In the same way, the PBMC control culture with the stimulated medium showed an equal or higher Cell Density during the time kinetics studied. Therefore, it is possible to conclude about which cell viability was equal or greater than 72 hours after the start of the culture. By comparing in all the experiments where proliferation was activated by the PHA factor, a significant decrease in Cell Density can be concluded in the area close to the chip. An explanation of the phenomenon can be explained by observing the microphotographs of Fig. 7.4. During two moments of the experiment, cellular fields close to the chip with PMMA were captured. At $t = 24$ hours (Fig. 7.4(a), 7.4(b) and 7.4(c)) an increase in Cell Density was observed in the neighborhood of the sample but not strictly at the sample edge. At $t = 72$ hours (Fig. 7.4(d)) the photomicrograph was captured with a lateral increase of less than $4x / 0.1$ WD 10 mm but with greater work distance. In this image, it was impossible to quantify the number of monocytes on the chip edge due to the high number of adherent cells. The image of Fig. 7.4(d) showed a cellular halo on the chip edge while its surroundings had a very low Cell Density. The same phenomenon was captured for the PBMC+PHA+PMMA+HAp group. The above, associated in the same way to the very high cellular adherence to the bone implant 72 hours after the start of the culture.

Cellular biology is a field of study that has allowed to understand different processes and mechanisms that occur in the cell under different conditions. During homeostasis or cell stress, various physiological or immunological factors can be understood that are directly or indirectly related to the synthesis of associated proteins for a wide variety of pathologies. Factors such as growth, inflammation, clonogenicity, immunosuppression, among others, can be altered by endogenous and exogenous agents under homeostasis or cell stress states (Falcão, et al., 2014).

Peripheral blood mononuclear cells (PBMC) have been studied comparatively for various purposes including inflammation. In the radiotherapeutic field, the dose and the dose rate have been analyzed as exogenous agents in cobalt therapy treatments. For a study where the inflammatory response was evaluated for two doses, 2 Gy and 10 Gy, a significant difference was found at 48 h after exposure of the cultures in vitro between the dose rates used for each of these two doses, probably by the damage caused in the vital functions and its impact on the recovery time of the cells (Falcão, et al., 1998).

The modulation of the immune response in PBMC cultures of patients infected with *S. Mansoni* was also studied and focused on the expression of the immunoglobulin IL-10 (Interleukin-10) in which a reduction in the formation of granulomas was evidenced (Falcão, et al., 1998; Malaquias, et al., 1997). In these in vitro cell culture studies, the analysis of the immune response based on the different established controls is imperatively remarkable. These controls have a very important role to suggest possible treatments to the different pathologies that are studied both at the level of cellular and molecular biology.

In the radiotherapeutic field, seeds based on I-125 and Pd-103 have been proposed as radioactive sources of interstitial use for prostate cancer. One of the greatest advantages of using this Brachytherapy technique is the easy to deposit the greatest amount of absorbed dose in the tumor, which is known as in situ procedure (Emami, 1998; Trinidad, et al., 2012). Computational simulations performed on highly differentiated tissues using the MCNP-5 (Monte Carlo N-particle v.5) and SISCODES (Computational System for Neutron and Photon Dosimetry by Stochastic Methods) showed a significant dose reduction in the pelvic region with the use of a source of Pd-103 compared to I-125 prostate implants. The study also highlights the requirement to put carefully implants according to clinical protocols (Emami, 1998; Trinidad, et al., 2012).

7.5. Conclusion

The cellular adhesion was one of the phenomena found in all the groups exposed to the bone cement chips. The cellular phenomenon surrounding the edge of the bone chips indicated high compatibility and it would be possible to infer that due to the exposure of the monocytes to the material there wasn't detriment to the cell viability. Therefore, it can be concluded that the exposure to the bone implant didn't present a toxic response, even in a non-commercial 1:1 ratio of the PMMA+HAp system. Comparing the results found with other studies carried out by other researchers, it is possible to infer the existence of inflammatory processes depending on the size of the PMMA particles and possibly due to that high adhesion and cellular aggregation was found at the chips edge. An important aspect found at the wells background was the detection of a significant number of HAp crystals. Possibly due to the detachment of these particles due to the cellular activity of the PBMC in the bone implant. Future perspectives would be aimed at confirming the phagocytic function of macrophages derived from monocytes, found in other studies. It

would also be possible to study signaling processes performed by PBMC cells in the calcium biophosphates bioceramics which could guide the cellular function of osteoclasts and osteoblasts in bone tissues.

7.6. References

- Campos, T. P. R. & D'alessandro, R., 2006. Brasil, Patente N° PI 0605721-7 B1.
- Chikaura, H. et al., 2016. Effect of particle size on biological response by human monocyte-derived macrophages. *Biosurface and Biotribology*, Volume 2, pp. 18-25.
- Dalby, M. J., 2001. Initial interaction of osteoblasts with the surface of a hydroxyapatite-poly(methylmethacrylate) cement. *Biomaterials*, 22(13), pp. 1739-1747.
- Dalby, M. J., 2002. Increasing hydroxyapatite incorporation into poly(methylmethacrylate) cement increases osteoblast adhesion and response. *Biomaterials*, 23(2), pp. 569-576.
- de la Calle, A. B., González-González, G., Fornés, C. & Martínez-Calderón, F., 2006. 153Sm-EDTMP (SAMARIO) for the treatment of metastatic bone pain. *Rev. Soc. Esp. Dolor*, Volume 3, pp. 159-163.
- Donanzam, B. A., 2012. *Bioceramicas com Ho-166 e Sm-153: sintese, caracterização e avaliação dosimetrica em radiovertebroplastia..* Belo Horizonte (MG): Universidade Federal de Minas Gerais.
- Donanzam, B. A., Campos, T. P. R., Dalmázio, I. & Valente, E. S., 2013. Synthesis and characterization of calcium phosphate loaded with Ho-166 and Sm-153: a novel biomaterial for treatment of spine metastases. *J Mat Sc: Mat in Med*, Volume 24, pp. 2873-2880.
- Emami, B., 1998. *Principles and practice of radiation oncology. Oral Cavity*. 3 ed. Philadelphia: In: Perez CA, Brady LW editors.
- Falcão, P. L., Cuperschmid, E. M., Trindade, B. M. & Campos, T. P. R., 2014. Transporting growth factor- β matrix metalloproteinase secretion in cell culture from ex-vivo PBMC after exposure to UV radiation. *J. Biol. Reg. & Homeost. Agents*, 28(2), pp. 333-340.
- Falcão, P. L. et al., 1998. Human schistosomiasis mansoni: IL-10 modulates the in vitro granuloma formation. *Parasite Immunology*, Volume 20, pp. 447-454.

- Falcão, P. et al., 2015. Enhancement of viability of radiosensitive (PBMC) and resistant (MDA-MB-231) clones in low-dose-rate cobalt-60 radiation therapy. *Radiol. Bras*, 48(3), pp. 158-165.
- Gazzinelli, G., Katz, N. & Rocha, R. S., 1983. Immune responses during human schistosomiasis mansoni. X. Production and standardization of an antigen-induced mitogenic activity by peripheral blood mononuclear cells from treated, but not active cases of schistosomiasis. *J Immunol*, Volume 130, pp. 2891-5.
- Georgy, B. A., 2008. Metastatic Spinal Lesions: State-of-the-Art Treatment Options and Future Trends. *Am J Neuroradiol*, Volume 29, pp. 1605-1611.
- Gerszten, P. C., 2007. The Role of Minimally Invasive Techniques in the Management of Spine Tumors: Percutaneous Bone Cement Augmentation, The Role of Minimally Invasive Techniques in the Management of Spine Tumors: Percutaneous Bone Cement Augmentation. *Orthop Clin N Am*, Volume 38, pp. 441-450.
- Gerszten, P. C. et al., 2005. Combination kyphoplasty and spinal radiosurgery: a new treatment paradigm for pathological fractures. *J Neurosurg Spine*, Volume 3, pp. 296-301.
- Guerra, N. B., Hernández, M. L. & Santos, R. G., 2010. Acrylic bone cement modified whit hydroxyapatite/vinyl acetate. Mechanical, thermoanalytical characterization and in vitro bioactivity. *Polímeros*, 20(2), pp. 98-106.
- Harel, R. & Angelov, L., 2010. Spine metastases: Current treatments and future directions. *European Journal of Cancer*, Volume 46, pp. 2696-2707.
- Jäger, M. & Wilke, A., 2003. Comprehensive biocompatibility testing of a new PMMA-HA bone cement versus conventional PMMA cement in vitro. *J Biomater Sci Polymer Edn*, 14(11), pp. 1283-1298.
- Klimo, P., Meic, J. & Schmidt, H., 2004. Surgical Management of Spinal Metastases. *The Oncologist Neuro – Oncology*, 9(2), pp. 188-196.
- Legeros, R. Z. et al., 2003. Biphasic calcium phosphate bioceramics: preparation, properties and applications. *J Mater Sci Mater Med*, 14(3), pp. 201-209.
- Macedo, R. D., 2005. *Radiovertebroplastia para Tratamento de Neoplasias Malignas óseas da Coluna Vertebral: Avaliação da proposta e da viabilidade*. Belo Horizonte (MG): Dissertation - Universidade Federal de Minas Gerais.
- Malaquias, L. C. C. et al., 1997. Cytokine Regulation of Human Immune Response to *Schistosoma mansoni*: Analysis of the role of IL-4, IL-5 and IL-10 on peripheral

- blood mononuclear cell responses. *Scand. J Immunol*, Volume 46, pp. 393-398.
- Ramstedt, S. et al., 2010. Inflammatory response to injectable biomaterials for stabilization of vertebral compression fractures. *Trends. Biomater. Artif. Organs*, 24(1), pp. 1-10.
- Trinidad, B. M. et al., 2012. Comparative dosimetry of prostate brachytherapy with I-125 and Pd-103 seeds via SISCODES/MCNP. *Radiol. Bras.*, 45(5), pp. 267-272.
- Vallo, C. I., 1999. Polymethylmethacrylate-based bone cement modified with hydroxyapatite. *J. Biomed Mater Res*, 48(2), pp. 150-158.

8. CONSIDERAÇÕES FINAIS

A Radiovertebroplastia é apresentada como uma nova proposta terapêutica para tratamentos de metástases ósseas. As metástases ósseas que produzem complicações neurológicas constituem o alvo dessa nova proposta. Principalmente aquelas metástases que geram compressão interna nas peças ósseas precisam de prioridade no atendimento em pacientes oncológicos. Os tratamentos paliativos em pacientes com metástases envolvem terapias de radiação, entre elas a radioterapia conformacional e o IMRT. O IMRT principalmente é planejado nos serviços de rádio-oncologia para diminuir a dose absorvida nos tecidos saudáveis. Quando a medula espinhal recebe uma dose absorvida superior a permitida, existe alta probabilidade que o paciente desenvolva complicações neurológicas após do tratamento paliativo nas metástases vertebrais. A *mielitis* aparece como um efeito indesejado, mas inevitável nos pacientes oncológicos com metástases vertebrais. Muitas propostas radioterápicas apareceram durante os últimos 30 anos entre elas o uso sistêmico de $^{153}\text{Sm-EDTMP}$; entretanto, o radionuclídeo acoplado ao fármaco não atinge eficientemente todas as metástases devido à radio-resistência das células cancerosas e da pobre biodistribuição do fármaco. Essa nova proposta, a Radiovertebroplastia é baseada no acoplamento da radiação *in situ* a um procedimento ortopédico minimamente invasivo, já frequentemente usado em pacientes com osteoporose. O uso *in situ* da radionuclídeo de emissão beta acoplado em um cimento ósseo é inserida no local da metástase aumentando a dose absorvida na vértebra, portanto, aumentando, a janela terapêutica e diminuindo a probabilidade de administrar dose radiotóxica nos órgãos de risco próximos ao implante.

O estudo da dosimetria com os radionuclídeos propostos mostraram seu desempenho. O Y-90 foi o radionuclídeo que apresentou a melhor janela terapêutica para o tratamento paliativo de possíveis metástases vertebrais radio-resistentes. Além disso, o Ho-166 mantém boa perspectiva para ser incorporado como alternativa para o tratamento *in situ*. O Sm-153 não apresentou um desempenho radioterapêutico apropriado para esse tipo de tratamento, mas possivelmente poderá ser utilizado em outros procedimentos *in situ*, em locais cujos ossos sejam finos e superficiais, como mãos e pés.

Após o decaimento do radionuclídeo, o compósito toma outra função. Este faz parte dos

processos de restauração e estabilidade das peças ósseas afetadas pelas metástases. É importante aprofundar o conhecimento sobre o material principalmente para esta finalidade. Estudos térmicos feitos permitiram compreender a natureza do polímero (Polimetilmetacrilato - PMMA) usado como um dos componentes do cimento ósseo. A calorimetria exploratória diferencial (DSC) conferiu a existência de uma transição vítrea em torno de 103 °C, acima dessa temperatura crítica o material continua seu processo de desnaturação e de degradação que indicam liberação de outros produtos como CO₂ e H₂O avaliados na termogravimetria (TG). Outro aspecto importante do PMMA é a natureza hidrofóbica do composto. A hidroxiapatita (HAp), outro dos constituintes do material cimentício, também mostrou a presença da água presa na rede cristalina amorfa. O fenômeno provavelmente acontece pela capacidade higroscópica do HAp. A água é retida pelo HAp devido a um número determinado de dipolos elétricos entre ³²P e grupos (OH)⁻ que interagem em certa faixa de distância intermolecular na rede do HAp. Essas características contrárias nos constituintes primários do cimento ósseo PMMA+HAp produzem reações de segregação favorecendo a geração de poros no material após a mistura e a polimerização do PMMA. Estudos mecânicos feitos no sistema PMMA+HAp para uma proporção de 1:1 mostrou um comportamento mecânico no range do tecido ósseo trabécular ou esponjoso. O que infere na possibilidade de uma otimização da composição do cimento para favorecer a difusão células de medula vermelha óssea no implante no corpo vertebral. Estudos de citotoxicidade mostraram alta aderência ao implante ósseo de células de monócitos (PBMC). Essa alta agregação supõe múltiplos processos de dinâmica celular ativada nas células PBMC devido à exposição ao material de implante. Uma das perspectivas dessa linha de pesquisa envolve avaliar se existem fenômenos de sinalização dos monócitos devido à agregação destes na superfície do cimento.

Uma das perspectivas futuras desse trabalho é encaminhada à investigação da viabilidade celular da linhagem MDA-MB-231 exposto a cimento ósseo radioativo (1-x)PMMA+xHAp+y^AMHAp, sendo M o radionuclídeo beta acoplado ao cimento. Outros possíveis estudos em modelos animais envolver avaliar a viabilidade do uso do implante radioativo para identificar a janela terapêutica do procedimento em seu conjunto.

A. APÊNDICE - FUNDAMENTOS DA TERMODINÂMICA

a TRANSIÇÕES DE FASE

No estado sólido, a descrição termodinâmica permite por meio de variáveis de estado, tais como: pressão, temperatura, entalpia, entropia, energia livre, etc. (p , T , H , F etc., respetivamente) compreender a natureza e propriedades físicas das substâncias. A estabilidade de tais características físicas definidas na forma dimensional e geométrica em redes Bravais é chamada de fase e depende diretamente do comportamento das variáveis de estado. Geralmente, o estudo das transformações de fase é feito usando as variáveis de estado (T , V) em relação a funções como a energia livre de *Helmholtz* F e as variáveis (p , T) em relação à entalpia livre de Gibbs G em condições de equilíbrio ou fora do equilíbrio termodinâmico. Sabe-se que uma fase é estável quando é caracterizada por um potencial mínimo de F e constante T e V , ou um mínimo de G e constante p e T ou um mínimo de H e constante S e p ou um mínimo de U e constante S e V ou um máximo de entropia S e constante U e V . Frequentemente, o equilíbrio do estado pode ser modificado pela aplicação de uma perturbação térmica ou mecânica. Para um sistema sólido se transformar ou mudar de fase, a estabilidade deve passar para o limite do equilíbrio, onde a variação da entropia é zero e esse estado é conhecido como metaestável. Uma aplicação direta desses critérios, conhecida como o critério de estabilidade de *Gibbs-Duhem*, indica que o estado de equilíbrio estável corresponde à fase em que há um mínimo de energia G e quando esses limites são cruzados, o sistema está em uma fase de transição em que há um limite de pontos críticos determinados pelas variáveis de estado.

O estudo das fases de uma substância pode ser compreendido por meio de um diagrama que estabelece relação das transformações das fases em função de uma variável de estado independente, por exemplo, a temperatura T ou a pressão p . Em um sistema, é possível definir a variância ν como o número total de variáveis que caracterizam o sistema, N o número de variáveis térmicas, c o número de componentes, ϕ o número de fases e r o número de reações entre os componentes no caso aconteçam.

$$\nu = c - r - N - \varphi \quad (\text{A.1})$$

Quando um sistema contém vários componentes, é natural que várias fases coexistam e que novas sejam formadas quando uma variável de estado é alterada. Abaixo temos um exemplo de um diagrama de fase de dois componentes *A* e *B* (Fig. A.1.).

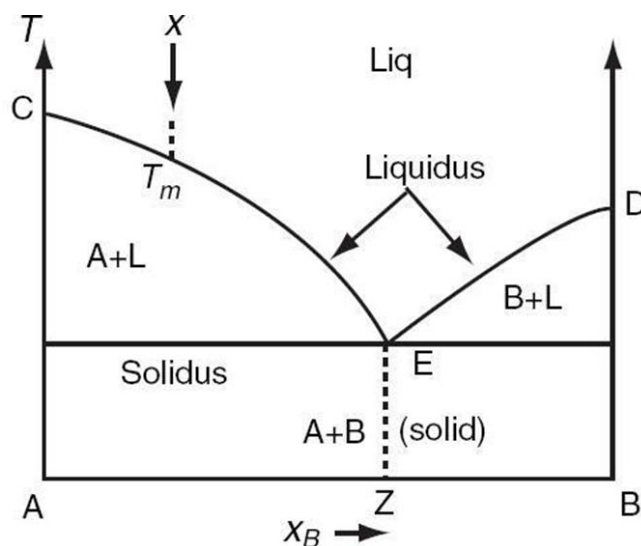


Figura A.1 O diagrama de fase de um sistema binário dois componentes *A* e *B*. Na parte mais baixa, a coexistência dos componentes no estado sólido é observada. O diagrama de fase está definido em termos de temperatura e concentração.

É possível classificar as transições de fase com base nos potenciais termodinâmicos, conforme foi proposto por *Paul Ehrenfest* em 1933 (PAPON, LEBLOND, & MEIJER, 2002).

- Transições de primeira ordem: aquelas são acompanhadas pela descontinuidade das quantidades termodinâmicas, tais como: entropia e densidade, associadas às primeiras derivadas dos potenciais termodinâmicos. Na transição de fase, estas derivadas de primeira ordem do potencial apresentam descontinuidades.
- Transições de segunda ordem: neste caso, os potenciais termodinâmicos e suas primeiras derivadas são contínuos, enquanto algumas das segundas derivadas aproximam-se de zero ou aproximam-se assintoticamente ao infinito no ponto de transição em relação às variáveis de estado.

$$S = -\left(\frac{\partial G}{\partial T}\right)_p, \quad V = \left(\frac{\partial G}{\partial p}\right)_T, \quad V = \left(\frac{\partial(G/T)}{\partial(1/T)}\right) \quad (\text{A.2})$$

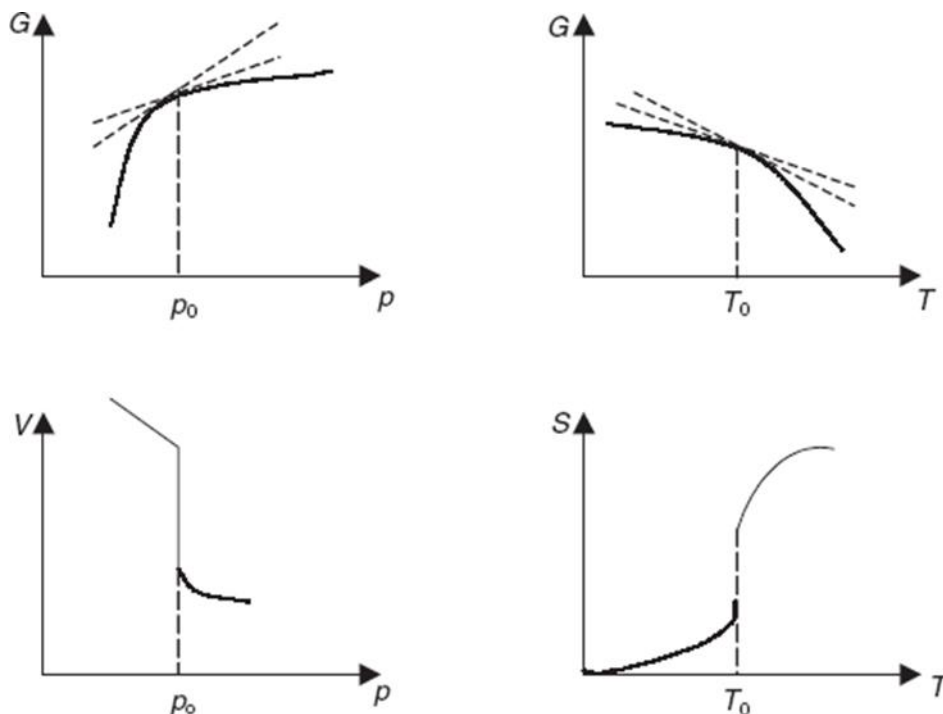


Figura A.2 Os gráficos a seguir são característicos de transições de primeira ordem, os potenciais termodinâmicos são contínuos e as quantidades associadas V e S são descontínuos.

$$\frac{C_p}{T} = -\left(\frac{\partial^2 G}{\partial T^2}\right)_p = \left(\frac{\partial S}{\partial T}\right)_p, \quad \kappa_T V = -\left(\frac{\partial^2 G}{\partial p^2}\right)_T = -\left(\frac{\partial V}{\partial p}\right)_T \quad (\text{A.3.})$$

Onde C_p e κ_T são a capacidade calorífica a pressão constante e constante de compressibilidade a temperatura constante, respectivamente.

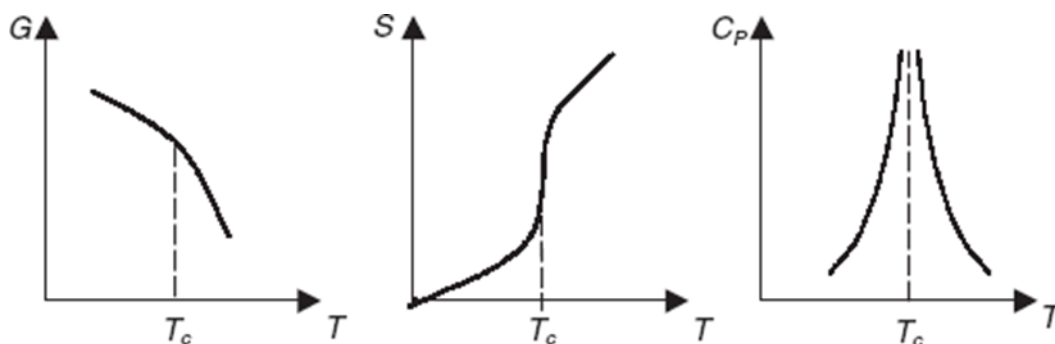


Figura A.3 As transições de segunda ordem, as primeiras derivadas dos potenciais termodinâmicos são contínuas, mas algumas das segundas derivadas divergem.

Em termos gerais, podem ser estabelecidos dois tipos de categorias de transição:

- Transições nas quais nenhuma das fases pode ser distinguida devido a propriedades intrínsecas, de modo que apenas são caracterizadas por uma mudança na estrutura ou simetria do material.
- Transições nas quais uma das fases aparece com uma nova propriedade física; essas também podem ser associadas à mudança de simetria ou estrutura geométrica.

Muitas substâncias no estado sólido sob uma transição de fase têm uma mudança na estrutura associada à disposição dos átomos devido à mudança na simetria do cristal. Normalmente, essas mudanças são caracterizadas por transformações de fase de maior simetria induzidas pelos deslocamentos dos átomos no sólido. Em essência, você pode determinar dois tipos de transições estruturais:

- Transições de ordem/desordem
- Transições de deslocamento

As transições ordem/desordem normalmente associadas a propriedades elétricas de alguns cristais. Enquanto as transições de deslocamento estão associadas ao deslocamento dos átomos na rede cristalina de suas posições de equilíbrio devido à rotação molecular que acontece com a rede perturbada e mudando mesmo assim o parâmetro da rede do cristal. Naturalmente, esse tipo de transições de mudanças estruturais são consideradas transições de primeira ordem.

Transições de segunda ordem, por exemplo: ferromagnetismo, supercondutividade ou transições de metálicas/isolantes. Normalmente, eles estão sujeitos a propriedades de tipo elétrico e magnético de alguns sólidos e não necessariamente têm uma mudança de estrutura. Existe uma variedade de mecanismos que descrevem a evolução das transições de fase, portanto, é razoável que as transições não ocorram instantaneamente, isso implica que a formação das fases depende das mudanças nos parâmetros termodinâmicos envolvendo a formação de microestruturas conhecidas como núcleos. Esse fenômeno de nucleação ocorre durante a cristalização de líquidos quando os núcleos são formados por agregados moleculares. A nucleação também é possível quando algumas moléculas

constituintes do material podem se difundir em agregados moleculares, formando assim uma nova fase. A aparência dos núcleos da nova fase implica a criação de interfaces entre duas fases e a ocupação ou distribuição em toda a estrutura cristalina.

Nucleação. A nucleação é fundamentalmente governada pelo fenômeno de difusão postulado nas *Leis de Fick*. Neste fenômeno, os movimentos de átomos ou moléculas ocorrem nos três estados da matéria representados em deslocamentos em determinadas distâncias, que é definida pela dinâmica de um grande número de transições de fase que tornam possível a nucleação.

A difusão permite que um sistema físico atinja o estado de equilíbrio, como ocorre nos mecanismos de condução. As *leis de Fick* são apresentadas de tal forma que se evidencia a relação entre concentração de partículas e tempo.

Leyes de Fick:

$$J = -D \cdot \nabla n \quad (\text{A.4})$$

$$\frac{\partial n}{\partial t} = D \cdot \nabla^2 n \quad (\text{A.5})$$

A difusão da matéria envolve o movimento de átomos ou moléculas em um sólido ou fluido que deve ter a energia suficiente para movimentar as partículas da sua posição de equilíbrio. Nos sólidos, as imperfeições definidas como as posições disponíveis ou as vagas facilitam o fenômeno de difusão, mas é fundamental que as partículas possam atravessar a energia potencial para que a rede se transforme em uma nova fase. Em geral, o coeficiente de difusão depende de a energia necessária para o fenômeno ocorrer.

$$D = D_0 e^{\left(\frac{W}{kT}\right)} \quad (\text{A.6})$$

Na equação anterior se descreve o fenômeno de difusão, onde W é a energia de ativação associada ao mecanismo. O valor depende do tipo de mecanismo e da natureza da fase. A formação de novas fases em torno da temperatura de transição, a formação de novos agregados ou núcleos implica a aparência de interfaces entre as fases iniciais e a nova fase, por isso o tamanho crítico do núcleo é decisivo na formação da nova fase ou na reversibilidade do mecanismo.

Este estudo despertou o interesse científico e vários modelos foram desenvolvidos para compreender a formação de novas fases devido ao fenômeno da nucleação. Tal é o caso do **Modelo de Volmer** em uma transição líquido/sólido em que é obtida uma relação entre a mudança de entalpia associada à nucleação e o raio crítico de formação dos núcleos da nova fase. O aspecto mais importante deste modelo para que a nucleação seja possível é que a transição seja completa é que o líquido deve ser super-resfriado. Outro modelo é o **Modelo de Lindemann**, que prevê de forma empírica e satisfatória a fusão de sólidos.

Outro aspecto fundamental desses mecanismos de transição está diretamente relacionado à duração do fenômeno. Esses processos dependentes do tempo são divididos em dois tipos: fenômenos de transporte e fenômenos de relaxamento. Nos fenômenos de transporte há uma tendência para o equilíbrio no sistema, enquanto nos fenômenos de relaxamento não ocorre transporte, mas há uma mudança nos graus de liberdade do sistema.

b. ANÁLISE TÉRMICA

Usando muitas das considerações da termodinâmica é possível estudar diferentes materiais empregando técnicas experimentais que descrevem algumas propriedades das substâncias. Existem várias técnicas de análise térmica, como termometria e dilatométrica, que se baseiam na medição da temperatura devido ao contato térmico e alterações macroscópicas em variáveis de estado, como o volume. Existe outro grupo de técnicas baseadas na calorimetria que envolve a medição de quantidades extensivas do calor.

A calorimetria foi desenvolvida principalmente em meados do século XVIII quando se chamava apenas o estudo calórico. Existem principalmente dois métodos de análise calorimétrica térmica, calorimetria exploratória diferencial clássica (DSC – Differential Scanning Calorimetry) e a mais recente, calorimetria exploratória modulada por temperatura (MDSC – Modulated Differential Scanning Calorimetry).

Sabemos que o calor é uma manifestação da energia, além que o calor e o trabalho descrevem a troca de energia entre os sistemas termodinâmicos. Em quase todas as

técnicas experimentais, a calorimetria é realizada a pressão constante, de modo que a medida do calor é a mudança na entalpia de acordo com a termodinâmica. A entalpia livre G , é conhecida como função Gibbs ou potencial termodinâmico e é utilizada como medida de estabilidade termodinâmica. Em resumo, a calorimetria envolve a medição do calor de três maneiras:

- Determinação de mudanças de temperatura
- Além disso, mudanças de estado
- Comparação de energia química, elétrica ou mecânica

De acordo com essas possibilidades na medição da calorimetria, essas mudanças ou comparações podem ser apreciadas usando calorimetria isotérmica ou adiabática. Na calorimetria isotérmica o sistema é fechado e as mudanças são observadas em relação à temperatura do laboratório. Na calorimetria adiabática, a temperatura do interior do calorímetro aumenta sem que exista o fluxo de calor com o meio ambiente. Na calorimetria diferencial, utilizam-se dois calorímetros duplos, que permitem uma troca de temperatura dos calorímetros com os arredores. Geralmente, esta troca é linear e é realizada em uma faixa de temperatura.

As aplicações da calorimetria permitem a determinação de impurezas em um composto e estudos termoquímicos também podem ser realizados. O cálculo das impurezas geralmente é feito ao estudar os pontos de fusão do sistema componente e isso apresenta uma tendência a diminuir devido às impurezas presentes. Os estudos de termoquímica são realizados em calorímetros adiabáticos e em calorímetros de varredura diferencial (*DSC*) para determinar a entalpia do composto, com a ajuda experimental da capacidade de calor. O cálculo das entalpias representa os calores da reação no sistema que, em última instância, está relacionado às energias de ligação do composto.

A calorimetria exploratória diferencial (*DSC*) é uma técnica na qual as medições podem ser feitas e analisadas por meio de curvas de aquecimento e resfriamento para obter características quantitativas no procedimento. A temperatura é medida continuamente e a técnica diferencial é utilizada para avaliar o fluxo de calor na amostra e para determinar as perdas de calor entre a referência e a amostra. Existem duas técnicas de análise térmica

DTA (Differential Thermal Analysis) que permitem determinar principalmente o diagrama de fase, as temperaturas de transição e as reações químicas. Além disso, existe a *DSC* (Calorimetria Exploratória Diferencial) que permite medir quantitativamente o fluxo de calor. Os desenvolvimentos operacionais deste sistema estão relacionados à alta precisão na determinação das mudanças de temperatura e à diminuição da perda de calor devido ao tamanho pequeno das amostras e às razões de aquecimento rápidas. Em seguida, é apresentado um pequeno esquema de um Calorímetro Exploratório Diferencial, no qual a plataforma de referência e a plataforma de amostra estão presentes.

A taxa do fluxo de calor da amostra calorimétrica é calculada na amostra e sua cápsula ou alíquota, a referência calorimétrica, é normalmente uma cápsula vazia, o procedimento é realizado com taxa de troca de temperatura e a capacidade calorífica. A capacidade calorífica é uma medida a pressão e a composição constante

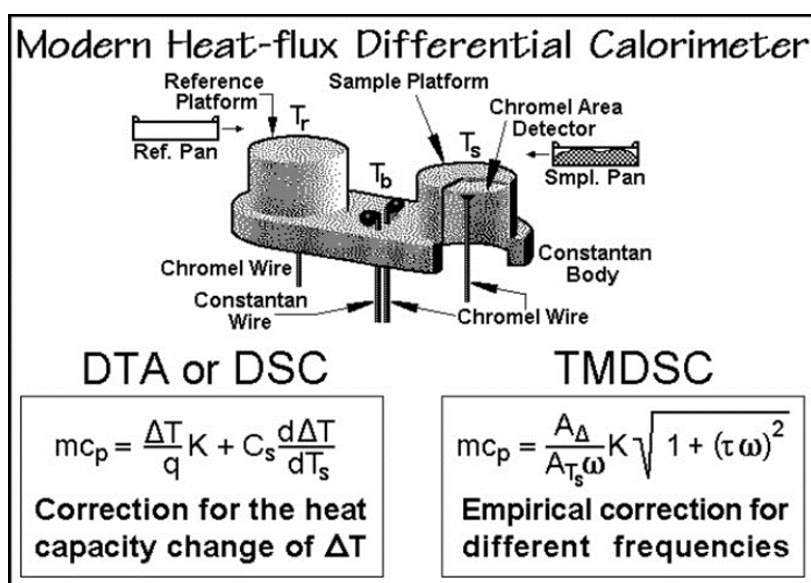


Figura A.4 Calorímetro exploratório diferencial.

As duas equações apresentadas na figura permitem determinar o calor específico a pressão constante da amostra para o DTA ou DSC e para a MDSC. De forma simples, a Capacidade Calorífica do sistema de cápsula de amostra pode ser determinada de acordo com o esquema (sistema amostra – alíquota C_s)

$$C_s = (mc_p + C_r) \quad (A.7)$$

onde C_r é a capacidade calorífica da referência e é C_p o calor específico a pressão constante da amostra. A capacidade de calor a pressão constante pode ser expressa em termos de entalpia e temperatura $C_p = \left(\frac{\partial H}{\partial T}\right)_{p,n}$ (A.8) Os potenciais ou funções termodinâmicas de Gibbs são:

$$H = \int C_p dT, S = \int (C_p / T) dT, G = H - TS \quad (\text{A.9})$$

A análise desenvolvida no *DSC* pode ser qualitativa na medida em que são interpretados os picos ou as anomalias observadas nos termogramas lançados pelo sistema operacional, essas anomalias podem ser exotérmicas ou endotérmicas e a área que eles definem representa a mudança na entalpia ao redor um ponto crítico no sistema, sendo essa uma análise quantitativa. Os pontos críticos são aqueles em que há evidências de um fenômeno de transição no sistema devido às características térmicas dessas técnicas. Esses pontos correspondem às temperaturas críticas de transição. Em resumo, esta técnica de análise permite a determinação do teor de calor da substância devido à diferença na condução térmica entre a alíquota de alumínio contendo a amostra e a alíquota vazia de alumínio. O fluxo de calor ou energia que é absorvido pela amostra é apresentado como uma função da temperatura no intervalo especificado pelo operador. A representação gráfica é apresentada pelo sistema operacional do equipamento e, dependendo da estrutura do sistema, é viável determinar qualitativamente as transições possíveis que são apresentadas. Então, a potência

é: $\phi(T) = \left(\frac{\partial Q}{\partial t}\right)_p$ (A.10), lembre-se que a capacidade calorífica de uma substância a

pressão constante é: $C_p = \left(\frac{\partial Q}{\partial T}\right)_{p,n}$ (A.11). Então, se você deriva o poder calórico ou o

fluxo de calor $\phi(T)$ em relação à temperatura que você obtém:

$$\frac{\partial \phi}{\partial T} = \frac{\partial}{\partial t} \left(\frac{\partial Q}{\partial T}\right)_p \quad (\text{A.12.}), \text{ portanto, a derivada do fluxo é uma medida direta relacionada}$$

à capacidade calorífica da substância. Uma técnica experimental para determinar a perda de massa devido às diferentes reações que a amostra sofre à medida que os ciclos térmicos se desenvolvem é a análise termogravimétrica (*TGA*). Essas reações químicas em muitas

sustâncias são devidas à degradação ou desidratação que ocorre na formação de novas ligações após as transições nas quais o vapor de água e/ou o dióxido de carbono são produzidos.

B. APÊNDICE – ALGUNS FUNDAMENTOS DE DOSIMETRIA

a. GERALIDADES DA DOSIMETRIA

A dosimetria de radiações estabelece uma relação entre a dose absorvida ou a taxa de dose resultante da interação produzida pela radiação ionizante na matéria. Mais em geral, refere-se à determinação por medição ou cálculo dessa quantidade, bem como outros aspectos radiologicamente relevantes, tais como: exposição, kerma, fluência, dose equivalente, energia transmitida, entre outros. A dose geralmente absorvida é medida através de cálculos baseados em relacionamentos previamente definidos. Para estabelecer esta relação e assim determinar essa quantidade, são utilizados dispositivos que são capazes de fornecer uma leitura que é uma medida da dose absorvida depositada em um volume sensível pela radiação ionizante. Se a dose não for homogênea no volume sensível, a leitura é uma medida de algum tipo de valor médio. Idealmente, a leitura é proporcional à dose absorvida em cada elemento de volume.

A idealização ocorre com frequência na prática, mas nem sempre pode ser aproximada dosimetricamente. A maioria dos dosímetros apresenta algum grau de não linearidade em pelo menos algum intervalo de sua dose ou também pode ocorrer devido a fatores de acoplamento entre a leitura dos dispositivos devido à medição entre o sinal e a dose. A interpretação de uma leitura dosimétrica em termos da quantidade desejada é o problema central na dosimetria. Para estabelecer uma relação entre a leitura de um dispositivo dosimétrico e a dose absorvida, foi proposto um modelo simples conhecido como Modelo de Teoria da Cavidade, que consiste em um volume V em que a radiação deposita doses por ionização, o volume é coberto por uma parede. A cavidade, ou seja, o volume V pode ser líquido, sólido ou gasoso dependendo do tipo de dosímetro. A parede do dosímetro pode cumprir uma série de funções, tais como: uma fonte secundária de partículas carregadas que contribuem para a dose no volume, fornecendo equilíbrio de partículas carregadas ou equilíbrio transitório de partículas carregadas, travando partículas carregadas que se originam fora da parede, protegendo o volume V de influências mecânicas ou danos, umidade, luz, campos eletrostáticos ou de radiofrequência, entre outras funções.

Portanto, dependendo do propósito dosimétrico do desenho do dispositivo para determinar a dose absorvida, ele desempenhará um papel importante, como a espessura da parede do dispositivo ou seu tamanho, a fim de medir as quantidades que dependem das características do dispositivo. Os campos locais de fótons e nêutrons ou as características dos campos secundários de partículas carregadas.

Existem vários aspectos fundamentais no estudo dosimétrico, tais como: a medida de dose absoluta, que determina a dose absorvida no volume de um dosímetro sem necessidade de calibração em um campo de radiação conhecido. A precisão e a exatidão, a primeira determina a reprodutibilidade das medidas dosimétricas, repetindo suas medidas e a outra expressa a proximidade das medidas dos valores esperados com os valores reais da quantidade medida. O intervalo de dose, que é determinado a partir da sensibilidade da dose ao longo do intervalo medido e que é desejável apresentar um comportamento linear com a dose para fácil calibração e interpretação. Também é importante considerar a leitura de fundo e o limite de baixa dose ou dose zero que afetam substancialmente as medidas realizadas na dosimetria pessoal. O limite máximo do range de dosagem para um dosímetro é apresentado principalmente por razões instrumentais e pelas características intrínsecas do dosímetro (saturação). A estabilidade tanto antes como depois da irradiação é outra característica que afeta significativamente a medida da dose e que pode estar relacionada com o dano sofrido pelo dosímetro pela exposição a radiação ou outros fatores externos que podem ocorrer durante o armazenamento do dispositivo. A dependência energética de um dosímetro é, em princípio, a dependência da leitura pela quantidade dosimétrica estudada sobre a energia cinética da radiação à qual o dispositivo foi exposto.

Há vários dispositivos que permitem correlacionar a leitura com a dose absorvida no domínio da física médica, especialmente no range de diagnóstico e a imagem médica onde o nível de exposição do paciente pode variar de acordo com a técnica utilizada, mas, em princípio, a dose absorvida em comparação com a radioterapia, é muito menor na maioria dos casos. Além disso, no caso da radioterapia, a energia dos feixes é muito maior e a dose a ser determinada é considerada em profundidade, enquanto no caso de diagnóstico a maior dose que pode ser depositada na pele é de maior preocupação. Esses aspectos técnicos são levados em consideração para os diferentes fins com os quais os diferentes

tipos de dosímetros são usados, uma classe de dosímetros frequentemente utilizados pelos serviços de radiofísica hospitalar são os dosímetros de termoluminescência conhecidos como *TLD* pelo acrônimo em inglês. Comercialmente, existem vários tipos de *TLDs* de acordo com a finalidade para o que são utilizados, empresas como a Harshaw Company US especializam-se na fabricação e comercialização de chips de termoluminescência com referências TLD-100 (LiF:Mg,Ti) e TLD-400 (CaF₂:Mn) entre outros. Na maioria deles, as propriedades relacionadas à dosimetria da termoluminescência foram estudadas, mas os mecanismos físicos que estão correlacionados com a exposição ou a dose absorvida ainda não são totalmente compreendidos. Portanto, algumas questões do fenômeno da termoluminescência são apresentadas para aprofundar nas ideias importantes da técnica dosimétrica.

b. MODELO FÍSICO DA TERMOLUMINISCÊNCIA

O processo físico que dá origem à termoluminescência é facilmente compreendido se a distribuição dos elétrons em um sólido cristalino for levada em consideração. Na mecânica quântica, os estados de energia do elétron são quantificados, ou seja, há apenas uma série de possíveis valores para a energia associada ao elétron. Uma vez que os elétrons estão sujeitos a um potencial variável periódico, a solução da equação de *Schrödinger* determina uma série de intervalos ou bandas de energia permitidos, enquanto todos os outros valores constituem as bandas proibidas ou as *gaps* de energia.

No zero absoluto de temperatura, todos os elétrons estão localizados nos níveis permitidos de menor energia, denominando o nível de Fermi (N_F) ao máximo valor de energia possível para um elétron nessa situação; portanto, a 0 ° K todos os níveis de energia abaixo da N_F estarão cheios, enquanto os níveis de energia mais altos ficarão vazios. A banda de maior energia que aparece total ou parcialmente cheia é chamada de banda de valência (*BV*), sendo a banda de condução (*BC*) a próxima banda mais alta e, dependendo de como o N_F é posicionado em relação a essas bandas, teremos os diferentes tipos de substâncias: isolantes, condutores ou semicondutores.

O arranjo descrito na Fig. B.1. seria o correspondente a um cristal ideal; no entanto, em

um cristal real, há uma série de alterações reticulares (defeitos) tais como vagas disponíveis, impurezas, etc., que causam a aparência de possíveis valores de energia para o elétron dentro do gap de energia. Esses valores discretos, ao contrário das bandas, não estão presentes em todo o cristal, mas estão localizados em seus defeitos mesmos.



Figura B.1 Arranjo do nível de Fermi (N_F), em relação às bandas de valência (BV) e de condução (BC) em (a) isolantes, (b) semicondutores e (c) condutores.

Nesta situação, à medida que a temperatura aumenta, a agitação térmica favorece as transições eletrônicas e os elétrons estão progressivamente localizados em níveis de energia mais elevados. Estas transições eletrônicas não são apenas produzidas por variações de temperatura, mas também a incidência de radiações de alta energia, tanto eletromagnéticas (raios-X, raios gama) quanto corpusculares (elétrons, prótons, nêutrons, partículas alfa ou beta, etc.), eles produzem a ionização atômica no cristal, causando uma troca energética entre a radiação incidente e os elétrons do sólido, que aumentam sua energia e fazem uma transição para a banda de condução. É o processo chamado ionização por irradiação. Uma vez que a radiação aumenta o número de elétrons deslocalizados pela banda de condução, a probabilidade de serem presas nas armadilhas aumenta, portanto, quanto mais intensa ou mais extensa é a irradiação, maior a densidade das armadilhas ocupadas.

Durante a irradiação, o material absorve uma certa quantidade de energia que resulta na criação de pares de elétrons-oculos ($e^- - h^+$), excitando elétrons para a banda de condução e deixando seus respectivos oculos na valência (passo 1, Fig. B.2.). Ambos os tipos de cargas podem se mover através de suas respectivas bandas e depois de um curto período de tempo

se recombinam (recombinação imediata) radiativas ou não-radiativas (passo 2).

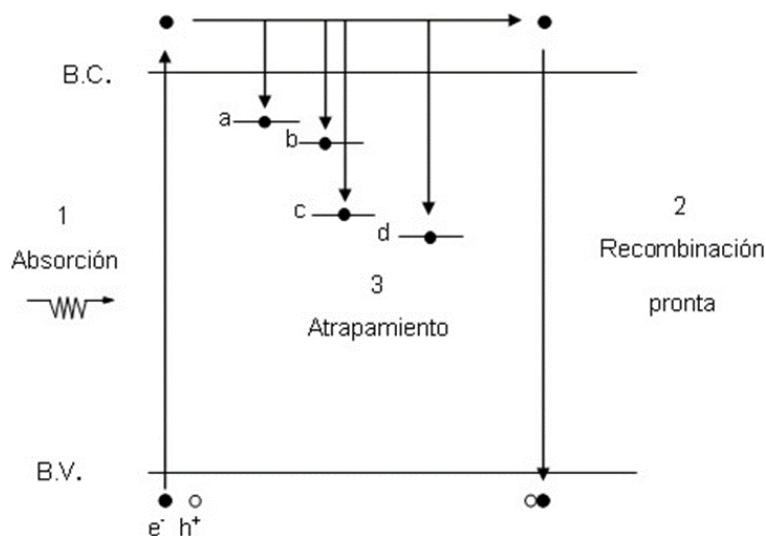


Figura B.2 Esquema do processo de (1) absorção de energia de radiação ionizante, (2) recombinação pronta e (3) estabilização de parte da energia absorvida pela captura de portadores de carga.

Este segundo passo representa o retorno quase imediato ao estado fundamental antes da irradiação. As armadilhas (níveis intermediários no intervalo de banda) são estados metaestáveis de imperfeições da rede que podem atrair um elétron ou um oco e são responsáveis por uma pequena fração da energia absorvida pelo material que está sendo armazenado uma vez que a irradiação tem concluído (passo 3). Se um elétron dentro de um certo nível do espaço requer menos energia para fazer a transição para a banda de condução do que para realizar um processo de recombinação com um intervalo na banda de valência, é dito estar em uma armadilha. O conceito de armadilha vem da maior ou menor probabilidade de um tipo de transição ou outro. Na Fig. B.3. Todo o processo é representado esquematicamente.

À medida que a temperatura aumenta gradualmente, as cargas presas nas armadilhas mais próximas da banda de condução serão aquelas que são primeiro excitadas, sendo deslocadas na referida faixa a temperaturas mais baixas; obviamente, as cargas presas em armadilhas mais profundas exigirão mais energia para ser liberada (passo 4, Fig. B.3.). O tempo que o elétron permanece em uma armadilha depende da temperatura, de modo que, à medida que aumenta, diminui, liberando o elétron da sua armadilha quando um

determinado estado de agitação térmica é alcançado, o que é necessário para superar a barreira do potencial da armadilha.

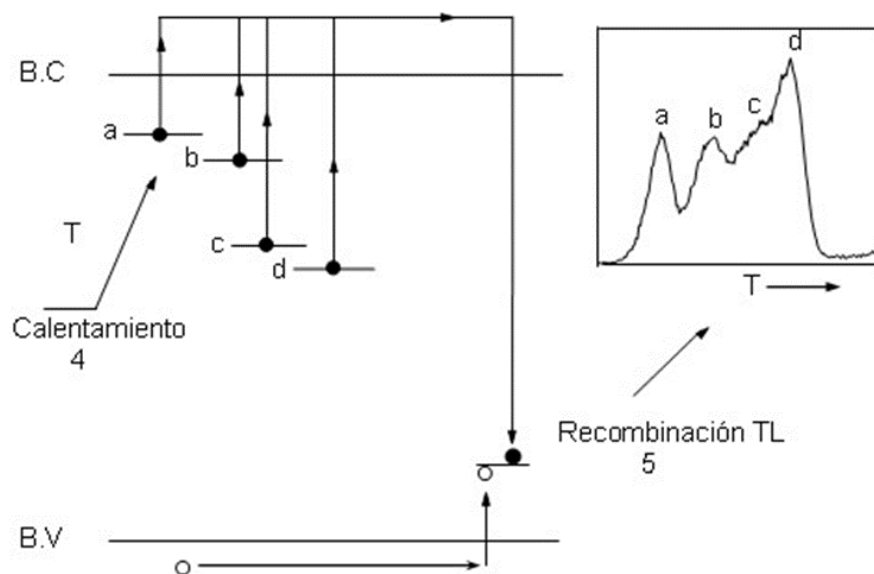


Figura B.3 Diagrama do esvaziamento térmico das diferentes armadilhas e relação com os picos de intensidade TL. (4) A temperatura do dosímetro é aumentada gradualmente produzindo sucessivamente a transição eletrônica das armadilhas (com profundidades a, b, c e d) para o BC. (5) Após um curto período de tempo na banda de condução, ocorre uma redução de energia, dando origem a uma recombinação radioativa e gerando a curva TL.

Uma vez que eles deixam a armadilha, e com o material em alta temperatura, a probabilidade de um processo recombinante (tanto radioativo quanto não radioativo) aumenta. Qualquer uma dessas recombinações, se for radioativa, causa luminescência (passo 5). Todo esse processo ocorre durante o processo de aquecimento (ou leitura) do dosímetro (Fig. B.3.).

A posição dos máximos de temperatura (T_m) que aparecem na curva TL está relacionada aos parâmetros de captura que, para cada uma das armadilhas, dependem da profundidade da mesma (E) e do fator de frequência (s). Assumindo uma cinética de primeira ordem (onde o processo de recombinação ocorre diretamente após a estimulação térmica e, portanto, a intensidade TL é proporcional à concentração de elétrons presos que deixam as armadilhas), este processo pode ser ajustado para uma equação tipo geral:

$$\frac{\beta E}{kT_m^2} = n^b s \exp\left(-\frac{E}{kT}\right) \quad (\text{B.1.})$$

onde β é a taxa de aquecimento, n é o número de portadores de carga envolvidos no processo, b é a ordem da cinética determinada empiricamente (assumindo a primeira ordem $b = 1$), s é um fator que depende da frequência de vibração térmica (ν), o coeficiente de transmissão da armadilha (χ) e de um fator de entropia ($\exp\left(\frac{S}{k}\right)$) sendo k a constante de Boltzmann. O modelo descrito irá corresponder a uma distribuição discreta de armadilhas (Martini *et al.* (MARTINI, SPINOLO, & VEDDA, 1994)).

No entanto, em muitas ocasiões, principalmente em materiais naturais, um modelo próximo foi observado a partir do descrito acima e corresponde a uma distribuição contínua de armadilhas onde os picos TL não são caracterizados por um único valor de E e s , mas por uma distribuição de tempos de semivida (τ) de elétrons em armadilhas muito próximas umas das outras (distribuição contínua de armadilhas). O valor de τ na posição do máximo é definido por:

$$\tau = \frac{1}{s_i} \exp\left(-\frac{E}{kT}\right) = \left[\nu \chi_i \exp\left(-\frac{S_i}{k}\right) \right]^{-1} \exp\left(-\frac{E}{kT}\right) \quad (\text{B.2.})$$

A intensidade da luz, que é o número de recombinações radiativas produzidas por um número de elétrons por um tempo τ , é expressa como:

$$I = -\frac{dn}{d\tau} = np \quad (\text{B.3.})$$

Onde p é a probabilidade de escapar do elétron da armadilha, que é função da temperatura e da profundidade do mesmo. Os picos do espectro de uma curva TL ou curva de desexcitação térmica não fornecem informações sobre a natureza dos centros emissores correspondentes nem dos centros de captura de elétrons. Conforme mencionado acima, essa informação deve ser obtida por outras técnicas. Muitos estudos propuseram sistemas de distribuição contínua de armadilhas que, de acordo com o acima, a seguinte equação será satisfeita:

$$I \rightarrow A \exp\left(-\frac{E_a}{kT}\right) \quad (\text{B.4.})$$

O que simplifica muito a relação entre a sinal I e a ordem cinética b . Onde A é uma constante e independente de b , além disso, é possível estabelecer uma relação funcional

entre $\ln I$ versus $1/T$, o que permitirá obter a inclinação da linha, sendo a energia de ativação necessária para superar o potencial das armadilhas e k a constante de **Boltzmann** em electron-volts com um valor aproximado de $8,6173 \times 10^{-5} \text{ eV/K}$.

c. DOSIMETRIA COM FILME RADIOCRÔMICO

Chama-se reação radiocrômico à coloração direta de um meio pela absorção de radiação quando são irradiados. Inicialmente sofrem uma polimerização parcial que altera sua transmitância, tornando-a mais escura na luz visível. Esta opacidade é proporcional à dose recebida. O filme radiocrômico (FRC) tem sido usado como dosímetro para altas doses ($10^4 - 10^6 \text{ Gy}$). No entanto, essas doses estão fora da faixa clínica, pois em uma sessão de radioterapia podem ser alcançadas doses de cerca de 2 Gy; é por isso que o FRC atual, como o EBT-2, foi adaptado para ser sensível a doses entre 1 cGy e 40 Gy.

O componente ativo é igual ao seu antecessor, EBT, com número atômico eficaz (Z_{eff} de acordo com o fabricante = 6,89), o que se torna muito semelhante ao da água ($Z_{\text{eff}} = 7,3$), em termos de densidade. A camada sensível deste filme radiocrômico contém principalmente carbono (42,3%), hidrogénio (39,7%) e oxigénio (16,2%) e, em proporções muito pequenas, de azoto (1,1%), de lítio (0,3%) e cloro (0,3%).

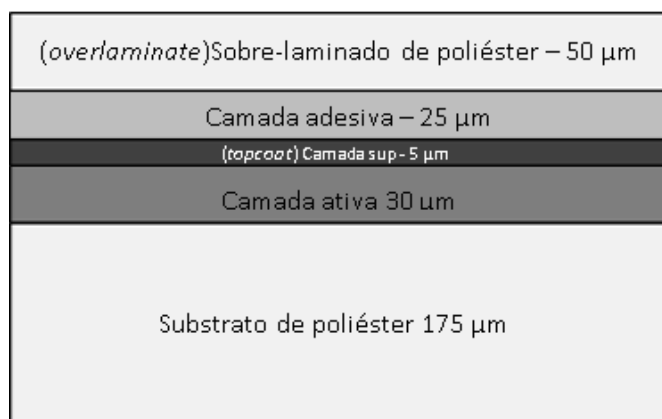


Figura B.4 Configuração do FRC Gafchromic® EBT2

A camada ativa é feita sobre um substrato de poliéster, seguido de um acabamento que adere a uma camada adesiva. Finalmente, tem uma sobre laminação de poliéster; as dimensões de cada camada são detalhadas na Figura B.4. folhas de poliéster ajudar a

proteger a camada ativa de danos mecânicos e permitir que o filme mergulhado em água durante algumas horas, à custa de penetração de água (1 a 2 mm) nas bordas. No entanto, a maioria das irradiações é realizado com fantasmas de acrílico para não molhar o filme.

Várias vantagens têm EBT-2 em relação aos seus antecessores, dois deles é que a camada ativa e revestimento superior foram alteradas para polímero sintético natural, que proporciona alta controle de fabricação e, portanto, a sua composição química. E o mais importante, a presença de uma tinta amarela na sua camada ativa fornece menos sensibilidade à luz visível e os raios ultravioletas, de tal modo que não necessita de um quarto escuro para manipular o filme.

Os FRC EBT-2 tem no seu espectro de absorção a 636 nm e um máximo secundário em 585 nm. Os comprimentos de onda correspondem às cores vermelha e amarela, respectivamente; estes valores foram medidos pelo fabricante e independentemente por Butson *et al.* (BUTSON, CHEUNG, YU, & ALNAWAF, 2009). O espectro de absorção completa de uma película irradiada com diferentes valores de dose mostradas na Figura B.5, são claros os picos, e pode ver que o pico de 636 nm é o maior valor OD_{net} . Portanto, quando um filme é escaneado (colorido), o canal vermelho é preferido, pois é mais sensível que os outros (por exemplo, azul ou verde), no entanto, o verde que faz parte do pico secundário também pode ser uma boa opção de análise.

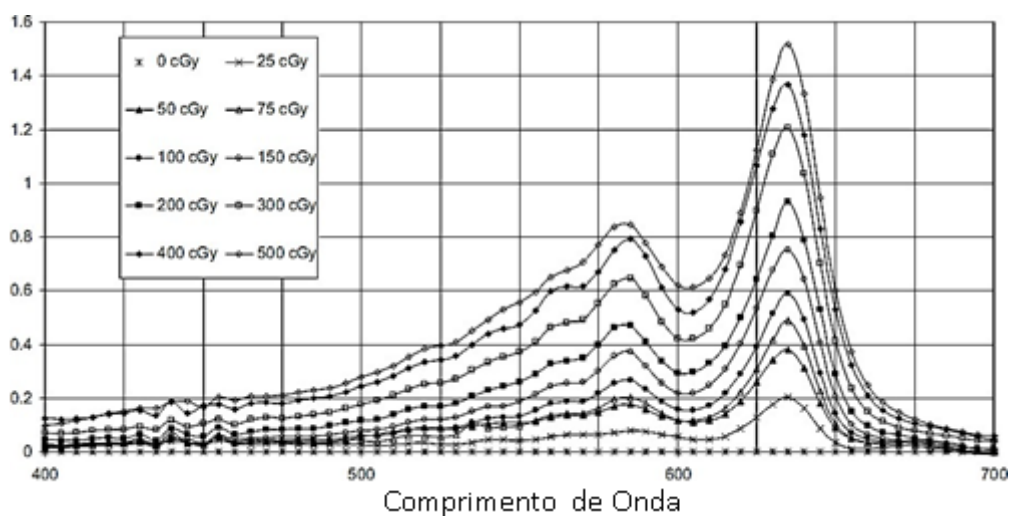


Figura B.5 Espectro de absorção líquida do EBT2 quando irradiado na faixa de 0-500 cGy. Imagem adaptada de Butson *et al.*

Finalmente, sabe-se que um filme radiográfico tem uma sensibilidade dependente da energia, no entanto, os filmes EBT-2, devido à sua composição química, os tornam pouco dependentes de energia para fótons e elétrons. Para a faixa de energia clínica (2 - 15 MeV), variações muito pequenas são observadas entre 1 e 2%, para a mesma dose. Portanto, uma calibração feita em uma energia pode ser usada para dosimetria em qualquer outra energia, pelo menos em primeira instância, mas é recomendável realizar uma calibração em cada energia. Deve-se levar em conta que cada novo lote de filmes deve ser calibrado independentemente.

Função de relacionamento entre dose e OD_{net}

Existem muitas propostas para ajustar dados experimentais, entre os quais estão aqueles que usam polinômios como proposto por Devic *et al* e Ferreira *et al.*, onde a função tem a seguinte forma:

$$D_{fit} = a \cdot OD_{net}^n + b \cdot OD_{net} \quad (B.5)$$

onde a , b e n são os parâmetros de ajuste. Observe que a equação (B.5) depende do OD_{net} que está relacionado à proporção de leituras I_{unexp}/I_{exp} e necessário corrigir a heterogeneidade do scanner. Se o valor do pixel bruto é usado, uma correção de heterogeneidade deve ser feita, especialmente se a dose esperada é alta dose. Outra função utilizada é baseada em funções racionais, como proposto pelo fabricante e Micke *et al*.

$$D_{fit} = \left(\frac{a + b \cdot OD_{net}}{OD_{net} - c} \right) \quad (B.6)$$

Finalmente a última expressão utilizada foi um polinômio de grau 3 com origem zero ordenada com a seguinte forma:

$$D_{fit} = a \cdot OD_{net}^3 + b \cdot OD_{net}^2 + c \cdot OD_{net} \quad (B.7)$$

Para escolher a melhor curva, são levadas em consideração as recomendações de Bouchard *et al*, que estabelecem as seguintes condições para a curva de calibração:

1. percorrer a origem das coordenadas
2. ser uma função crescente.
3. A função deve ter um ou nenhum ponto de inflexão na área de interesse.
4. Se houver um ponto de virada, ele estará no intervalo de 0 a $0,5 OD_{net}$, máximo.

Finalmente, recomenda-se que as funções de ajuste, no caso de um polinômio, sejam de grau dois ou três, porque a incerteza aumenta proporcionalmente com o grau da função de ajuste.

C. APÊNDICE – ANÁLISE MECÂNICA

As propriedades mecânicas de um material são todas aquelas características que permitem diferenciá-lo de outras, do ponto de vista do comportamento mecânico.

Elasticidade e plasticidade

Elasticidade é a propriedade de um material para recuperar sua forma inicial, uma vez que uma força não é mais aplicada a ele. A plasticidade é a propriedade oposta: a deformação plástica é mantida mesmo quando a força cessa. As proporções da resistência total suportada em condições de comportamento elástico e plástico podem ser expressas da seguinte forma:

$$\textit{elasticidade} = \sigma_{ult} - \sigma_y$$

$$\textit{plasticidade} = (\sigma_{ult} - \sigma_y) / \sigma_{ult}$$

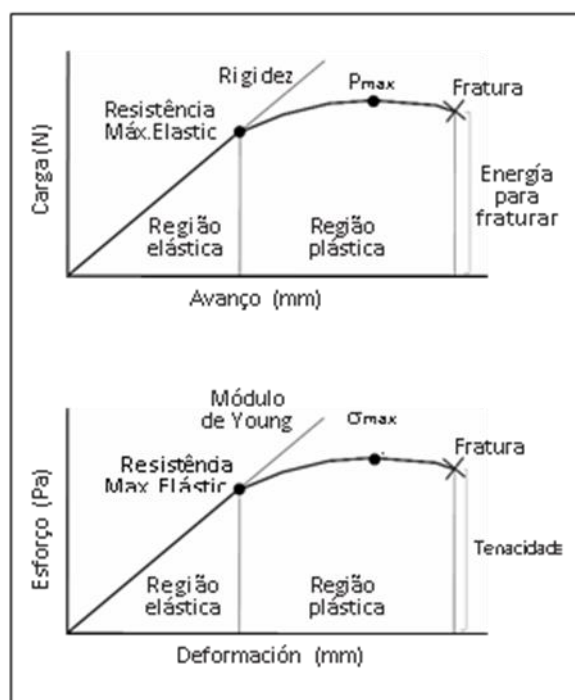


Figura C.1 Princípios biomecânicos utilizados na determinação das propriedades mecânicas do osso. Curva de deslocamento de carga (acima) e curva de tensão-deformação (abaixo) após a normalização do primeiro usando as dimensões do objeto testado

Às vezes, quando um corpo é submetido à ação de uma força, o corpo é capaz de retornar toda a energia usada para deformá-lo quando a força cessa (comportamento elástico). No entanto, em algumas circunstâncias isso não é possível, a deformação sofrida (comportamento plástico) é irreversível. Se submetemos um osso à ação progressiva de uma força, os dois tipos de deformação ocorrem sucessivamente (Figura C.1.), de modo que se diz que o osso tem um comportamento elástico-plástico. A partir da curva tensão-deformação, podemos obter uma grande quantidade de informações sobre as propriedades do material. Uma primeira região na qual a tensão e deformação são proporcionais (região linear da curva correspondente à região elástica, a Lei de Hooke) e uma outra região que não é recuperada é distinto a forma original do objeto, mesmo que a carga não seja aplicada (área de plástico ou deformação irreversível). O ponto de transição entre a região elástica e a região plástica é chamado de ponto de resistência máxima elástica (tensão de máxima resistência elástica, σ_y) que estima a capacidade de um material se deformar sem sofrer microfaturas. Em uma região plástica o ponto correspondente à tensão máxima (tensão máxima próxima à ruptura, σ_{ult}), a partir do qual, o material sofre microfaturas responsáveis de uma queda de tensão. Portanto, a deformação sofrida pela amostra aumenta até o ponto da fratura. Em uma situação ideal o comportamento plástico não aconteceria e o ponto de resistência elástica máxima seria equivalente ao ponto de fratura. Nesse caso em uma proveta cilíndrica vai acontecer o seguinte:

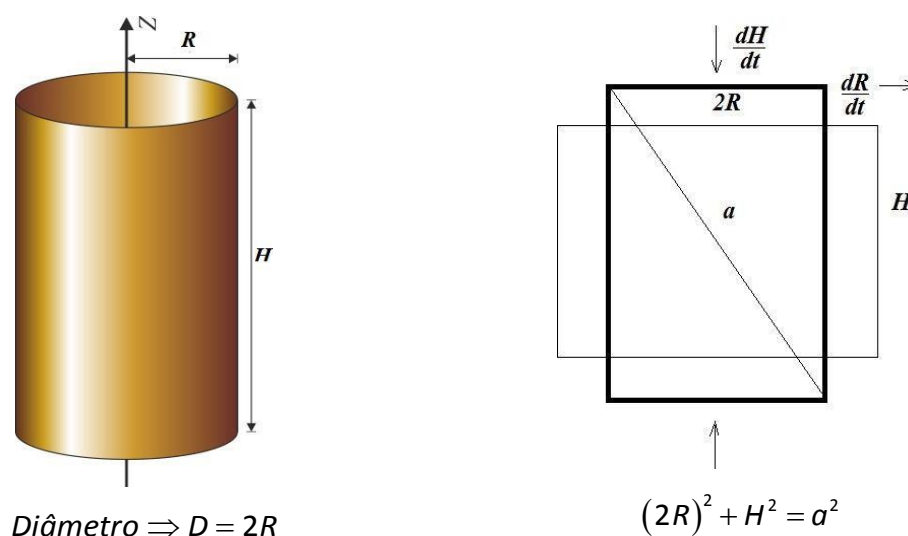


Figura C.2 Deformação do bloco de prova ideal, $dH/dt = -dR/dt$

Em um teste de esforço vs deformação nestas condições ideais:

$$8R \cdot R' + 2H \cdot H' = 0 \rightarrow 4R \cdot R' = H \cdot H' \rightarrow H = 2(2R) \rightarrow H = 2D \quad (C.1)$$

Nos testes de compressão é determinado o módulo de Young, devido aos efeitos de atrito entre as placas e as superfícies da amostra, e aos danos sofridos nas próprias superfícies durante a obtenção das amostras. Para minimizar esses efeitos, amostras cilíndricas com relação de comprimento-diâmetro de 2:1 são recomendadas como foi demonstrado anteriormente.

É muito importante conferir que as superfícies das extremidades sejam paralelas para evitar erros durante o teste. Atualmente, as placas de compressão auto-ajustáveis estão disponíveis para compensar a falta de alinhamento das superfícies. Em um teste a amostra é carregada em compressão ou tração a força é constante (N/s) ou deslocamento constante (m/s) e os dados de força e encurtamento ou alongamento da amostra são coletados através do transdutor de força e extensômetro. O esforço pode ser calculado como:

$$\sigma = \frac{P}{A} \quad (C.2)$$

onde P é a carga aplicada e A a área da seção transversal da amostra. A deformação será calculada como:

$$\varepsilon = \frac{\delta}{H_0} \quad (C.3)$$

Onde δ é o deslocamento da amostra e H_0 o comprimento inicial da amostra. Desta forma, podemos obter uma curva de tensão-deformação. Na curva podemos calcular o módulo de Young como a inclinação da região do gráfico reto (região elástica):

$$E = \frac{\Delta\sigma}{\Delta\varepsilon} \quad (C.4)$$

A área sob a curva tensão-deformação representa o valor da tenacidade (u) do material. O valor máximo de tensão (σ_{ult}) é uma característica da resistência da probeta às forças de tração ou compressão.

D. REFERÊNCIAS DOS APÊNDICES

- AITKEN, M. J. (1971). *Thermoluminescence dating-studies in archaeological science*. London: Academic Press London.
- ARRÁNS, R., MIRAS, H., ORTIZ-SEIDEL, M., TERRÓN, J. A., MACIAS, J., & ORTIZ-LORA, A. (2009). Dosimetria con películas radiocrómicas. *Rev. Fis. Med.*, 10(2), 83- 104.
- ATTIX, F. H. (2004). *Introduction to radiological physics and radiation dosimetry*. KGaA: WILEY-VCH Verlag GmbH and Co.
- BUTSON, M. J., CHEUNG, T., YU, P. K., & ALNAWAF, H. (2009). Dose and absorption spectra response of EBT2 Gafchromic film to high energy x-rays. *Australasian Physical & Engineering Sciences in Medicine*, 32(4), 196-202.
- JOHNS, H. E., & CUNNINGHAM, J. R. (1969). *The Physics of Radiology*. Springfield: American Lectures Series
- MARTINI, M., SPINOLO, G., & VEDDA, A. (1994). Phosphorescence and thermally stimulated luminescence of amorphous SiO₂. *Solid State Commun*, 91(9), 751-756.
- PAPON, P., LEBLOND, J., & MEIJER, P. H. (2002). *The Physics of Phase Transitions, Concepts and Applications* (2d. ed.). Paris: Springer.
- REIF, F. (1965). *Fundamentals of statistical and thermal physics*. New York: McGraw-Hill. REIF, F. (1967). *Statistical Physics: Berkeley Physics Course* (Vol. 5). New York: McGraw-Hill.
- WUNDERLICH, B. (2005). *Thermal Analysis of Polymeric Materials*. Berlin: Springer-Verlag

E. ANEXOS

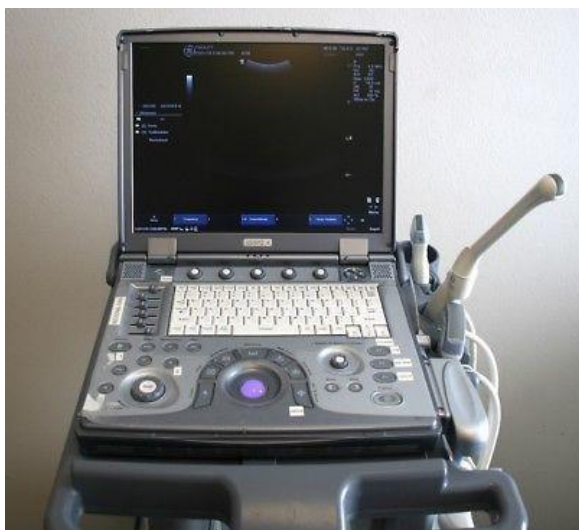
a. Imagem Médica



(a)



(b)



(c)



(d)

Figura E.1 Equipamentos para tratamento das imagens. (a) Equipe portátil de Raios-X BR 100 (b) Scanner de transmissão HP Scanjet G4050 (c) Equipe portátil ecográfica GE LOGIQe (d) Fantoma de coluna de animal

b. Análise Térmica

(a)



(b)



(c)

Figura E.2 Análise Térmica. (a) Termobalança METTLER TGA Analysis Equipment (b) Termômetro Digital de baixa resolução com comunicação para porta serial RS232 (c) Calorímetro Exploratório Diferencial DSC-60 Shimadzu

c. Análise Mecânica

Figura E.3 Equipamento para ensaios mecânicos INSTRON 5582 com sistema de aquisição de dados Bluehill© Software

d. Citotoxicidade

(a)



(b)



(c)



(d)

Figura E.4 Equipamentos para o estudo da Citotoxicidade. (a) Centrífuga CentriBio Modelo 80-2b (b) Leitor ELISA STAT FAX 303 Plus Microstrip Reader (c) Incubadora com CO₂ Shel Lab (d) Microscópios

e. Trabalhos publicados em revistas, congressos e em processo de submissão

Capítulo 1.

Revista Radioterapia Mineira.

Carlos Julio Montaña (M. Sc., doutorando), Tarcísio Passos Ribeiro de Campos (Prof. Titular, PhD). Possibilidades de um cimento ósseo radioativo em metástases ósseas - uma revisão. ISSN 2446 – 8967. Indexação IBICT.

<http://www.radioterapiamineira.org/#/cimentoosseoradioativo/>.

Capítulo 2

Acta Ortopédica Brasileira.

Carlos Julio Montaña (M. Sc., doutorando), Tarcísio Passos Ribeiro de Campos (Prof. Titular, PhD). Considerações sobre cimento radioativo de PMMA com agregado de HAp-Sm-153, Ho-166 ou Re-188 para tratamento de metástases ósseas.

Acta Ortop Bras. 2019;27(1):64-8

DOI: <http://dx.doi.org/10.1590/1413-785220192701190288>

<https://www.actaortopedica.com/>.

Capítulo 3

Artigo extenso. Congresso 1

Montaña, C. J., Nogueira, L. B. and T. P. R. Campos. Physical distribution and radiological contrast of cements implanted in vitro vertebrae. Terceira Semana de Engenharia Nuclear e Ciências das Radiações - **SENCIR 2016**. AP-35. 4 a 6 de outubro de 2016, Belo Horizonte.

Capítulo 4

Artigo 3 – Revista Técnica.

Carlos J. Montaña, Bruno R.S. Lemos, Maria I. Yoshida, Natanael G.S. Almeida, Maria T.P. Aguilar, Tarcísio P.R. Campos. Hydroxyapatite influence on the thermal and mechanical properties of a possible radioactive bone cement. A espera da decisão.

Capítulo 5

Artigo extenso. Congresso 2

Carlos J. Montaña, Adolfo H. M. Silva, Maria H. Araujo and Tarcísio P.R. Campos. Influence of hap on the polymerization processes of a possible radioactive bone cement. International Nuclear Atlantic Conference - **INAC 2017**. E03-27, October 22-27, 2017. Belo Horizonte.

Capítulo 6

Artigo 4 – Revista Técnica.

Carlos J. Montaña, Bruno M. Mendes and Tarcísio P.R. Campos. Computational dosimetric evaluation using a radioactive bone cement based on PMMA+HAp with optimal radiological contrast. Em processo de ajuste e submissão.

Capítulo 7

Artigo 5 – Revista Técnica.

Carlos J. Montaña, Olga L. M. Moreno, Patrícia L. Falcão and Tarcísio P.R. Campos. Cytotoxicity study in PBMC cultures due to exposition of a possible radioactive-bone cement based in PMMA-HAp. Em processo de ajuste e submissão.